

Many-body Theory of Electric Dipole Moments of Atoms and its Implications for the Standard Model of Particle Physics

A thesis

submitted for the degree of
Doctor of Philosophy
In The Faculty of Science

To

The Department of Physics
University of Mangalore, Mangalore

by

K. Venkata Phani Lata



Indian Institute of Astrophysics

Bangalore 560 034, INDIA

September 2007

To my mother, Smt. Santha Kumari

DECLARATION

I hereby declare that the matter contained in this thesis titled “**Many-body Theory of Electric Dipole Moments of Atoms and Its Implications for the Standard Model of Particle Physics**” submitted to the Mangalore University, Mangalagangothri for the award of Ph.D degree is the result of the investigations carried out by me at the Indian Institute of Astrophysics, Bangalore, under the supervision of Prof. Bhanu Pratap Das. This work has not been submitted for the award of any degree, diploma, associateship, fellowship etc. of any university or institute. The results presented herein have not been subjected to scrutiny.

Prof. Bhanu Pratap Das
(Thesis Supervisor)

K.Venkata Phani Lata
(Ph.D. Candidate)

Indian Institute of Astrophysics
Bangalore 560 034, INDIA
September, 2007

CERTIFICATE

This is to certify that the thesis entitled “**Many body theory of Electric Dipole Moments of Atoms and its implications for the Standard Model of Particle Physics**” submitted to the University of Mangalore by Ms.K. Venkata Phani Lata for the award of the degree of Doctor of Philosophy in the faculty of Science, is based on the results of the investigations carried out by her under my supervision and guidance, at the Indian Institute of Astrophysics, Bangalore. This thesis has not been submitted for the award of any degree, diploma, associateship, fellowship etc. of any university or institute.

Prof. Bhanu Pratap Das
(Thesis Supervisor)

Indian Institute of Astrophysics
II Block, Koramangala
Karnataka
September, 2007

Acknowledgements

First and foremost, I would like to express my sincere thanks and gratitude to my supervisor, Prof. Bhanu Pratap Das, for giving me the encouragement, support and guidance at all stages of my thesis work. He has been the best example for his patience and perseverance. Without his unconditional support, both at the research and personal level, it would have been impossible to bring this piece of work to this stage. I also thank him for exposing me to many interesting areas of physics. It was a great experience to learn physics from an excellent teacher like him. I am extremely fortunate to be a part of his group at IIA.

It is my pleasure to thank Dr. Angom Dilip Kumar Singh, Physical Research Laboratory, for his immense support, guidance and encouragement all through my work. I consider myself fortunate to have got a chance to work with him. I venerate all the discussions that we've had, where we had sorted out things in the most scientific and natural way. His honest feedbacks have helped me immensely both in my research and personal front. It wouldn't be an exaggeration to say that he was my unofficial co-guide.

I also thank Prof. Govind Nayak, Head of the physics department, Mangalore University, and Ms. Soni, who were extremely cooperative in all the formalities related to my registration at the Mangalore University. I take this opportunity to thank Prof. Vijaya Kumar for the excellent discussions we had at PRL and his timely help concerning the University formalities.

I thank Dr. Rajat Chaudhuri for his guidance and useful comments at various stages of my work.

I express my sincere thanks to my first teacher Sri. Giri sir for everything. He was responsible for what I am, today. I thank him for all the parental care that he had given me through years. Words would'nt be sufficient to thank him for the selfless care and concern he has shown me.

I would like to thank the earlier Director of Indian Institute of Astrophysics Prof. Ramanath Cowsik and the present Director, Prof. Siraj Hassan, for the continuous

support and facilities provided to me, particularly the computational resources, without which it would not have been possible to complete my work. I also thank all the earlier and present members of the Board of Graduate Studies for helping me out with various problems during my stay at IIA and also for their support all through. I specially thank Prof. Hassan and Dr. Anupama for all the help they had given me. I also thank Dr. Vasundhara for her cooperation at some stages.

I thank Mrs. Vagishwari, Mrs. Christina Birdie and all the library staff for their all time cooperation concerning the accessing of the library and procuring papers which were not available in our library.

I thank Mr. J.S. Nathan and Dr. Baba Verghese, for their cooperation and support regarding all computer related problems. I also thank Prof. Jayanth Murthy for his help and support concerning the computational resources at the institute.

I specially thank Dr. Prajval Shastri for her care and concern during my stay at IIA. Her kind words of encouragement have helped me immensely in getting back to my work when I was at my low self.

I express my sincere thanks to Mr. Bhashyam and Mrs. Shantha for all the care and concern and for the delightful musical evenings we've had together.

I thank the IIA administrative staff for all the help they have given me from time to time. I thank Mrs. Jain and Mr. Shankar for their help and cooperation.

It has been a wonderful experience on the whole, to be a part of IIA. I must say that I have learnt very important lessons during my stay at IIA. I thank my friends - Raji for always lending me a helping hand, Preeti for always encouraging me and waking me up with chai in the morning, Mahesh for his kind words, Suresh for our wonderful discussions on topics related to food. I thank Sonjoy, for his cooperation and his concern for my work. I thank Ravi, Sankar, Manoj and all my JAP batchmates Poonam, Vikram, Anand, Malaya for their wonderful company. I thank Dr. Kathiravan for his kind help, especially concerning Mangalore University formalities. I thank my juniors - Nataraj, Nagaraj, Maiti, Veeresh, Vigeesh, Blesson, Ramya, Sampoorna, Ananth, Bharat, Tapan for all the fun we've had together. I thank Shaals for the precious moments we had

shared. I can never forget dunna (Haritha) for the influence she has made in my life and for always being there for me. Living with her has made a major positive influence on me - a completely new and fresh attitude, a new way of looking at everything. The pleasant time spent with Pratika will always be cherished.

I thank Prof. Debashis Mukherjee for the very exciting discussions we've had and admire his style of explaining physics in a crisp and transparent way. I thank Dr. Geetha Gopakumar and her family for the good time I have spent with them. I thank her for her supportive words and her encouragement at various occasions. I thank my group members, specially Dr. Chiranjib Sur for the many valuable discussions we have had all through. I have benefited a lot from them. I thank Dr. Holger Merlitz for his valuable suggestions at the time of completion of my thesis work.

I thank Prof. Anwar Kamal for his valuable guidance in building up my research career in physics.

I express my deepest gratitude towards the faculty of Hyderabad Central University, Dr. Prasanta K. Panigrahi, Prof. A.K. Kapoor, Prof. Chaturvedi, Prof. V. Srinivasan, Dr. M. Sivakumar, Prof. S.P. Tewari, Prof. V.S.S. Sastry, Prof. S.N. Kaul, Dr. Venu for the excellent training and the spirit of doing science that they have inculcated in me. I particularly thank Dr. Prasanta K. Panigrahi for inspiring me through his enthusiasm and energy which brings back the spirit of research in me. I consider myself to be extremely lucky to be the student of these great teachers, who have given a stimulating experience during my study at HCU. I also thank my batchmates of HCU for all the fun we've had while studying together and for making my stay at HCU a memorable one.

My special thanks to Prof. Rohini Godbole for her wonderful teaching, which has inspired me to a great extent and has kept my interests alive in particle physics.

I thank my friends in PRL - Sricharan, Murali, Rajneesh, Sarika, Pathak, Tarak, Jayendra, Saugata, Shashwathi, Bindu, Rashmi, Arpitha for all the help and for their valuable company during the time I spent there. It was a memorable experience to be in the company of my rakhee brother, NRMS, who was extremely helpful and ever enthusiastic about doing research. I also thank my uncle Prof. Devnath and aunt for their

wonderful company and for creating an inspiring environment and making me feel at home. The times I had spent at PRL were very crucial for me and without their cooperation and support, it would not have been possible for me to make fruitful use of my stay.

I thank my late grandfather for motivating me from my childhood to take up higher studies. His blessings and words of encouragement are always cherished.

I thank my loving parents, who have been encouraging and supporting me during these years of my stay away from them. I specially thank and express my deepest gratitude to my mother for sacrificing her desires, small and big, for the sake of my education. Her life through these years has had a very positive influence on me. There might be few like her who choose to be optimistic always and it is to her that I dedicate my thesis.

I also thank amma and anna for the excellent support, encouragement and their concern towards me and my work. I am very lucky to be a part of their family. I also thank my brother and vadina for all the good times we've had and for always being there. I thank Babu and Geetha for the company they have given me. I greatly cherish all the fun I had with my sisters, Sowmya and Ramya.

Last but not the least, I thank my husband, Kittu, for his wonderful company, his persistent efforts to inspire me to work and his enormous support always in spite of being victimized due to my frustrations at various occasions. His completely different attitude towards life has helped me discover a new personality in myself. It is impossible to quantify my "thanks" to him.

LIST OF PUBLICATIONS

1. Publications - (1)
2. Publications - (2)
3. Publications - (3)
4. Publications - (4)
5. Publications - (5)

Table of Contents

List of Tables	xii
List of Figures	xv
Abstract	xvi
1 Introduction	1
1.1 Atomic Electric Dipole Moments(EDM)	1
1.1.1 Closed and Open-Shell Atomic EDMs and their Implications . . .	4
1.2 Experiments on Atomic EDMs	6
1.3 Present Status of the EDM Experiments on Closed-Shell Atoms	8
2 Closed-shell Atomic Electric Dipole Moments	10
2.1 Atomic EDM Induced by Tensor-Pseudotensor Electron-Nucleus Interaction	11
2.2 Atomic EDMs Arising from the Nuclear Schiff Moment	13
3 Coupled Cluster Theory and its Application to Atomic EDMs	16
3.1 Coupled-Cluster Theory for Closed-Shell Systems	18
3.1.1 Unperturbed Coupled-Cluster Equations	18
3.1.2 EDM Perturbed Coupled-Cluster Equations	24
3.1.3 Reduction of the Perturbed Coupled-Cluster Equations to Unper- turbed Coupled-Cluster Equations	30
3.1.4 Non-Linear EDM Perturbed Coupled-Cluster Equations	33
3.1.5 Selection Rules for the Cluster Operators	35

3.2	Application of CC Theory to Atomic Electric Dipole Moments	37
3.2.1	Zeroth Order EDM	39
3.2.2	First Order EDM	42
3.3	Comparison of Coupled-Perturbed Hartree-Fock and Coupled-Cluster Theories	47
3.3.0.1	The Coupled-Perturbed Hartree-Fock Equations	47
3.3.0.2	CCEDM Equations	51
3.4	Comparison of Coupled-Cluster Theory with Configuration Interaction	55
3.5	Size Consistency and Size Extensivity	57
4	Computational Aspects of CC Theory of Closed-shell Atomic EDMs	60
4.1	Conventions and Symbols	60
4.2	Implementation of the Iterative Scheme	61
4.3	Complementary and Equivalent Diagrams	62
4.3.1	Four Particle Form of the Coulomb Operator	64
4.3.2	Two-Particle – Two-Hole Form of the Coulomb Operator	65
4.3.3	Three-Particle (Three-Hole) – One-Hole (One-Particle) Form of the Coulomb Operator	65
4.4	Intermediate Storage Scheme	67
4.5	Evaluation of Atomic EDM	72
5	Analysis of Hg EDM Results	74
5.1	Accuracy of the Single Particle Wavefunctions	75
5.2	Calculation of Correlation Energy	80
5.2.1	Application of CC Theory to Polarizability	81
5.2.1.1	Static Polarizability	81
5.2.2	Sample Calculation of Polarizability of ^{199}Hg	83
5.3	Linear CCEDM for Atomic Hg	84
5.3.1	Results for Hg EDM Induced by the P and T Violating T-PT Interaction	85

5.3.2	Results for Hg EDM Induced by the \hat{P} and \hat{T} Violating Nuclear Schiff Moment	86
5.3.3	Summary of the EDM Results for ^{199}Hg	87
5.4	Results for the CCEDM-CPHF Comparison	88
5.5	Implications of Atomic EDMs for Physics Beyond the Standard Model .	93
6	Conclusions and Future Directions	98
A	P and T Violation and Electric Dipole Moments	102
B	Classification of the CCEDM Diagrams	105
C	Technical Details of the CCEDM Program	107
D	The Tensor-Pseudotensor H_{EDM} Matrix Element	116
E	Radial Matrix Elements of the Nuclear Schiff Moment	120
F	Matrix Elements of the P and T Violating Nuclear Potential	124
G	Additional Notes	129
G.1	Matrix elements of the Coulomb operator	129
G.2	Matrix elements of the Induced Dipole Operator	130

List of Tables

1.1	Transformation of the D and J operators under P and T	2
1.2	Experiments in progress	9
5.1	Details of basis used in the CCEDM calculation	79
5.2	Results for correlation energy with basis sets of different sizes	81
5.3	Individual contributions for polarizability	84
5.4	Individual contributions for T-PT induced EDM	85
5.5	Individual contributions for NSM induced EDM	87
5.6	Summary of results for polarizability and the EDM induced by NSM, T-PT interactions	89
5.7	Basis used for CCEDM-CPHF calculations	89
5.8	Variation of the CPHF results with introduction of virtuals of higher an- gular momenta	90
5.9	Dominant contributions to the EDM in the CCEDM-CPHF framework .	91
5.10	Comparison of CPHF mixing coefficients and the CCEDM-CPHF $T^{(1)}$ amplitudes	92
E.1	Table of the possible κ values	121

List of Figures

1.1	Fundamental origin of observable EDMs	3
3.1	Physical realization of the coupled-cluster wavefunction	17
3.2	Notation used in the thesis	26
3.3	T1-T1 clock	26
3.4	T2-T1 block	27
3.5	T1-T2 block	27
3.6	T2-T2 block	28
3.7	CCEDM diagrams contributing to RHS of the CCEDM equations	28
3.8	CCEDM diagrams contributing to RHS of the CCEDM equations	29
3.9	Diagram representing $T^{(1)}$ - (a) $T_1^{(1)}$ (b) $T_2^{(1)}$	36
3.10	Diagrams representing the electric dipole operator	39
3.11	Diagrams contributing to $(De^{T^{(0)}})_1$	40
3.12	Diagrams contributing to $(De^{T^{(0)}})_2$	41
3.13	Effective diagrams for singles and doubles for zeroth order	42
3.14	Effective diagrams contributing to EDM	43
3.15	Effective diagrams at first order contributing to F1(A)	43
3.16	Open diagrams at first order for the term $(De^{T^{(0)}})_3$	44
3.17	Effective diagrams at first order for F2(A)	45
3.18	Effective diagrams at first order for F2(A)	45
3.19	Effective diagrams at first order for F2(B)	46
3.20	CPHF diagrams at zero and one order residual Coulomb interaction . . .	49
3.21	CPHF diagrams contributing to EDM	53

3.22	Diagrams contributing to EDM at the CPHF level	54
4.1	Notation for orbital lines	61
4.2	Equivalent diagrams	65
4.3	The <i>normal</i> and the <i>complementary</i> diagrams	66
4.4	The <i>normal</i> and the <i>complementary</i> diagrams	66
4.5	CCEDM diagrams arising from EDM-IMS diagrams	68
4.6	CCEDM diagrams arising from $V_N T_2^{(1)}$ and $V_N T_1^{(0)} T_1^{(1)}$	68
4.7	H_{EDM} perturbed hole-hole one-body IMS diagrams.	69
4.8	H_{EDM} perturbed particle-particle one-body IMS diagrams.	69
4.9	One-body V_N effective diagrams	70
4.10	Cluster diagrams from EDM-IMS diagrams	70
4.11	Two-body V_N effective diagrams	70
4.12	Cluster diagrams from V_N IMS diagrams	71
4.13	Cluster diagrams from V_N IMS diagrams	71
5.1	Relative percentage error for $5s_{1/2}$ and $6s_{1/2}$. The distance is presented in atomic units.	76
5.2	Relative percentage error for $4p_{1/2}$ and $5p_{1/2}$. The distance is presented in atomic units.	77
5.3	Relative percentage error for $4p_{3/2}$ and $5p_{3/2}$. The distance is presented in atomic units.	77
5.4	Relative percentage error for $4d_{3/2}$ and $5d_{3/2}$. The distance is presented in atomic units.	78
5.5	Relative percentage error for $4f_{5/2}$. The distance is presented in atomic units.	78
5.6	Correlation energy diagrams in linear coupled-cluster theory.	80
5.7	Leading diagrams contributing to pair correlation	86
B.1	Classification of CCEDM diagrams	105
B.2	Classification of CCEDM diagrams	106

C.1 CCEDM flow-chart 111
C.2 Loop structure for the driver routine 112
C.3 Loop structure for the driver routine (contd.) 113
C.4 Inclusion of EDM-IMS diagrams 114
C.5 Inclusion of one- and two-body Coulomb IMS diagrams 115

ABSTRACT

In this thesis titled “**Many-body theory of Electric Dipole Moments of Atoms and its Implications for the Standard Model of Particle Physics**”, we have carried out theoretical studies of the electric dipole moments (EDMs) of closed-shell atoms arising from the violations of P and T symmetries. It has been proved experimentally that parity is not a conserved quantity of nature. Weak interactions violate parity. CP violation was observed in the decay of neutral kaons, which means from the validity of the CPT theorem that there must be a violation of the time-reversal symmetry if the CPT is to be a conserved quantity. There has been no direct evidence of the time-reversal violation till the most recent experiments on the $B^0 - \bar{B}^0$ decays. Existence of a nonzero EDM on a non-degenerate physical system would be a direct unambiguous evidence of independent violations of the parity and time-reversal symmetries. In physical systems having degeneracy, there can be a non-zero EDM due to the mixing of opposite parity states. Such an EDM is not due to any discrete symmetry violation. An atom being a non-degenerate physical system, can have a nonzero EDM arising from various sources — parity and time-reversal violating electron-nuclear, electron-electron, interactions. In addition to this, an atomic EDM can also arise from the parity and time-reversal violating interactions at the nuclear, nucleon and the quark levels. Measurement of an atomic EDM and its comparison with the theoretical calculations of the enhancement factor $R = \frac{d_{\text{atom}}}{C_{\text{ptv}}}$, where C_{ptv} is the coupling constant associated with the parity and time-reversal violating interactions and d_{atom} is the atomic EDM, gives information about the

coupling constants which can be used to set stringent limits on the CP violating parameters at the fundamental level predicted by various models of particle physics - SUSY, left-right symmetric, multi-Higgs, etc. The connection between the atomic EDM and the fundamental CP -violating parameters at the quark-gluon level, involves nuclear shell-model and quantum chromodynamical calculations. Our calculation of the enhancement factor, being model independent, has the potential to test various particle physics models that describe physics beyond the Standard Model.

In the present work, we have calculated the EDM of ^{199}Hg ($Z = 80$), which is one of the most promising candidates experimentally. It has a nuclear spin $I = 1/2$ and hence its nucleus is a rich source of CP violating interactions arising at the nuclear, nucleon and at the elementary particle levels. This is due to the fact that the dominant interactions responsible for CP violation at various sectors in closed-shell atoms are highly sensitive to the nuclear spin. For example, the dominant source of ^{199}Hg atomic EDM is the nuclear Schiff moment which arises from the CP violation in the hadronic sector at the elementary particle level and the nuclear Schiff moment is related to the nuclear spin I .

In the present work, the various underlying many-body effects playing a crucial role in the atomic EDM of ^{199}Hg have been highlighted. We have calculated the enhancement factor for the EDM induced by the tensor-pseudotensor (coupling constant C_T) and the nuclear Schiff moment (coupling constant Q) using a very powerful relativistic many-body theory, the Coupled-Cluster theory (CCT). This has been applied for the calculation of EDMs of closed-shell atoms for the first time.

Coupled-cluster theory to all levels of excitation to all orders, is equivalent to all order many-body perturbation theory. Beyond second order it is very difficult to calculate atomic properties like EDM, etc because of the proliferation of terms in higher orders of the many-body perturbation theory. On the other hand, coupled-cluster theory contains, at a given level of order of excitation of the cluster operators, those effects, which would otherwise have occurred at a higher order in perturbation theory. We have applied coupled-cluster theory for the first time, to calculate closed-shell atomic electric dipole moments. The atomic EDM induced by nuclear Schiff moment (Q) and the tensor-pseudotensor interactions have been calculated using the coupled-cluster singles and doubles approximation, where only the correlations arising from singly and doubly excited cluster amplitudes are treated to all orders in the residual Coulomb interaction. We have also calculated the atomic polarizability of Hg and our results lie within the error bars of the measurement. Our EDM calculations give an improved limit on C_T , compared to an earlier calculation, where the correlation effects arising only from a few kinds of excitations, of 2-hole — 2-particle type have been treated to all orders. These effects form only a subset of the effects we have included in our present calculation. In the framework of the Standard Model of Particle Physics, the parameter C_T is zero and our calculated values of Q and C_T can be used to obtain new limits on quark-chromo EDMs and other fundamental coupling constants including the QCD vacuum angle. In other words, our values of C_T and Q can be used to test the Standard Model of Particle Physics.

**Many-body Theory of Electric Dipole Moments of
Atoms and its Implications for the Standard Model
of Particle Physics**

Chapter 1

Introduction

1.1 Atomic Electric Dipole Moments(EDM)

The three discrete symmetry operations under which the laws of physics were thought to be invariant till the year 1957 are parity (P), time-reversal (T) and charge conjugation (C). The search for violations of these symmetries could have profound implications for our understanding of particle physics. Of the three symmetries, P violation was observed by Wu.et al.[1] in 1957. Some years later, CP violation was observed in the neutral kaon system [2]. The three symmetries are linked by the CPT theorem [3] ¹ from which it can be inferred that CP -violation implies T violation.

The origin of parity violation can be discerned within the frame work of the Standard Model (SM) of particle physics through the weak interactions, but there is no clear understanding of the origin of time-reversal violation in nature. The presence of a nonzero electric dipole moment on a nondegenerate physical system is a direct signature of parity (P) and time-reversal (T) symmetry violations [4]. The total angular momentum of a physical system is related to its intrinsic EDM given by, $\mathbf{D} = d \mathbf{J}$, where \mathbf{J} is the total angular momentum, \mathbf{D} and d represent the intrinsic EDM its magnitude respectively. Table 1.1 illustrates the consequences of P and T violations on the intrinsic EDMs. Under a parity transformation \mathbf{D} being a vector changes sign and \mathbf{J} being a pseudo vector doesn't change sign, whereas under a time-reversal transformation \mathbf{J} changes sign and \mathbf{D} does not. The above table demonstrates in a simple way that for a system to

¹Any quantum theory, formulated on flat space time is symmetric under the combined action of CPT transformations, provided the theory respects (i) Locality (ii) Unitarity (i.e., conservation of probability) and (iii) Lorentz invariance.

Quantity	Parity	Time-reversal
\mathbf{D}	$\mathbf{D} = -\mathbf{D}$	$\mathbf{D} = \mathbf{D}$
\mathbf{J}	$\mathbf{J} = \mathbf{J}$	$\mathbf{J} = -\mathbf{J}$

Table 1.1: P, T violation for a nonzero EDM

have a nonzero EDM, both P and T have to be simultaneously violated. This can be rigorously proved for a nondegenerate physical system using some important ideas of quantum mechanics and is presented in Appendix A. Hence, it follows that atoms being nondegenerate physical systems can possess a nonzero intrinsic EDM if there are violations of P and T symmetries. They offer advantages from an experimental point of view, of being electrically neutral and hence can be subjected to external electric fields. In addition, atoms are rich sources of EDMs as we shall explain later in this chapter. They allow studies of CP or T violations in the leptonic, semi-leptonic and hadronic sectors. Searches for an atomic EDM can be broadly classified into the following categories - EDM of paramagnetic atoms (atoms having open-shell structure), EDMs of dia-magnetic atoms (atoms with closed electronic structure) and EDMs of nucleons, particularly EDM of the neutron. In this thesis, we discuss only the EDMs of diamagnetic atoms. Theoretical studies involve the parameterization of the atomic EDMs in terms of the CP -violating coupling constants at various levels as shown in Fig. 1.1 [5]. Some of the extensions of the Standard Model, like the multi-Higgs, Supersymmetry (SUSY) and left-right symmetric models, predict CP -violation at the level of elementary particles. The atomic EDMs can hence be expressed in terms of these coupling constants, with the knowledge of the CP -violating parameters of the intermediate - nuclear, nucleon and elementary particle sectors as shown in Fig. 1.1. As shown in the chart 1.1, we begin with the EDM of electron and quarks as well as the P and T violating interactions between electrons and quarks and quarks and quarks, which are predicted by certain extensions of the Standard Model [6]. Their manifestations at the levels of the nucleon and the nucleus are shown in Fig. 1.1. The P and T violating electron-nucleus interactions of of two types. As shown in the chart, one of them arises from the scalar-pseudoscalar currents and the other from

the tensor-pseudotensor currents, the former contributes to the EDM of an open-shell atom and the latter to the EDM of a closed-shell atom. In the present work, we focus on the EDMs arising in closed-shell atoms. The most dominant source of the closed-shell atomic EDMs is the nuclear Schiff moment (NSM) which is related to d_N through the nuclear spin.

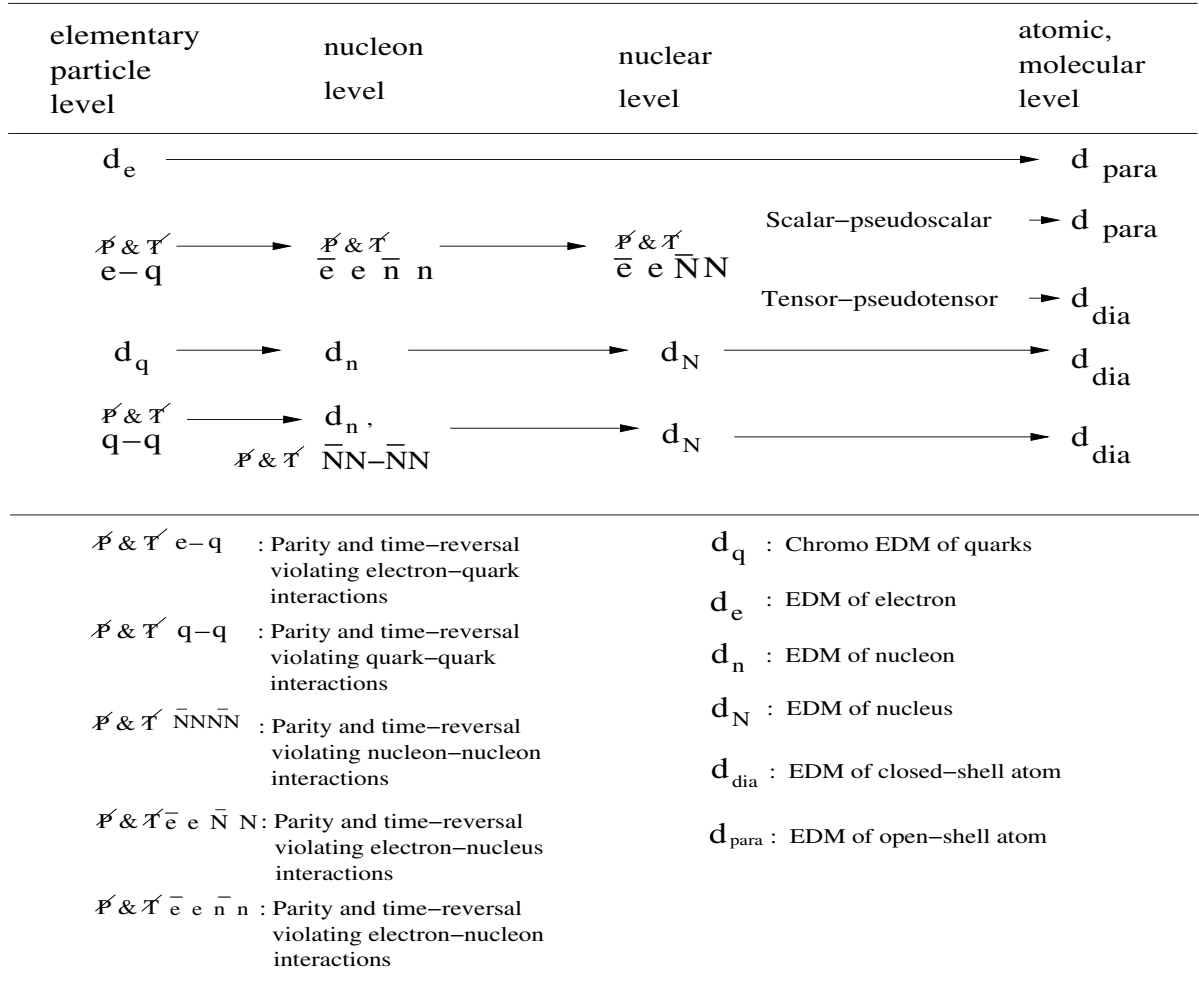


Figure 1.1: Origin of atomic EDM [5]. The chart shows the connection between the observable atomic EDMs (the atomic, molecular level) and the underlying CP violating interactions that produce them.

1.1.1 Closed and Open-Shell Atomic EDMs and their Implications

The permanent EDM of a physical system is aligned along its total angular momentum. This can be inferred from the Wigner-Eckart theorem [7]². Since the EDM of a closed-shell atom has zero total angular momentum from the electronic sector, the atomic EDM must lie along the nuclear spin. This EDM arises primarily from the CP -violating electron-nuclear interactions and the NSM. The electron-nuclear interactions, which violate T and P are the tensor-pseudotensor (T-PT)³ or the scalar-pseudoscalar (S-PS) interactions. In this thesis, we study atomic EDMs of closed-shell atoms which arise mainly from the T-PT electron-nuclear interactions and the nuclear Schiff moment. At the elementary particle level, the origin of closed-shell atomic EDMs is attributed to the P and T violating electron-quark interactions and quark-quark interactions which are predicted by the lepto-quark models [5]. The limits on the T-PT coupling constant (C_T) has been obtained from the comparison of the most recent experimental result of ¹⁹⁹Hg atomic EDM [8, 9],

$$d(^{199}\text{Hg}) = (-1.06 \pm 0.49 \pm 0.40) \times 10^{-28} \text{ e cm}$$

and the enhancement factor (ratio of atomic EDM to the coupling constant of the interaction in question) calculated by [10], using the coupled-perturbed Hartree-Fock theory,

$$d(^{199}\text{Hg}) = -6.0 \times 10^{-22} C_T \sigma_N \text{ e m}$$

where σ_N is the nuclear spin, which gives the limit on C_T ,

$$C_T = \left(1.77 \pm 0.82 \pm 0.67 \right) \times 10^{-9} \sigma_N$$

A nonzero value of C_T would imply physics beyond the Standard Model. The source of uncertainty in d_{Hg} is purely experimental, where the contribution comes from the

²Essentially which states that any vector pertaining to a system, must align with respect to the direction of the internal property of the system.

³In $\bar{e}e - \bar{N}N$ interaction, we treat the electron and the nuclear currents as the tensor and pseudotensor currents respectively, given by $\bar{\Psi}_e \sigma_{\mu\nu} \Psi_e$ and $\bar{\Psi}_N \sigma_{\mu\nu} \gamma^5 \Psi_N$.

systematic and the statistical errors. The uncertainty in C_T arises from the theoretical value of the ratio d_{atom}/C_T as well as the experimental result for d_{atom} . The uncertainty in the theoretical estimate of d_{atom}/C_T depends on the method used for the determination of C_T . Higher is the order of the Coulomb perturbation incorporated into the theory, higher is its accuracy. The accuracy of the calculations of enhancement factors would lead to a more stringent limit on C_T . Coupled-perturbed Hartree-Fock theory accounts for two-particle, two-hole kind of electron correlations to all orders in perturbation. In addition to these correlation effects, it is important to include the correlation effects that have not been accounted for by the coupled-perturbed Hartree-Fock theory. A more accurate atomic theory should be able to treat all kinds of electron correlations to all orders in perturbation, which includes four-particle, four-hole, three-particle—one-hole, etc effects. It is a challenge for many-body atomic theorists to be able to account for these important correlation effects and in this thesis, we have attempted to address this problem.

The NSM (denoted by operator S) is related to the EDM of the nucleus through the nuclear spin and can be caused by the nucleon-nucleon interactions or a nucleon EDM, which at the elementary particle level could arise from the interaction between the quarks and the chromo electric dipole moments of the quarks. The coupling constants associated with these interactions can be predicted by theories like multi-Higgs, SUSY [5, 11]. The dependence of the T-PT and NSM interactions on the nuclear spin makes closed-shell atoms, in particular, those having nonzero nuclear spin the best candidates to look for atomic EDMs sensitive to the nuclear sector. Closed-shell atoms can also give information on the electron EDM and scalar-pseudoscalar electron-nuclear interaction by considering the hyperfine interaction as a perturbation [12], but the limits on the corresponding coupling constants would not be as sensitive as those obtained from the paramagnetic atomic EDMs. For ^{199}Hg , the EDM induced by the NSM is calculated and parameterized in terms of the Schiff moment operator S . The most recent calculation by [13, 14] gives,

$$d_{\text{Hg}} = -2.8 \times 10^{-17} \left(\frac{S_{\text{Hg}}}{\text{efm}^3} \right) \text{e cm}$$

where S_{Hg} corresponds to the Schiff operator for ^{199}Hg . At the nucleon level, the operator S can be obtained in terms of the pion-nucleon coupling constants; pions being the dominant mediators of the nucleon-nucleon interactions (more detailed analysis is presented in Section 5.5 with our results) [15, 16]:

$$d_{\text{Hg}} = 3.92 \times 10^{-25} \eta_{\text{np}} \text{ e cm}$$

where η_{np} is an intermediate parameter that is related to the CP violating pion-nucleon coupling constant $\bar{g}_{\pi NN}$. This calculation involves nontrivial nuclear many-body physics, and it gives [17],

$$d_{\text{Hg}} = -3.92 \times 10^{-25} \times \left(\frac{G_F m_\pi^2}{\sqrt{2}} \right) g_{\pi NN} \bar{g}_{\pi NN} \text{ e cm}$$

where $g_{\pi NN}$ is the CP conserving pion-nucleon coupling constant. From the above, the observable atomic EDM can be expressed in terms of the chromo EDMs of quarks by [17],

$$d_{\text{Hg}} = -3.92 \times 10^{-25} \times \left(\frac{G_F m_\pi^2}{\sqrt{2}} \right) g_{\pi NN} \times 2 \left(\tilde{d}_u - \tilde{d}_d \right) \text{ e cm}$$

where \tilde{d}_d and \tilde{d}_u are chromo EDMs of the d and the u quarks respectively which are predicted by SUSY and the left-right symmetric models. The constant $\bar{g}_{\pi NN}$ is also related to θ_{QCD} , the QCD vacuum angle [18] by,

$$\bar{g}_{\pi NN} \approx -0.027 \theta_{\text{QCD}}$$

This allows us to constrain the value of θ_{QCD} through the ^{199}Hg atomic EDM.

1.2 Experiments on Atomic EDMs

The atomic calculations involve the calculation of ‘enhancement factor’ which is the atomic EDM parameterized in terms of the P and T violating coupling constants ($R = d_{\text{atom}}/C_{\text{ptv}}$), where C_{ptv} is the coupling constant associated with any P and T violating interaction. Comparing with the measured value of the atomic EDM, the value of C_{ptv}

can be extracted. Atoms are very excellent candidates for the search for atomic EDMs. In particular, heavy atoms are the preferred choices as the EDM scales as Z^2 or Z^3 . If a physical system has an intrinsic EDM d , then its interaction with the external electromagnetic field, in analogy with the interaction of the magnetic dipole moment μ is,

$$H_{\text{int}} = - \left(d\vec{E} + \mu\vec{B} \right) \cdot \frac{\vec{J}}{J}$$

where \vec{J} is the total angular momentum of the system. In the presence of external electric and magnetic fields, the EDM d and the magnetic dipole moment μ precess about the field axes. This precession is referred to as the Larmor precession. The basic idea in an EDM experiment is to measure the difference in the Larmor precession frequency corresponding to the parallel and anti-parallel configurations of \vec{E} with respect to \vec{B} [4],

$$\begin{aligned} \omega_1 &= \frac{2\mu|\vec{B}| + 2d|\vec{E}|}{\hbar} \\ \omega_2 &= \frac{2\mu|\vec{B}| - 2d|\vec{E}|}{\hbar} \\ \delta\omega &= \omega_1 - \omega_2 = \frac{4d|\vec{E}|}{\hbar} \end{aligned}$$

Therefore,

$$d = \frac{\hbar \delta\omega}{4|\vec{E}|}$$

Owing to the precision to which the frequency is to be measured, the EDM experiments are susceptible to a number of systematic effects like the motional magnetic fields, which is one of the most important sources of error. Atoms moving in an external electric field experience magnetic field in their rest frame, known as the motional magnetic field, given by, $\mathbf{B}_m = \mathbf{v} \times \mathbf{E}/c$. This field is odd in P and can mimic an EDM signal. The second important systematic effect comes from the leakage currents induced by the electric field. The leakage currents caused by high voltage are difficult to control and account for. Laser cooled atoms are excellent candidates for an EDM experiment. They offer the following advantages over the conventional beam and cell apparatus :

1. The environment is relatively perturbation free due to extremely low temperatures.

2. The average velocity of the atoms in the sample is nearly zero and hence there is zero, or negligible motional magnetic field effect.
3. They allow high coherence times as the atoms can maintain spin coherence for a relatively long time.
4. Low leakage currents.
5. It is possible to apply high electric fields as high as 100 kV/cm, as the sample region is small.

1.3 Present Status of the EDM Experiments on Closed-Shell Atoms

To date, the EDM experiment on ^{199}Hg gives the most sensitive limits on P and T violating coupling constants [8, 9]. ^{199}Hg has a nonzero nuclear spin, $I = 1/2$ and hence is very sensitive to the P and T violating interactions in the nuclear sector as both the nuclear Schiff moment, and the tensor-pseudotensor interactions, depend on the nuclear spin. Also, with $Z = 80$ it is sufficiently heavy which would enhance the relativistic effects, in turn enhancing the EDM. Any nonzero result for the ^{199}Hg EDM would indicate physics beyond the Standard Model. To set limits on specific models of CP violation, using atomic theory, the atomic EDM must be related to the CP violating parameters at the level of elementary particles. Our aim in this work is to improve the present limits for T-PT coupling constant and the Schiff moment which would in turn help in obtaining more accurate limits for the P and T violating coupling constants at the level of quarks and electrons. Limits on S can also be used to set further limits on the nucleon EDMs [19]. The Table 1.3 summarizes the on-going EDM experiments on closed-shell atoms. For experiments on various other atomic systems, see [20].

With the present apparatus the EDM of ^{199}Hg was measured to be [8, 9]

$$d(^{199}\text{Hg}) = (-1.06 \pm 0.49 \pm 0.40) \times 10^{-28} \text{e cm}$$

Atomic system	Present limit of EDM measured $ d_{\text{atom}} $ (e cm)	Laboratory
^{199}Hg	$< 2.1 \times 10^{-28}$	Univ. of Washington, Seattle
Xenon	$(0.7 \pm 3.3 \pm 0.1) \times 10^{-27}$	Princeton University
Radium	In progress	Argonne National Laboratory
Ytterbium	In progress	Kyoto University
Radon isotopes	In progress	University of Michigan

Table 1.2: Ongoing experiments on closed-shell atoms

There is further scope of improving the sensitivity of the measurement by a factor of 4, which could further improve the above result.

Chapter 2

Closed-shell Atomic Electric Dipole Moments

Atomic EDM can arise from one/more of the following sources :

- EDM of an electron d_e .
- P, T - odd electron-nucleon interactions which could be ‘scalar’ (scalar-pseudoscalar), ‘tensor’ (tensor-pseudotensor) or ‘pseudo-scalar’ (pseudoscalar-scalar) couplings.
- P, T - odd electron-electron couplings (this interaction gives a negligible contribution as its strength cannot be as large as the electron-nucleus interaction where the contributions to the electron-electron interactions do not add up coherently and hence do not scale as Z^2 or Z^3 , where Z is the atomic number).
- EDMs originating in the nucleus (NSM) due to the presence of P and T violating interactions at the level of quarks.

Electric dipole moments of closed-shell atoms arise predominantly from the ‘tensor’ kind of the electron-nucleus interaction and the NSM produced by the P and T violating interactions in the nucleus[5]. This is mainly due to the electronic and nuclear structure and related effects in closed-shell atomic systems [4], which will be discussed in subsequent sections.

2.1 Atomic EDM Induced by Tensor-Pseudotensor Electron-Nucleus Interaction

Consider the atomic EDM arising from P, T - odd electron-nucleon interactions and treat the nucleus nonrelativistically. The interaction Hamiltonian has the form,

$$H_{e-N}^{\text{EDM},T} = iG_F C_T \sqrt{2} \sum_i \sigma_N \cdot \gamma_i \rho_N(r) \quad (2.1)$$

where, G_F is the Fermi's coupling constant, C_T represents the T-PT coupling constant, $\rho_N(r)$ is the nuclear density and $\gamma_i = \beta\alpha_i$ represent Dirac matrices. The operator σ_N is the nuclear spin which is sometimes written in terms of the nuclear spin \mathbf{I} in this thesis. This interaction is responsible for the mixing of opposite parity electronic states producing a nonzero atomic EDM and it is this dependence of the $H_{e-N}^{\text{EDM},T}$ on the nuclear spin that makes closed-shell atoms having *nonzero* nuclear spin to be more sensitive to this interaction. The above form can be arrived at, starting from the second quantized form of the H_{EDM} operator,

$$H_{\text{EDM}} = \frac{iC_T G_F}{\sqrt{2}} [\bar{\Psi}_N \sigma_{\mu\nu} \Psi_N] [\bar{\Psi}_e \gamma^5 \sigma_{\mu\nu} \Psi_e] \quad (2.2)$$

Consider the term, $(\bar{\Psi}_N \sigma_{\mu\nu} \Psi_N)$. We have, $\bar{\Psi}_N = \Psi_N^\dagger \gamma_0$. Hence,

$$\begin{aligned} \gamma_0 \sigma_{\mu\nu} &= \gamma_0 \frac{i}{2} [\gamma_\mu \gamma_\nu - \gamma_\nu \gamma_\mu] \\ &= 0 \text{ if } \mu = \nu \\ &= i \gamma_0 \gamma_\mu \gamma_\nu \text{ if } \mu \neq \nu \end{aligned} \quad (2.3)$$

Using $\{\gamma_\mu, \gamma_\nu\} = 0$, we have,

$$\begin{aligned} i \gamma_0 \gamma_\mu \gamma_\nu &= i \gamma_0 [\gamma_0 \gamma_i + \gamma_i \gamma_\nu]_{(i \neq \nu)} \\ &= i \gamma_i + i \gamma_0 \gamma_i \gamma_\nu \\ &= i \gamma_i + i \alpha_i \gamma_\nu \\ &= i (\gamma_i + \alpha_i \gamma_\nu) \end{aligned} \quad (2.4)$$

Substituting the expression for $\gamma_0\sigma_{\mu\nu}$ from Eq. (2.4) in Eq. (2.2),

$$H_{\text{EDM}} = \frac{iC_T G_F}{\sqrt{2}} \left[i \Psi_N^\dagger (\gamma_i + \alpha_i \gamma_\nu)_{(i \neq \nu)} \Psi_N \right] \left[\bar{\Psi}_e \gamma^5 \sigma_{\mu\nu} \Psi_e \right] \quad (2.5)$$

Consider the second term of Eq. (2.5),

$$\begin{aligned} \bar{\Psi}_e \gamma^5 \sigma_{\mu\nu} \Psi_e &= \Psi_e^\dagger \gamma_0 \gamma_5 (i \gamma_\mu \gamma_\nu) \Psi_e \\ &= i \Psi_e^\dagger \gamma_0 \gamma_5 \gamma_\mu \gamma_\nu \Psi_e \\ &= -i \Psi_e^\dagger \gamma_5 \gamma_0 \gamma_\mu \gamma_\nu \Psi_e \\ &= -i \Psi_e^\dagger \gamma_5 (\gamma_i + \alpha_i \gamma_\nu \Psi_e) \end{aligned} \quad (2.6)$$

where $[\nu = 0, \alpha_i \gamma_0 = -\gamma_0 \alpha_i = -\gamma_0 \gamma_0 \gamma_i = -\gamma_i]$ Now, Eq. (2.5) becomes,

$$\begin{aligned} H_{\text{EDM}} &= \frac{iC_T G_F}{\sqrt{2}} \left[\Psi_N^\dagger (\gamma_i + \alpha_i \gamma_\nu)_{(i \neq \nu)} \Psi_N \right] \left[\Psi_e^\dagger \gamma_5 (\gamma_i + \alpha_i \gamma_\nu) \Psi_e \right] \\ &= \frac{iC_T G_F}{\sqrt{2}} \left[\Psi_N^\dagger (\gamma_i + \alpha_i \gamma_0 + \alpha_i \gamma_j) \Psi_N \right] \left[\Psi_e^\dagger \gamma_5 (\gamma_i + \alpha_i \gamma_0 + \alpha_i \gamma_j) \Psi_e \right] \\ &= \frac{iC_T G_F}{\sqrt{2}} \left[\Psi_N^\dagger \alpha_i \gamma_j \Psi_N \right] \left[\Psi_e^\dagger \gamma_5 \alpha_i \gamma_j \Psi_e \right] \\ &= \frac{iC_T G_F}{\sqrt{2}} \left[\Psi_N^\dagger \beta \gamma_i \gamma_j \Psi_N \right] \left[\Psi_e^\dagger \gamma_5 \beta \gamma_i \gamma_j \Psi_e \right] \\ &= \frac{iC_T G_F}{\sqrt{2}} \left[\Psi_N^\dagger \alpha_i \beta \alpha_j \Psi_N \right] \left[\Psi_e^\dagger \gamma_5 \alpha_i \beta \alpha_j \Psi_e \right] \\ &= \frac{iC_T G_F}{\sqrt{2}} \left[\Psi_N^\dagger \beta \alpha_i \alpha_j \Psi_N \right] \left[\Psi_e^\dagger \gamma_5 \beta \alpha_i \alpha_j \Psi_e \right] \end{aligned} \quad (2.7)$$

Consider

$$\begin{aligned} \alpha_i \alpha_j &= \begin{pmatrix} 0 & \sigma_i \\ \sigma_i & 0 \end{pmatrix} \times \begin{pmatrix} 0 & \sigma_j \\ \sigma_j & 0 \end{pmatrix} \\ &= \begin{pmatrix} \sigma_i \sigma_j & 0 \\ 0 & \sigma_i \sigma_j \end{pmatrix} \\ &= \sigma_i \sigma_j \mathbf{I} \end{aligned} \quad (2.8)$$

where \mathbf{I} is the identity matrix and σ_i are the Pauli spin matrices. Consider,

$$\begin{aligned}
 \gamma^5 \alpha_k &= \begin{pmatrix} 0 & -I \\ -I & 0 \end{pmatrix} \times \begin{pmatrix} 0 & \sigma_k \\ \sigma_k & 0 \end{pmatrix} \\
 &= \begin{pmatrix} -\sigma_k & 0 \\ 0 & -\sigma_k \end{pmatrix} \\
 &= -\begin{pmatrix} \sigma_k & 0 \\ 0 & \sigma_k \end{pmatrix} \\
 &= i \epsilon_{ijk} \gamma^5 \alpha^k \\
 &= i (2 \mathbf{I})
 \end{aligned} \tag{2.9}$$

Treating the nucleus nonrelativistically,

$$\begin{aligned}
 H_{\text{EDM}} &= \frac{i C_T G_F}{\sqrt{2}} [2 \mathbf{I}] [\Psi_e^\dagger \gamma^5 \beta \gamma^5 \alpha_k \Psi_e] \rho_N(r) \\
 &= \frac{2i C_T G_F \sqrt{2}}{2} \beta \alpha \mathbf{I} \rho_N(r) \\
 &= (i C_T G_F) (\sqrt{2}) (\beta \alpha \cdot \mathbf{I}) \rho_N(r)
 \end{aligned} \tag{2.10}$$

For an N-electron system, the above equation becomes,

$$H_{\text{EDM}} = (i C_T G_F) (\sqrt{2}) \sum_i (\gamma_i \cdot \mathbf{I}) \rho_N(r) \tag{2.11}$$

Note that the nuclear density $\rho_N(r)$ is proportional to the atomic number Z . The product of the Dirac matrices, (β & α) is an off-diagonal matrix, hence the matrix element of the H_{EDM} between the spinors which are proportional to \sqrt{Z} , and the dependence of the β matrix on Z , finally results in the scaling of the enhancement factor (the ratio $d_{\text{atom}}/C_{\text{ptv}}$, C_{ptv} is the P and T violating coupling constant) as $^2 Z^3$. This suggests that heavy atoms are preferred candidates for EDM experiments.

2.2 Atomic EDMs Arising from the Nuclear Schiff Moment

According to Schiff's theorem [21], the EDM of a point like nucleus is completely screened by the atomic electrons and hence it cannot be measured [22]. If a set of charged particles

²See Appendix D for H_{EDM} matrix elements

with EDMs, are in equilibrium under their mutual electrostatic forces, the first order correction to the energy due to the interaction of EDM with external electric field is zero. Consider an atom as a set of quantum mechanical charged particles, placed in an external electric field. The atom gets polarized and hence this induced charge distribution produces an internal field to cancel the external electric field. Hence, there can be no net force on the atom or the nucleus. This cancellation of the internal and external fields is exact for a point nucleus, but not for a finite one. The $s_{1/2}$ and the $p_{1/2}$ electrons have nonzero densities inside the nucleus. The nuclear Schiff moment arises due to the P and T odd nuclear interactions. The interaction of this P and T odd potential with the electron is responsible for the mixing of the opposite parity atomic wavefunctions and gives rise to an atomic EDM.

The electrostatic potential produced by the Schiff moment is of the form [15]

$$\Phi_{\text{SM}}(\vec{R}) = 4\pi\vec{S} \cdot \vec{\nabla}\delta(\vec{R})$$

for nonrelativistic electrons, where \vec{R} is the electron coordinate, \vec{S} is the Schiff moment operator and $\delta(\vec{R})$ is the Dirac-delta function. Now the contact interaction $-e\Phi_{\text{SM}}$ mixes the s and $p_{1/2}$ orbitals and produces EDMs in atoms. Using integration by parts and property of Dirac delta function, the matrix element between the s and $p_{1/2}$ atomic states is given by

$$\left\langle S \left| -e\Phi_{\text{SM}} \right| P \right\rangle = 4\pi e\vec{S} \cdot (\nabla\Psi_s^\dagger\Psi_p)_{R=0} = \text{constant}$$

is finite. The general P , T odd electrostatic potential inside the nucleus, is derived by [23] and a detailed derivation is presented in the Appendix F. A more rigorous expression for the nuclear potential arising from the nuclear Schiff moment is given by [23]:

$$\Phi_{\text{SM}}(\vec{R}) = -3\frac{\vec{S} \cdot \vec{R}}{B} \rho(R) \tag{2.12}$$

where $B = \int R^4\rho(R)dR$. The Hamiltonian of the interaction of electrons with this potential is

$$H_{\text{SM}} = 3e\frac{\vec{S} \cdot \vec{R}}{B} \rho(R) \tag{2.13}$$

If $\rho(R)$ is considered as the normalized density function, which is 1 for $R < R_N - \delta$ and $R > R_N + \delta$, where R_N is the nuclear radius, then the dimension of B is L^5 . Substituting in Eq. (2.13), we obtain the dimension of S as QL^3 . If $\rho(R)$ is considered as the usual nuclear density (dimension L^{-3}), then the dimension of B becomes $= L^4 \times QL^{-3} \times L = QL^2$. Substituting the dimensions of all quantities in Eq. (2.13), the dimension of S now becomes $= \frac{Q^2}{L} \times \frac{L^3}{Q} \times \frac{L^2}{L} = Q L^3$. Further, considering the quantization direction as \hat{z} , the Eq. (2.13) can be reduced to

$$H_{\text{SM}} = 15 \frac{S z}{R_N^5} e$$

We retain the quantity $\rho(R)$ throughout our calculation. Hence, we use

$$\begin{aligned} \Phi_{\text{SM}}(\vec{R}) &= -3 \frac{\vec{S} \cdot \vec{R}}{B} \rho(R) \\ &= -3 \frac{S R \cos \theta}{B} \rho(R) \end{aligned}$$

in spherical polar coordinates. The matrix elements of H_{SM} in terms of the single particle orbitals are given by³,

$$\begin{aligned} \left\langle \Phi_{ks_{1/2}} \left| H_{\text{SM}} \right| \Phi_{mp_{1/2}} \right\rangle &= (3 S e) \left(-\frac{1}{3} \right) \\ &\int_0^\infty \left[P_a(r) P_b(r) + Q_a(r) Q_b(r) \right] \frac{\rho(R)}{B} R dR \end{aligned} \quad (2.14)$$

The matrix element $\langle \Phi_{mp_{1/2}} | H_{\text{SM}} | \Phi_{ks_{1/2}} \rangle$ can be derived in a similar way and is found to be exactly the same as Eq. (2.14).

³See AppendixE for derivation

Chapter 3

Coupled Cluster Theory and its Application to Atomic EDMs

Calculation of physical properties of many-body quantum systems primarily involves the calculation of many-body wavefunctions. The accuracy of such a calculation hence, depends upon the accuracy of the many-body wavefunctions. Consider an atomic system composed of N particles. Let $|\Psi_0\rangle$ be the ground state exact wavefunction of the system and E be its total exact energy. The reference state of a system corresponds to the ground state configuration of the system. The exact state and the exact energy can be determined starting from the reference state of the physical system, constructed from the single particle wavefunctions of the N constituents. The best choice of a many-particle reference state is the Slater determinant, $|\Phi_0\rangle$. For an atom, the Slater determinant describes the Fermi vacuum (core) state, constructed from the set of occupied orbitals. These single particle orbitals are solutions of the Hartree-Fock equation in the independent particle model and satisfy the Pauli's exclusion principle, described in detail in [24]. A more realistic picture is that the particles are not moving independently due to their mutual interactions, termed as the electron-electron correlation. Coupled-cluster (CC) theory [25, 26, 27, 28] is a way to treat these correlations systematically, in which the exact atomic state is realized as the state of the atom where all possible electron correlations to all orders in terms of exciting clusters are accounted for. The operators that describe these excitations are known as the cluster operators. It can be imagined that two particles in the occupied space interact with each other via Coulomb interaction and get excited to unoccupied space. This can be mathematically described by the action of

an operator T_2 on the reference state $|\Phi_0\rangle$, to produce a state $T_2|\Phi_0\rangle$. The new state is formed by a double excitation in the reference state giving rise to two ‘holes’ and consequently creating two ‘particles’ outside the reference state. A similar process can occur where, two pairs of particles excite themselves independently. This can be achieved by acting T_2 twice on the reference state $|\Phi_0\rangle$, with the inclusion of a statistical weighing factor of $(\frac{1}{2!})$ to avoid counting pairs twice. The resulting contribution to the exact state from the two double excitations is now $(\frac{1}{2!}) T_2^2|\Phi_0\rangle$. This process of excitation of independent pair of particles from the reference state is obtained by $(\frac{1}{m!}) T_2^m|\Phi_0\rangle$, which describes the amplitude of excitation of m independent pairs. All the double excitation amplitudes can be superposed to give the total amplitude $\sum_{m=0}^{\infty} (\frac{1}{m!}) T_2^m|\Phi_0\rangle = \exp(T_2)|\Phi_0\rangle$. Similarly, the amplitudes for the simultaneous excitation of three particles can be described by $T_3|\Phi_0\rangle$ and the total contribution of all triple excitations can be obtained by summing over all the independent triplets, $\sum_{p=0}^{\infty} (\frac{1}{p!}) T_3^p|\Phi_0\rangle$. Also, the simultaneous independent excitation of m pairs and p triplets is given by $\frac{1}{p!m!} T_2^m T_3^p|\Phi_0\rangle$. Summing over p and m , the total amplitude is given by $\exp(T_2 + T_3)|\Phi_0\rangle$. Proceeding as above, for an N electron system, all possible single, double, triple and so on to n -tuple excitations can be obtained from the wavefunction $\exp(T_1 + T_2 + T_3 + \dots + T_N)|\Phi_0\rangle$. The operator $\exp(T_1)$ produces single particle excitations and hence the total *exact* atomic wavefunction can be described by the wavefunction $|\Psi\rangle = e^{(\sum_{n=1}^N T_n)}|\Phi_0\rangle$. This is the exact atomic state in the coupled-cluster formulation and T is known as the cluster operator. Throughout the thesis we consider only the correlations giving rise to single and double excitations, to all orders and the exact atomic Hamiltonian is the approximate relativistic Dirac-

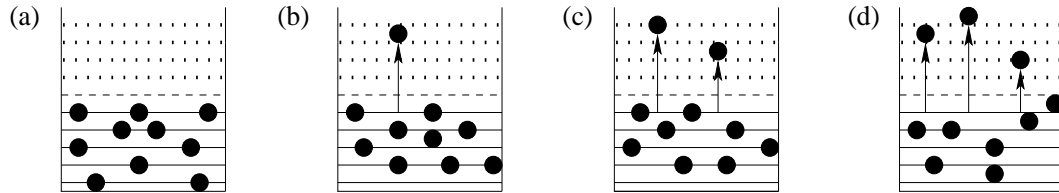


Figure 3.1: Physical realization of the coupled-cluster wavefunction - (a) represents Fermi vacuum, (b),(c),(d) represent single (T_1), double ($T_1^2/2!, T_2$) and triple ($T_1^3/3!, T_1T_2, T_3$) excitations respectively [25].

Coulomb Hamiltonian described in the next section. Also, the above formulation of the

many-body exact state is valid precisely for a closed-shell atomic system. The exact wavefunction of an atom of open-shell structure is obtained by partitioning the excitations into three parts - excitations from the core to virtual, core to valence and valence to virtual shells, described by an additional operator S . The many-body exact state now becomes, $|\Psi\rangle = e^T e^S |\Phi_0\rangle$. This thesis deals only with the coupled-cluster theory applied to closed-shell atomic systems. CC theory applied to open-shell atomic systems is explained in [29].

3.1 Coupled-Cluster Theory for Closed-Shell Systems

3.1.1 Unperturbed Coupled-Cluster Equations

The starting point of setting up the coupled-cluster equations is the relativistic atomic Hamiltonian in the Dirac-Coulomb approximation,

$$H = \sum_i^N \left[c\boldsymbol{\alpha}_i \cdot \mathbf{p}_i + \left(\beta_i - \mathbf{1} \right) c^2 + V_N(r_i) \right] + \sum_{i<j}^N \frac{1}{r_{ij}} \quad (3.1)$$

where, c is velocity of light, α and β are the Dirac matrices, $1/r_{ij}$ is the Coulomb potential energy between two electrons, in atomic units ($m_e = 1$, $|e| = 1$ and $\hbar = 1$) and $V_N(r_i)$ is the nuclear potential. In the above Hamiltonian, the rest mass energy is subtracted from the total energy eigenvalues. This is the Hamiltonian of an atomic system considering only the inter electron electrostatic interactions. The single particle equations are obtained by approximating the two-electron term in Eq. (3.1) by a central field potential $U_{\text{DF}}(i)$, known as the Dirac-Fock potential [24, 30], then

$$H_{\text{DC}} = \sum_i^N \left[c\boldsymbol{\alpha}_i \cdot \mathbf{p}_i + \left(\beta_i - \mathbf{1} \right) c^2 + V_N(r_i) + U_{\text{DF}}(i) \right] + V_{\text{es}} \quad (3.2)$$

Define the residual Coulomb interaction V_{es} as,

$$V_{\text{es}} = \left(\sum_{i<j}^N \frac{1}{r_{ij}} - U_{\text{DF}}(i) \right)$$

The above Hamiltonian in Eq. (3.2) can be rewritten as,

$$H_{\text{DC}} = H_0 + V_{\text{es}}$$

where

$$H_0 = \sum_{i=1}^N h_0(i)$$

and

$$V_{\text{es}} = - \sum_{i=1}^N u_i + \sum_{i<j}^N r_{ij}^{-1}$$

The non-central (or) correlation effects are included by treating V_{es} as a perturbation. The single electron wavefunctions satisfy the relativistic many-particle Schrödinger equation [24, 30]

$$\left[c\boldsymbol{\alpha}_i \cdot \mathbf{p}_i + (\beta_i - 1)c^2 + V_N(r_i) + U_{\text{DF}}(i) \right] \left| \psi_a \right\rangle = \epsilon_a \left| \psi_a \right\rangle \quad (3.3)$$

where $|\psi_a\rangle$ are the single electron wavefunctions in the two component form,

$$\left\langle \mathbf{r} \left| \psi_a \right\rangle = \frac{1}{r} \begin{pmatrix} P_{n_a \kappa_a}(r) \chi_{\kappa_a m_a}(\theta, \phi) \\ i Q_{n_a \kappa_a}(r) \chi_{-\kappa_a m_a}(\theta, \phi) \end{pmatrix} \quad (3.4)$$

where $P_{n_a \kappa_a}(r)$ and $Q_{n_a \kappa_a}(r)$ are the large and small components of the single electron wavefunction respectively and the angular part is a product of the orbital and spin angular momenta of the electrons, given by

$$\chi_{\kappa_a m_a}(\theta, \phi) = \sum_{m_a^l, m_a^s} \left| l_a m_a^l \right\rangle \times \left| s_a m_a^s \right\rangle \left\langle l_a, m_a^l, s_a, m_a^s \left| J_a, M_a \right\rangle \right.$$

where l_a and s_a are the orbital and the spin angular momenta of the electron respectively, angular momenta, m_a^l , m_a^s are their projections, J_a , M_a , the total angular momentum and its projection. Here, a denotes the quantum numbers needed to specify the electron. The quantity $\langle l_a, m_a^l, s_a, m_a^s | J_a, M_a \rangle$ are the Clebsch-Gordan coefficients. The orbital part are the spherical harmonics and the terms involving spin are the Dirac spinors. These single electron wavefunctions are simultaneous eigen functions of J , J_z , L and S .

κ , the relativistic quantum number, is the eigenvalue of the operator $K = -1 - 2\mathbf{L} \cdot \mathbf{S}$, given in terms of j and l , $\kappa = -\left(j + \frac{1}{2}\right) a$, where $a = +1$ for $l = \left(j - \frac{1}{2}\right)$ and $a = -1$ for $l = \left(j + \frac{1}{2}\right)$ [31, 32]. The many-electron wavefunction of an atomic system with the Hamiltonian given in Eq. (3.2), is the Slater determinant obtained by constructing the linear combinations of the single particle wavefunctions respecting the Pauli's exclusion principle, and is given by

$$\left| \Psi \right\rangle = \sqrt{\frac{1}{N!}} \begin{vmatrix} \psi_a(1) & \psi_a(2) & \cdots & \psi_a(N) \\ \psi_b(1) & \psi_b(2) & \cdots & \psi_b(N) \\ \cdots & \cdots & \cdots & \cdots \\ \psi_n(1) & \psi_n(2) & \cdots & \psi_n(N) \end{vmatrix} \quad (3.5)$$

where the coefficient $\sqrt{1/N!}$ is the normalization constant, and a single particle orbital $\psi_i(j)$ represents the wavefunction of electron with the space coordinate j and specified by the set of quantum numbers i . Throughout the thesis, we denote a, b, c, \dots for occupied orbitals (holes) and p, q, r, s, \dots for unoccupied orbitals (particles). The challenging problem in atomic many-body theory is to solve the Hamiltonian Eq. (3.2) with V_{es} as perturbation to all orders. Solving Eq. (3.3) variationally by minimizing the energy functional with respect to the form of orbitals and by imposing orthonormality condition [24], the Hartree-Fock equation is obtained as

$$\left(h^0 + g^0 - \epsilon_a^0 \right) \left| \psi_a^0 \right\rangle = 0; \quad (3.6)$$

where h^0 and g^0 are the single and two-particle operators respectively in Eq. (3.2), together termed as the Fock operator f^0 . The subscript 0 refers to the equation without the EDM perturbation. The operator g^0 is the central field approximation of the two-electron Coulomb interaction

$$g^0 \left| \psi_a^0 \right\rangle = \sum_{b=1}^{N_{\text{occ}}} \left[\left\langle \psi_b^0 \left| v \right| \psi_b^0 \right\rangle \left| \psi_a^0 \right\rangle - \left\langle \psi_b^0 \left| v \right| \psi_a^0 \right\rangle \left| \psi_b^0 \right\rangle \right]$$

where $v = 1/r_{ij} = 1/r_{12}$ is the two-electron operator and the sum runs over all occupied orbitals. Substituting for g^0 , the Eq. (3.6) becomes

$$h^0 \left| \psi_a^0 \right\rangle + \sum_{b=1}^{N_{\text{occ}}} \left[\left\langle \psi_b^0 \left| v \right| \psi_b^0 \right\rangle \left| \psi_a^0 \right\rangle - \left\langle \psi_b^0 \left| v \right| \psi_a^0 \right\rangle \left| \psi_b^0 \right\rangle \right] - \epsilon_a^0 \left| \psi_a^0 \right\rangle = 0 \quad (3.7)$$

Eq. (3.7) is the Hartree-Fock equation. The perturbed equations are obtained by introducing the P and T violating tensor-pseudotensor interaction Hamiltonian in addition to the residual Coulomb interaction. The wavefunctions and the Hamiltonian are perturbed by the H_{EDM} interaction thereby giving the perturbed Hartree-Fock equations demonstrated in the next few pages.

The many-body Schrödinger equation of the Dirac-Coulomb Hamiltonian for an atomic system, in a state $|\Psi\rangle$ in the CC formalism is given by

$$H|\Psi\rangle = E|\Psi\rangle \Rightarrow He^{T^{(0)}}|\Phi_0\rangle = Ee^{T^{(0)}}|\Phi_0\rangle$$

where the superscript on $T^{(0)}$ is used to distinguish the unperturbed cluster operator from the the EDM perturbed cluster operator, introduced in the subsequent sections of this thesis. Operating from left side by $e^{-T^{(0)}}$

$$e^{-T^{(0)}}He^{T^{(0)}}|\Phi_0\rangle = E|\Phi_0\rangle$$

Expressing H in normal ordered form, $H = H_N + E_{\text{DF}}$, where $E_{\text{DF}} = \langle\Phi_0|H|\Phi_0\rangle - \langle\Phi_0|H_N|\Phi_0\rangle$ is the Dirac-Fock energy. Then,

$$e^{-T^{(0)}}\left(H_N + E_{\text{DF}}\right)e^{T^{(0)}}|\Phi_0\rangle = E|\Phi_0\rangle \quad (3.8)$$

Projecting Eq. (3.8) with singly and doubly excited states $\langle\Phi_a^r|$ and $\langle\Phi_{ab}^{rs}|$ respectively and restricting the cluster operator $T^{(0)}$ to $T^{(0)} = T_1^{(0)} + T_2^{(0)}$, the single and double excitation cluster amplitude equations are obtained. The second quantized form of the cluster operators is given by

$$\begin{aligned} T_1^{(0)} &= \sum_{a,p} a_p^\dagger a_a \mathbf{t}_a^p |\Phi_0\rangle \\ T_2^{(0)} &= \sum_{a,p,b,q} \frac{1}{2!} a_p^\dagger a_q^\dagger a_b a_a \mathbf{t}_{ab}^{pq} |\Phi_0\rangle \end{aligned} \quad (3.9)$$

and

$$\begin{aligned} \sum_{i=1}^N h_0(i) &= \sum_i a_i^\dagger a_i \epsilon_i \\ V &= - \sum_{ij} a_i^\dagger a_j \langle i|u|j\rangle + \frac{1}{2} \sum_{ijkl} a_i^\dagger a_j^\dagger a_l a_k \langle ij|r_{ij}^{-1}|kl\rangle \end{aligned} \quad (3.10)$$

Each term in the above equations can be represented diagrammatically described in detail in the later sections and in this thesis all subsequent calculations are performed using the diagrammatic approach. Expanding $\left(e^{-T^{(0)}} H_N e^{T^{(0)}}\right)$ using Campbell-Baker-Hausdorff expansion,

$$\begin{aligned}
 e^{-T^{(0)}} H_N e^{T^{(0)}} &= H_N + \left[H_N, T^{(0)} \right] + \frac{1}{2!} \left[\left[H_N, T^{(0)} \right], T^{(0)} \right] + \frac{1}{3!} \left[\left[\left[H_N, T^{(0)} \right], T^{(0)} \right], T^{(0)} \right] \\
 &\quad + \frac{1}{4!} \left[\left[\left[\left[H_N, T^{(0)} \right], T^{(0)} \right], T^{(0)} \right], T^{(0)} \right] \tag{3.11}
 \end{aligned}$$

Examining the Eq. (3.11), the first term H_N is a *connected*¹ term as it contains only one vertex of H_N . The second term $[H_N, T^{(0)}]$ is also *connected* using $[H_N, T^{(0)}] = \left\{ \overline{H_N T^{(0)}} \right\} - \left\{ \overline{T^{(0)} H_N} \right\}$, where the curly brackets refer to normal ordering². Considering a general term, $[H_N, T^{(0)}]^{(n)} = \left[[H_N, T^{(0)}]^{(n-1)}, T^{(0)} \right]$. Any n th commutator would consist of all *connected* terms, provided the $(n-1)$ th commutator is *connected*. Hence the term $\left(e^{-T^{(0)}} H_N e^{T^{(0)}}\right)$ is built only from *connected* terms. Using $\left\{ \overline{T^{(0)} H_N} \right\} = 0$, we get,

$$\begin{aligned}
 e^{-T^{(0)}} H_N e^{T^{(0)}} &= H_N + \left\{ \overline{H_N T^{(0)}} \right\} + \left\{ \overline{H_N T^{(0)} T^{(0)}} \right\} + \left\{ \overline{H_N T^{(0)} T^{(0)} T^{(0)}} \right\} + \\
 &\quad \left\{ \overline{H_N T^{(0)} T^{(0)} T^{(0)} T^{(0)}} \right\} \tag{3.12} \\
 &= \left(H_N e^{T^{(0)}} \right)_c
 \end{aligned}$$

where, the curly brackets in the above equation represent normal ordering of the operators within the brackets, the symbol above the operators represents *contraction* and the subscript c represents completely *connected* terms. Two operators, under this symbol

¹For any two objects H_N and $T^{(0)}$, we have $\overline{H_N T^{(0)}} = H_N T^{(0)} - \left\{ \overline{H_N T^{(0)}} \right\}$

²Two operators A and B in second quantization form are said to be normal ordered if the creation operator associated with a core (a_{core}^\dagger) or the annihilation operator associated with the virtual (a_{virtual}) appears on the right side of the rest of the operators in the product AB.

are said to be *contracted* if their respective creation and annihilation operators *contract* with each other, always in pairs of one creation and one annihilation operator, in all possible ways. Substituting the above in Eq. (3.8) and projecting from left hand side by singly and doubly excited determinantal states,

$$\left\langle \Phi_a^r \left| \left\{ \left(\overline{H_N e^{T^{(0)}}} \right)_c \right\} \right| \Phi_0 \right\rangle = 0 \quad (3.13)$$

$$\left\langle \Phi_{ab}^{rs} \left| \left\{ \left(\overline{H_N e^{T^{(0)}}} \right)_c \right\} \right| \Phi_0 \right\rangle = 0 \quad (3.14)$$

Expanding $\left(\overline{H_N e^{T^{(0)}}} \right)_c$,

$$\begin{aligned} & \left\langle \Phi_a^r \left| \left\{ \overline{H_N T^{(0)}} + \overline{H_N T^{(0)} T^{(0)}} + \overline{H_N T^{(0)} T^{(0)} T^{(0)}} + \overline{H_N T^{(0)} T^{(0)} T^{(0)} T^{(0)}} \right\} \right| \Phi_0 \right\rangle \\ & \quad = - \left\langle \Phi_a^r \left| H_N \right| \Phi_0 \right\rangle \\ & \left\langle \Phi_{ab}^{rs} \left| \left\{ \overline{H_N T^{(0)}} + \overline{H_N T^{(0)} T^{(0)}} + \overline{H_N T^{(0)} T^{(0)} T^{(0)}} + \overline{H_N T^{(0)} T^{(0)} T^{(0)} T^{(0)}} \right\} \right| \Phi_0 \right\rangle = \\ & \quad - \left\langle \Phi_{ab}^{rs} \left| H_N \right| \Phi_0 \right\rangle \end{aligned} \quad (3.15)$$

Note that the maximum number of $T^{(0)}$ operators contributing to the *contraction* in the above equation is four, due to the two-body nature of H_N . Since we use the approximation $T^{(0)} = T_1^{(0)} + T_2^{(0)}$, Eq. (3.15) can be written in the matrix form as,

$$\begin{pmatrix} H_{11}(T_1^{(0)}, T_2^{(0)}) & H_{12}(T_1^{(0)}, T_2^{(0)}) \\ H_{21}(T_1^{(0)}, T_2^{(0)}) & H_{22}(T_1^{(0)}, T_2^{(0)}) \end{pmatrix} \begin{pmatrix} T_1^{(0)} \\ T_2^{(0)} \end{pmatrix} = \begin{pmatrix} -H_{10} \\ -H_{20} \end{pmatrix} \quad (3.16)$$

where the terms on the right hand side are independent of $T_1^{(0)}$ and $T_2^{(0)}$ and the dressed Hamiltonian matrix elements on the left hand side are dependent on the $T^{(0)}$ amplitudes. In the above equation, the size of the column vector is N , which is equal to the sum of the single and the double excitations and the matrix on the left hand side is of dimension $N \times N$.

Combining the above equations,

$$\mathbf{A}(T^{(0)})T^{(0)} = \mathbf{C} \quad (3.17)$$

where A is dependent on $T^{(0)}$ and C is independent of $T^{(0)}$. This is a nonlinear matrix equation which should be solved in a self-consistent way to obtain the unperturbed cluster amplitudes.

3.1.2 EDM Perturbed Coupled-Cluster Equations

The H_{EDM} operator is a single-particle EDM operator and has the same diagrammatic representation as the electric dipole operator and the one-body part of V (Eq. (3.10)). Consider the H_{EDM} perturbed Schrödinger equation for the atomic Hamiltonian H .

$$\left(\tilde{H}\right)|\Psi\rangle = \left(E\right)|\Psi\rangle \quad (3.18)$$

where $\tilde{H} = H + \lambda H_{\text{EDM}}$ and $|\Psi\rangle = e^T|\Phi_0\rangle = e^{T^{(0)} + \lambda T^{(1)}}|\Phi_0\rangle$. Taking terms upto one order in λ ,

$$\tilde{H}e^{T^{(0)}}\left(1 + \lambda T^{(1)}\right)|\Phi_0\rangle = Ee^{T^{(0)}}\left(1 + \lambda T^{(1)}\right)|\Phi_0\rangle$$

Substituting for \tilde{H} in the above equation,

$$\left(H + \lambda H_{\text{EDM}}\right)e^{T^{(0)}}\left(1 + \lambda T^{(1)}\right)|\Phi_0\rangle = Ee^{T^{(0)}}\left(1 + \lambda T^{(1)}\right)|\Phi_0\rangle$$

Comparing λ^0 and λ^1 terms on both sides,

$$\left(He^{T^{(0)}}\right)|\Phi_0\rangle = Ee^{T^{(0)}}|\Phi_0\rangle \quad (3.19)$$

and

$$\left(He^{T^{(0)}}T^{(1)} + H_{\text{EDM}}e^{T^{(0)}}\right)|\Phi_0\rangle = Ee^{T^{(0)}}T^{(1)}|\Phi_0\rangle \quad (3.20)$$

Multiplying Eq. (3.19) by $T^{(1)}$ on both sides,

$$T^{(1)}He^{T^{(0)}}|\Phi_0\rangle = ET^{(1)}e^{T^{(0)}}|\Phi_0\rangle \quad (3.21)$$

Using the normal ordered form of $H = H_N + E_{\text{DF}}$, Eq. (3.20) becomes,

$$\left(H_N e^{T^{(0)}} T^{(1)} + H_{\text{EDM}} e^{T^{(0)}} \right) \left| \Phi_0 \right\rangle = \left(\Delta E_{\text{corr}} e^{T^{(0)}} T^{(1)} \right) \left| \Phi_0 \right\rangle \quad (3.22)$$

since $T^{(0)}$ and $T^{(1)}$ commute and $E_{\text{corr}} = E - E_{\text{DF}}$. Operate Eq. (3.22) on both sides by $e^{-T^{(0)}}$,

$$\left(\overline{H}_N T^{(1)} + \overline{H}_{\text{EDM}} \right) \left| \Phi_0 \right\rangle = \Delta E_{\text{corr}} T^{(1)} \left| \Phi_0 \right\rangle \quad (3.23)$$

Operating by $e^{-T^{(0)}}$ on Eq. (3.21) and converting H into normal form,

$$T^{(1)} \overline{H}_N \left| \Phi_0 \right\rangle = \Delta E_{\text{corr}} T^{(1)} \left| \Phi_0 \right\rangle \quad (3.24)$$

subtracting Eq. (3.23) from Eq. (3.24),

$$\left[\overline{H}_N, T^{(1)} \right] \left| \Phi_0 \right\rangle = -\overline{H}_{\text{EDM}} \left| \Phi_0 \right\rangle \quad (3.25)$$

where $\overline{O} = e^{-T^{(0)}} \hat{O} e^{T^{(0)}}$ where \hat{O} is any operator. The equation for the coupled-cluster perturbed singles and doubles can be derived from the basic equation, Eq. (3.25) by projecting on both sides of the equation with singly and doubly excited determinantal states.

$$\begin{aligned} \left\langle \Phi_a^r \left[\overline{H}_N, T^{(1)} \right] \left| \Phi_0 \right\rangle &= -\left\langle \Phi_a^r \left| \overline{H}_{\text{EDM}} \left| \Phi_0 \right\rangle \right. \right\rangle \\ \left\langle \Phi_{ab}^{rs} \left[\overline{H}_N, T^{(1)} \right] \left| \Phi_0 \right\rangle &= -\left\langle \Phi_{ab}^{rs} \left| \overline{H}_{\text{EDM}} \left| \Phi_0 \right\rangle \right. \right\rangle \end{aligned} \quad (3.26)$$

which are equivalent to

$$\begin{aligned} \left\langle \Phi_a^r \left\{ \overline{H}_N T^{(1)} \right\} \left| \Phi_0 \right\rangle &= -\left\langle \Phi_a^r \left| \overline{H}_{\text{EDM}} \left| \Phi_0 \right\rangle \right. \right\rangle \\ \left\langle \Phi_{ab}^{rs} \left\{ \overline{H}_N T^{(1)} \right\} \left| \Phi_0 \right\rangle &= -\left\langle \Phi_{ab}^{rs} \left| \overline{H}_{\text{EDM}} \left| \Phi_0 \right\rangle \right. \right\rangle \end{aligned} \quad (3.27)$$

These equations are the H_{EDM} perturbed coupled-cluster equations and are termed as CCEDM equations in this thesis. Further expanding $T^{(1)}$, these equations can be recast in the form of a system of linear matrix equations,

$$\begin{aligned} H_{11} T_1^{(1)} + H_{12} T_2^{(1)} &= -H_{10} \\ H_{21} T_1^{(1)} + H_{22} T_2^{(1)} &= -H_{20} \end{aligned} \quad (3.28)$$

where H_{11} , H_{12} , H_{21} , H_{22} are dressed Hamiltonian matrix elements and H_{10} and H_{20} are the dressed H_{EDM} matrix elements. The above equation can be expressed more compactly as $\mathbf{A}T^{(1)} = \mathbf{C}$, where the matrices \mathbf{A} and \mathbf{C} are independent of the $T^{(1)}$ amplitudes. The Eq. (3.28) is classified into four blocks, T1-T1, T1-T2, T2-T1 and T2-T2 ; where T1-T1 and T1-T2 contain the diagrams contributing to the $T_1^{(1)}$ equation through singles and doubles respectively, and T2-T1 and T2-T2 contain the diagrams contributing to the $T_2^{(1)}$ equation through singles and doubles respectively. The diagrams contributing to the CCEDM equations with zero orders in $T^{(0)}$ are shown in Fig. 3.3, 3.4, 3.5, 3.6. The diagrams 3.7 and 3.8 represent the terms present on the right hand side of the CCEDM equations. The diagrammatic representation of the operators is shown in Fig. 3.2.

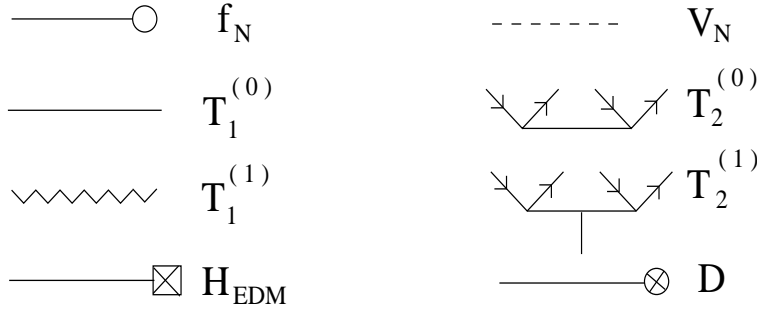


Figure 3.2: Notation. f_N and V_N denote the one- and two- electron parts of H_N respectively.

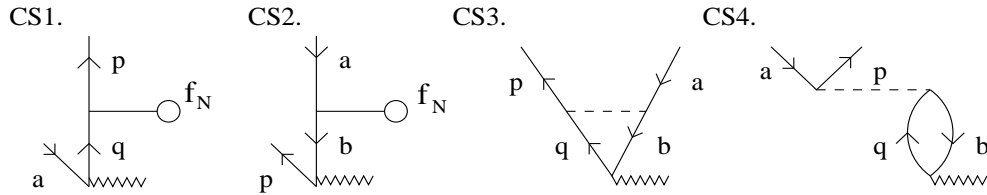


Figure 3.3: Diagrams contributing to T1-T1 block.

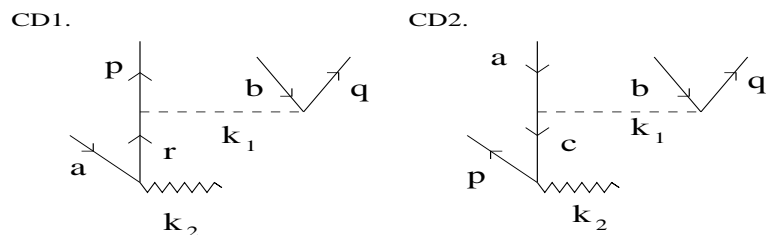


Figure 3.4: Diagrams contributing to T2-T1 block

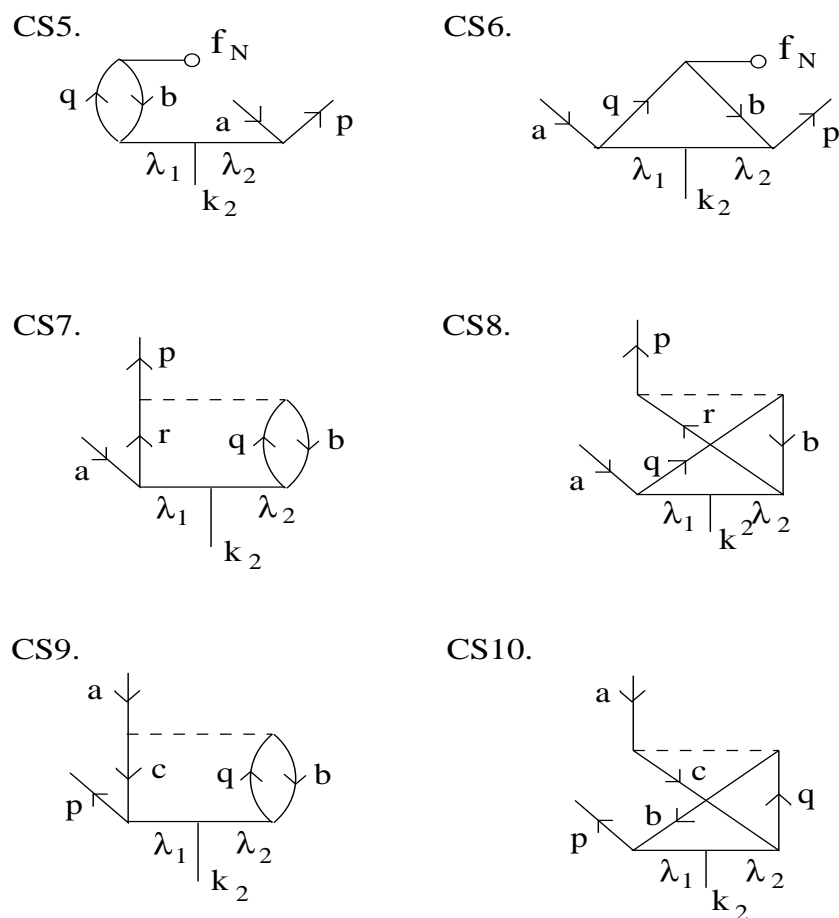


Figure 3.5: Diagrams contributing to T1-T2 block

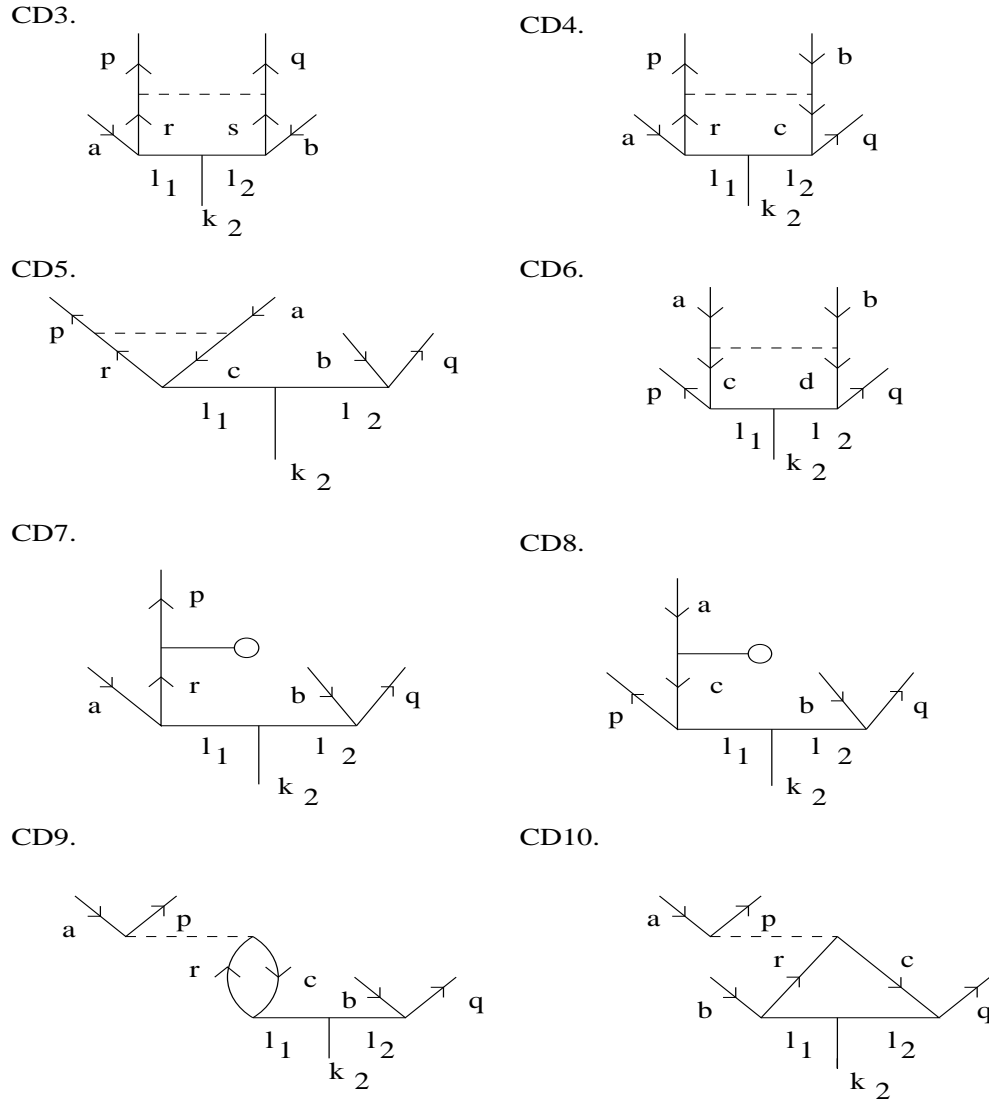


Figure 3.6: Diagrams contributing to T2-T2 block

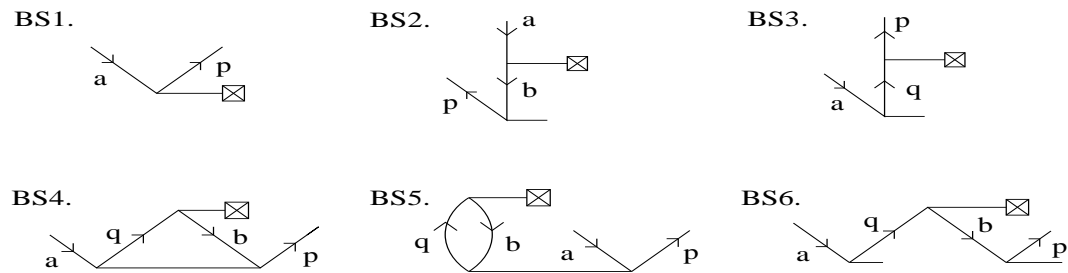


Figure 3.7: Diagrams contributing to the right hand side of the singles CCEDM equation.

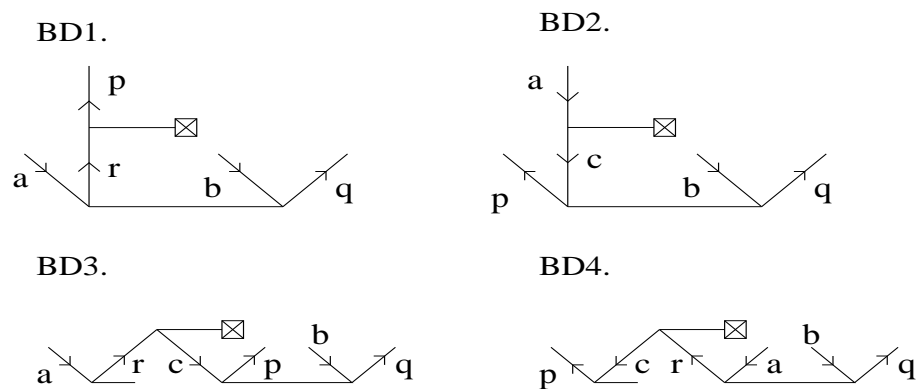


Figure 3.8: The diagrams contributing to the right hand side of the doubles CCEDM equation.

3.1.3 Reduction of the Perturbed Coupled-Cluster Equations to Unperturbed Coupled-Cluster Equations

In the absence of an external perturbation such as the EDM interaction, the EDM perturbed CC equations given by Eq. (3.27) can be reduced to the unperturbed CC equations given by Eq. (3.14). Hence, the unperturbed cluster amplitudes assume the role of the perturbed cluster amplitudes and the CC equation can be solved to obtain the unperturbed cluster amplitudes. This exercise can serve as a good check for the CCEDM code. This can be implemented at two stages — linear and nonlinear in the $T^{(0)}$ operator. The calculation of the unperturbed amplitudes from CCEDM equations in the limit $H_{\text{EDM}} \rightarrow 0$ at the linear level is discussed in the next few pages. Consider the CC equations (Eq. (3.14)) with upto one order in $T^{(0)}$ (linearised CC equations),

$$\left\langle \Phi_a^r \left| \left\{ H_N + \overline{H_N T^{(0)}} \right\} \right| \Phi_0 \right\rangle = 0 \quad (3.29)$$

$$\left\langle \Phi_{ab}^{rs} \left| \left\{ H_N + \overline{H_N T^{(0)}} \right\} \right| \Phi_0 \right\rangle = 0 \quad (3.30)$$

(Note that in the present section, we have renamed T in Eq. (3.14) as $T^{(0)}$.) Since we use the approximation $T^{(0)} = T_1^{(0)} + T_2^{(0)}$,

$$\left\langle \Phi_a^r \left| H_N \right| \Phi_0 \right\rangle + \left\langle \Phi_a^r \left| \left\{ \overline{H_N T_1^{(0)}} + \overline{H_N T_2^{(0)}} \right\} \right| \Phi_0 \right\rangle = 0 \quad (3.31)$$

$$\left\langle \Phi_{ab}^{rs} \left| H_N \right| \Phi_0 \right\rangle + \left\langle \Phi_{ab}^{rs} \left| \left\{ \overline{H_N T_1^{(0)}} + \overline{H_N T_2^{(0)}} \right\} \right| \Phi_0 \right\rangle = 0 \quad (3.32)$$

The above equations can be written in the form,

$$H_{11}T_1^{(0)} + H_{12}T_2^{(0)} = -H_{10} \quad (3.33)$$

$$H_{21}T_1^{(0)} + H_{22}T_2^{(0)} = -H_{20} \quad (3.34)$$

where the right hand side of the above equations is independent of $T^{(0)}$. The above equations can be combined to give,

$$\mathbf{A}T^{(0)} = \mathbf{C} \quad (3.35)$$

where \mathbf{A} and \mathbf{C} are independent of T . This is a linear matrix equation. Now, consider the CCEDM equations (Eq. (3.27)),

$$\left\langle \Phi^* \left| \left[\overline{H}_N, T^{(1)} \right] \right| \Phi_0 \right\rangle = - \left\langle \Phi^* \left| \overline{H}_{\text{EDM}} \right| \Phi_0 \right\rangle \quad (3.36)$$

where $|\Phi^*\rangle$ is a singly or doubly excited Slater determinant. The linearised CCEDM equations are obtained by approximating, $\overline{H}_N \approx H_N$ and $\overline{H}_{\text{EDM}} \approx H_{\text{EDM}}$. This gives for singles,

$$\left\langle \Phi_a^r \left| \left[H_N, T^{(1)} \right] \right| \Phi_0 \right\rangle = - \left\langle \Phi_a^r \left| H_{\text{EDM}} \right| \Phi_0 \right\rangle \quad (3.37)$$

where $T^{(0)}$ assume the role of of $T^{(1)}$. In the absence of the EDM perturbation, on the right hand side of the Eq. (3.37), H_{EDM} is replaced by H_N . Also, the $T^{(0)}$ amplitudes take the role of the $T^{(1)}$ amplitudes. Hence the singles equation becomes,

$$\left\langle \Phi_a^r \left| \left\{ \overline{H_N T^{(0)}} \right\} \right| \Phi_0 \right\rangle = - \left\langle \Phi_a^r \left| H_N \right| \Phi_0 \right\rangle \quad (3.38)$$

In the left hand side of the Eq. (3.38), the terms of $\{\overline{H_N T^{(0)}}\}$ contributing to the singles and linear in $T^{(0)}$ arise only from the (2-hole — 2-particle) (diagrams CS3, CS4 Fig. 3.3), (3-particle — 1-hole) (diagrams CS7, CS8 Fig. 3.5), (3-hole — 1-particle) (diagrams CS9, CS10 Fig. 3.5) and particle-particle (CS1, Fig. 3.3) and hole-hole (CS2 Fig. 3.3) form of the residual Coulomb operator. With the inclusion of only these diagrams and under the linear approximation, in the absence of the H_{EDM} perturbation, Eq. (3.38) becomes mathematically equivalent to the unperturbed CC equations, Eq. (3.32). Similar changes for the CCEDM equation for doubles gives,

$$\left\langle \Phi_{ab}^{rs} \left| \left\{ \overline{H_N T^{(0)}} \right\} \right| \Phi_0 \right\rangle = - \left\langle \Phi_{ab}^{rs} \left| H_N \right| \Phi_0 \right\rangle \quad (3.39)$$

For the doubles, the diagrams contributing to the left hand side are (4-hole) (diagram CD6 Fig. 3.6), (4-particle) (diagram CD3 Fig. 3.6), (3-particle — 1-hole) (diagrams CD1, CD2 Fig. 3.4), (2-particle — 2-hole) (diagrams CD4, CD5, CD9, CD10 Fig. 3.6) and particle-particle (CD7) and hole-hole (CD8) (Fig. 3.6). The Eq. (3.38) and Eq.

(3.39),

$$\left\langle \Phi_a^r \left| \overline{H_N T^{(0)}} \right| \Phi_0 \right\rangle = - \left\langle \Phi_a^r \left| H_N \right| \Phi_0 \right\rangle \quad (3.40)$$

$$\left\langle \Phi_{ab}^{rs} \left| \overline{H_N T^{(0)}} \right| \Phi_0 \right\rangle = - \left\langle \Phi_{ab}^{rs} \left| H_N \right| \Phi_0 \right\rangle \quad (3.41)$$

are the ‘unperturbed’ deduced from the linear CCEDM equations in the limit of $H_{\text{EDM}} \rightarrow 0$ and can be represented in terms of elements of a matrix as

$$H'_{11} T_1^{(0)} + H'_{12} T_2^{(0)} = H'_{10} \quad (3.42)$$

$$H'_{21} T_1^{(0)} + H'_{22} T_2^{(0)} = H'_{20}$$

where H'_{10} and H'_{20} are the Coulomb matrix elements on the RHS of Eq. (3.41) and (3.41) respectively and H'_{11} , H'_{12} and H'_{21} , H'_{22} represent the matrix elements on the LHS of Eq. (3.41) (3.41) respectively. These are equivalent to the coupled-cluster equations Eq. (3.34). The term $\langle \Phi_a^r | H_N | \Phi_0 \rangle = 0$ on the right hand side of Eq. (3.41), due to Brillouin’s theorem ¹. The singles equation after substituting $T^{(0)} = T_1^{(0)} + T_2^{(0)}$ becomes,

$$\left\langle \Phi_a^r \left| \overline{H_N T_1^{(0)}} + \overline{H_N T_2^{(0)}} \right| \Phi_0 \right\rangle = 0$$

For the initial guess, set the matrix elements of $T_2^{(0)} = 0$ and hence

$$\left\langle \Phi_a^r \left| \overline{H_N T_1^{(0)}} \right| \Phi_0 \right\rangle = \sum_I \left\langle \Phi_a^r \left| H_N \right| \Phi_I \right\rangle \left\langle \Phi_I \left| T_1^{(0)} \right| \Phi_0 \right\rangle = 0$$

For a given value of I , the matrix elements of $T_1^{(0)} = 0$. The initial guess values for the doubles cluster amplitudes are obtained from the doubles equation by setting $T_1^{(0)} = 0$,

$$\left\langle \Phi_{ab}^{rs} \left| \overline{H_N T_2^{(0)}} \right| \Phi_0 \right\rangle = - \left\langle \Phi_{ab}^{rs} \left| H_N \right| \Phi_0 \right\rangle \quad (3.43)$$

The matrix elements on the right hand side of Eq. (3.43) reduce to

$$\left\langle \Phi_{ab}^{rs} \left| H_N \right| \Phi_0 \right\rangle = \left\langle rs \left| v \right| ab \right\rangle - \left\langle rs \left| v \right| ba \right\rangle$$

¹This states that the Hamiltonian H_N does not connect the determinantal states which differ by a single excitation and hence there can be no first order mixing of such states

and the initial guess for $T_2^{(0)}$ becomes,

$$= - \frac{\left[\langle rs | v | ab \rangle - \langle rs | v | ba \rangle \right]}{\epsilon_a + \epsilon_b - \epsilon_p - \epsilon_q}$$

The Eq. (3.41) are then solved for the unknown $T^{(0)}$ amplitudes. Appropriate changes corresponding to the reduction of the perturbed CC equations to the unperturbed CC equations are made to the linear CCEDM program to calculate the unperturbed cluster amplitudes and the correlation energy.

3.1.4 Non-Linear EDM Perturbed Coupled-Cluster Equations

Consider the H_{EDM} perturbed singles and doubles cluster amplitudes equation (the prime denotes that the reference state and the excited Slater determinants are opposite in parity due to the parity odd perturbation)

$$\begin{aligned} \langle \Phi_a^{r'} | \left\{ \overline{H_N T^{(1)}} \right\} | \Phi_0 \rangle &= - \langle \Phi_a^{r'} | \left\{ \overline{H_{\text{EDM}}} \right\} | \Phi_0 \rangle \\ \langle \Phi_{ab}^{rs'} | \left\{ \overline{H_N T^{(1)}} \right\} | \Phi_0 \rangle &= - \langle \Phi_{ab}^{rs'} | \left\{ \overline{H_{\text{EDM}}} \right\} | \Phi_0 \rangle \end{aligned} \quad (3.44)$$

Expanding $\overline{H_N}$ in the equation for singles,

$$\begin{aligned} \langle \Phi_a^{r'} | \left\{ H_N + \overline{H_N T^{(0)}} + \frac{1}{2!} \overline{H_N T^{(0)} T^{(0)}} + \frac{1}{3!} \overline{H_N T^{(0)} T^{(0)} T^{(0)}} \right\} T^{(1)} | \Phi_0 \rangle \\ = - \langle \Phi_a^{r'} | \left\{ \overline{H_{\text{EDM}}} \right\} | \Phi_0 \rangle \end{aligned} \quad (3.45)$$

Using $T^{(1)} = T_1^{(1)} + T_2^{(1)}$,

$$\begin{aligned} \langle \Phi_a^{r'} | \left\{ H_N + \overline{H_N T^{(0)}} + \frac{1}{2!} \overline{H_N T^{(0)} T^{(0)}} + \frac{1}{3!} \overline{H_N T^{(0)} T^{(0)} T^{(0)}} \right\} T_1^{(1)} \\ + \left\{ H_N + \overline{H_N T^{(0)}} + \frac{1}{2!} \overline{H_N T^{(0)} T^{(0)}} + \frac{1}{3!} \overline{H_N T^{(0)} T^{(0)} T^{(0)}} \right\} T_2^{(1)} | \Phi_0 \rangle = - \langle \Phi_a^{r'} | \left\{ \overline{H_{\text{EDM}}} \right\} | \Phi_0 \rangle \end{aligned}$$

Similarly the double excitations satisfy the equation

$$\begin{aligned} & \left\langle \Phi_{ab}^{rs'} \left| \left\{ H_N + \overline{H_N T^{(0)}} + \frac{1}{2!} \overline{\overline{H_N T^{(0)}} T^{(0)}} + \frac{1}{3!} \overline{\overline{\overline{H_N T^{(0)}} T^{(0)}} T^{(0)}} \right\} T_1^{(1)} \right. \right. \\ & \left. \left. + \left\{ H_N + \overline{H_N T^{(0)}} + \frac{1}{2!} \overline{\overline{H_N T^{(0)}} T^{(0)}} + \frac{1}{3!} \overline{\overline{\overline{H_N T^{(0)}} T^{(0)}} T^{(0)}} \right\} T_2^{(1)} \right| \Phi_0 \right\rangle = - \left\langle \Phi_{ab}^{rs'} \left| \left\{ \overline{H_{\text{EDM}}} \right\} \right| \Phi_0 \right\rangle \end{aligned} \quad (3.46)$$

writing the equation for singles in terms of matrix elements,

$$\mathbf{A}_{11}(T^{(0)})T_1^{(1)} + \mathbf{A}_{12}(T^{(0)})T_2^{(1)} = -(H_{\text{EDM}})_0^1 \quad (3.47)$$

where

$$\begin{aligned} \mathbf{A}_{11}(T^{(0)})T_1^{(1)} &= \left\langle \Phi_a^{r'} \left| \left\{ H_N + \overline{H_N T^{(0)}} + \frac{1}{2!} \overline{\overline{H_N T^{(0)}} T^{(0)}} + \frac{1}{3!} \overline{\overline{\overline{H_N T^{(0)}} T^{(0)}} T^{(0)}} \right\} T_1^{(1)} \right| \Phi_0 \right\rangle, \\ \mathbf{A}_{12}(T^{(0)})T_2^{(1)} &= \left\langle \Phi_a^{r'} \left| \left\{ H_N + \overline{H_N T^{(0)}} + \frac{1}{2!} \overline{\overline{H_N T^{(0)}} T^{(0)}} + \frac{1}{3!} \overline{\overline{\overline{H_N T^{(0)}} T^{(0)}} T^{(0)}} \right\} T_2^{(1)} \right| \Phi_0 \right\rangle \end{aligned}$$

Similarly for the double excitations,

$$\mathbf{A}_{21}(T^{(0)})T_1^{(1)} + \mathbf{A}_{22}(T^{(0)})T_2^{(1)} = -(H_{\text{EDM}})_0^2 \quad (3.48)$$

where the matrices $\mathbf{A}_{21}(T^{(0)})$ and $\mathbf{A}_{22}(T^{(0)})$ are the coefficients of $T_1^{(1)}$ and $T_2^{(1)}$ operators in the doubles Eq. (3.46) respectively. The Eq. (3.47), Eq. (3.48) are nonlinear in $T^{(0)}$, but linear in $T^{(1)}$ and can be combined and written as

$$\begin{bmatrix} A_{11} & A_{12} \\ A_{21} & A_{22} \end{bmatrix} \begin{bmatrix} T_1^{(1)} \\ T_2^{(1)} \end{bmatrix} = \begin{bmatrix} B_1 \\ B_2 \end{bmatrix} \quad (3.49)$$

where

$$B_1 = -(H_{\text{EDM}})_0^1 = \left\langle \Phi_a^{r'} \left| \overline{H_{\text{EDM}}} \right| \Phi_0 \right\rangle$$

and

$$B_2 = -(H_{\text{EDM}})_0^2 = \left\langle \Phi_{ab}^{rs} \left| \overline{H}_{\text{EDM}} \right| \Phi_0 \right\rangle$$

These equations can be recast as,

$$\mathbf{A}(T^{(0)})T^{(1)} = \mathbf{B} \quad (3.50)$$

which are solved, to get the perturbed cluster amplitudes, where the $T^{(0)}$ amplitudes are assumed to be known. Splitting the matrix $\mathbf{A}(T^{(0)})$ in the above equation into diagonal and off-diagonal parts,

$$\mathbf{A}_{\text{diag}}(T^{(0)})T^{(1)} + \mathbf{A}_{\text{offdiag}}(T^{(0)})T^{(1)} = \mathbf{B}$$

gives an equation of the form

$$T^{(1)} = \frac{1}{\mathbf{A}_{\text{diag}}(T^{(0)})} \left[\mathbf{B} - \mathbf{A}_{\text{offdiag}}(T^{(0)})T^{(1)} \right] \quad (3.51)$$

This equation is solved iteratively until the self-consistently is achieved for the unknown $T^{(1)}$ amplitudes. That is, starting from an initial guess for the $T^{(1)}$'s, a new set of $T^{(1)}$'s are calculated, each time with the latest iterates. This process is repeated until convergence of the i th and the $(i - 1)$ th iterates. More details of the iterative scheme are presented in Section 4.2.

3.1.5 Selection Rules for the Cluster Operators

The tensor-pseudotensor electron-nucleus interaction Hamiltonian has the form (Eq. (2.1)),

$$H_{e-N}^{\text{EDM},T} = \frac{iG_F C_T}{\sqrt{2}} \sum_i \boldsymbol{\sigma}_N \cdot \boldsymbol{\gamma}_i \rho_N(r) \quad (3.52)$$

The operator in the electron space ($\boldsymbol{\gamma}_i$) is a vector of rank 1. The perturbed cluster amplitudes are associated with the electron space, which can be noted from the second quantization representation of the cluster operators (see Eq. (3.9)). The rank of the

interaction Hamiltonian must be incorporated into the cluster amplitudes and the diagrams representing them. Consider the diagrammatic representation of $T_1^{(1)}$ shown in Fig. 3.9(a). In terms of the multipole components

$$T_1^{(1)} = \sum_q (T_1^{(1)})_q^1 \quad (3.53)$$

Algebraically, $T_1^{(1)}$ can be written as

$$T_1^{(1)} = \sum_{a,p} a_p^\dagger a_a t_a^p \quad (3.54)$$

where, p is a particle, hence represented by an out-going line, and a is a hole represented by an incoming line, and t_a^p is the corresponding cluster amplitude. The rank of $T^{(1)}$ is denoted by $k_2 = 1$.

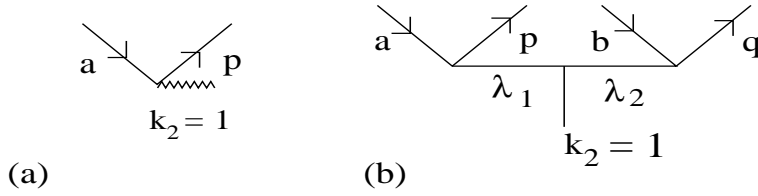


Figure 3.9: Diagram representing $T^{(1)}$ - (a) $T_1^{(1)}$ (b) $T_2^{(1)}$

The vertex formed by the orbital lines (a, p, k_2) in the $T_1^{(1)}$ diagram corresponds to the matrix element $\langle p|T_1^{(1)}|a\rangle$, and satisfies the triangular condition ³,

$$|J_a - 1| \leq J_p \leq J_a + 1,$$

and the magnetic quantum numbers satisfy,

$$m_a + m_p + q = 0,$$

where the J_i 's and m_i 's represent the total angular momenta and their projections respectively. The operator $T^{(1)}$ is odd under parity therefore,

$$(-1)^{l_a + l_p} = -1$$

³as dictated by the Wigner Eckart theorem for the matrix element of $T_1^{(1)}$

where l_i is the orbital angular momentum of the i th orbital. Consider the diagram representing $T_2^{(1)}$ operator. The vertices formed by the orbital indices (a, p, λ_1) , (b, q, λ_2) and $(\lambda_1, \lambda_2, k_2)$ satisfy the triangular conditions

$$|J_a - J_p| \leq \lambda_1 \leq J_a + J_p$$

$$|J_b - J_q| \leq \lambda_2 \leq J_b + J_q$$

$$|\lambda_1 - \lambda_2| \leq k_2 \leq \lambda_1 + \lambda_2$$

and the vertices satisfy,

$$(-1)^{l_a+l_p} = (-1)^{l_b+l_q}$$

Note that for the unperturbed cluster operator $T^{(0)}$ and the residual Coulomb operators preserve parity and hence, we have,

$$(-1)^{l_a+l_p} = (-1)^{l_b+l_q}$$

3.2 Application of CC Theory to Atomic Electric Dipole Moments

The EDM of the atom in the exact state $|\Psi'\rangle$ is

$$D_a = \frac{\langle \Psi' | D | \Psi' \rangle}{\langle \Psi' | \Psi' \rangle} \quad (3.55)$$

where D is the electric dipole operator and $|\Psi'\rangle$ is given by,

$$|\Psi'\rangle = |\Psi_0\rangle + \lambda |\Psi_0^{(1)}\rangle$$

where $|\Psi_0\rangle$ is the unperturbed state, λ is the perturbation parameter and $|\Psi_0^{(1)}\rangle$ is the first order correction to the unperturbed state due to the EDM perturbation. The exact state can be written in terms of the cluster operators as

$$|\Psi'\rangle = e^{T^{(0)} + \lambda T^{(1)}} |\Phi_0\rangle$$

where $|\Phi_0\rangle$ is the reference state. Retaining terms upto order λ ,

$$|\Psi'\rangle = e^{T^{(0)}} (1 + \lambda T^{(1)}) |\Phi_0\rangle$$

Substituting the above expression for $|\Psi'\rangle$ in Eq. (3.55) and keeping terms only of order λ , we obtain the expression for EDM ⁴,

$$D_a = \frac{\langle \Phi_0 | [\overline{D}T^{(1)} + T^{(1)\dagger}\overline{D}] | \Phi_0 \rangle}{\langle \Psi_0 | \Psi_0 \rangle} \quad (3.56)$$

which can also be written as,

$$D_a = \frac{\langle \Phi_0 | [\overline{\overline{D}}T^{(1)} + T^{(1)\dagger}\overline{\overline{D}}] | \Phi_0 \rangle}{\langle \Psi_0 | \Psi_0 \rangle} \quad (3.57)$$

where $\overline{D} = e^{T^{(0)\dagger}} D e^{T^{(0)}}$, using the fact that $T^{(1)}$ and D operators are odd and $T^{(0)}$ operator is even under parity, the bra and the ket vectors in the above expression must have the same parity. To simplify the calculations, we expand \overline{D} in the following manner,

$$\overline{D} = \left(1 + T^{(0)\dagger} + \frac{T^{(0)\dagger^2}}{2!} + \dots \right) D e^{T^{(0)}}$$

This can be written as [33]

$$\overline{D} = D e^{T^{(0)}} + \sum_{n=1}^{\infty} \frac{1}{n!} (T^{(0)\dagger})^n D e^{T^{(0)}} \quad (3.58)$$

The diagrams representing the electric dipole operator are shown in Fig. 3.10.

In Eq. (3.58), the one-body nature of the electric dipole operator D restricts the maximum possible *contractions* with $T^{(0)}$ to just two. Define

$$|\Phi_1\rangle = T^{(1)} |\Phi_0\rangle = (T_1^{(1)} + T_2^{(1)}) |\Phi_0\rangle,$$

⁴The symbol of *contraction* appears using $\overline{D}T^{(1)} = \overline{\overline{D}}T^{(1)} + \left\{ \overline{D}T^{(1)} \right\}$, where the curly brackets refer to normal ordering and the expectation value of normal ordered operator between the vacuum states is zero

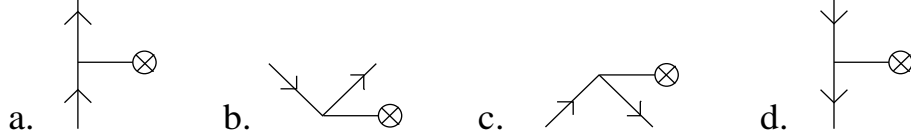


Figure 3.10: Diagrams representing the electric dipole operator

then

$$D_a = \frac{\langle \Phi_0 | \bar{D} | \Phi_1 \rangle + \langle \Phi_1 | \bar{D} | \Phi_0 \rangle}{\langle \Psi_0 | \Psi_0 \rangle} = 2 \frac{\langle \Phi_1 | \bar{D} | \Phi_0 \rangle}{\langle \Psi_0 | \Psi_0 \rangle} \quad (3.59)$$

The last step follows as the two terms are the complex conjugates of each other and give equal contributions. Substituting the expanded form of \bar{D}

$$\begin{aligned} D_a &= 2 \langle \Phi_1 | \left[D e^{T^{(0)}} + \sum_{n=1}^{\infty} \frac{1}{n!} (T^{(0)\dagger})^n D e^{T^{(0)}} \right] | \Phi_0 \rangle / \langle \Psi_0 | \Psi_0 \rangle \\ &= 2 \left[\langle \Phi_1 | D e^{T^{(0)}} | \Phi_0 \rangle + \langle \Phi_1 | \sum_{n=1}^{\infty} \frac{1}{n!} (T^{(0)\dagger})^n D e^{T^{(0)}} | \Phi_0 \rangle \right] / \langle \Psi_0 | \Psi_0 \rangle \end{aligned} \quad (3.60)$$

The complexity of the above expression can be mitigated by exploiting the fact that not all the terms containing the $T^{(0)\dagger}$ operators contribute to the infinite summation. In this scheme, the zeroth order D_a is terms without $T^{(0)\dagger}$ operator, first order D_a is terms having one order of $T^{(0)\dagger}$, and so on. The unlinked terms of the numerator cancel with the denominator and only linked terms contribute in the numerator.

3.2.1 Zeroth Order EDM

Consider the zeroth order contribution

$$D_a^0 = \langle \Phi_1 | D e^{T^{(0)}} | \Phi_0 \rangle$$

Expanding $\langle \Phi_1 |$

$$\langle \Phi_1 | D e^{T^{(0)}} | \Phi_0 \rangle = \underbrace{\langle \Phi_0 | T_1^{(1)\dagger} D e^{T^{(0)}} | \Phi_0 \rangle}_{Z_1} + \underbrace{\langle \Phi_0 | T_2^{(1)\dagger} D e^{T^{(0)}} | \Phi_0 \rangle}_{Z_2}. \quad (3.61)$$

The level of excitation (l.o.e) is the excitation number, assigned to a diagram taking into account the hole and particle creation and annihilations at the vertices of one and two-body diagrams. For example, the operators, T_1 and T_2 have l.o.e = 1 and 2 respectively since T_1 involves the annihilation of a hole a and the creation of a particle p and T_2 involves annihilation of two holes and creation of two particles. Then, T_1^\dagger and T_2^\dagger have l.o.e equal to -1 and -2 respectively. Since the operators $T_1^{(1)}$ and $T_2^{(1)}$ have fixed levels of excitation of $+1$ and $+2$ respectively, the possible terms contributing to the dressed dipole operator are restricted in Eq. (3.61). In other words, the term Z1 is nonzero only when $(De^{T^{(0)}})_1$ has l.o.e = 1 (indicated by the subscript). Similarly, for a nonzero Z2 contribution $(De^{T^{(0)}})_2$ must have a l.o.e = 2. Hence the terms finally contributing to zeroth order EDM can be read off as,

$$\left(De^{T^{(0)}}\right)_1 = \frac{1}{2!}DT_1^{(0)2} + DT_2^{(0)} + DT_1^{(0)} + D \quad (3.62)$$

$$\left(De^{T^{(0)}}\right)_2 = \frac{1}{3!}DT_1^{(0)3} + DT_1^{(0)}T_2^{(0)} + \frac{1}{2!}DT_1^{(0)2} + DT_2^{(0)} + DT_1^{(0)} \quad (3.63)$$

The diagrams of $(De^{T^{(0)}})_1$ and $(De^{T^{(0)}})_2$ are shown in Fig. 3.11 and Fig. 3.12 respectively. The linked diagrams of $(De^{T^{(0)}})_1$ are *connected*, but for $(De^{T^{(0)}})_{n \geq 2}$, *disconnected* diagrams also contribute.

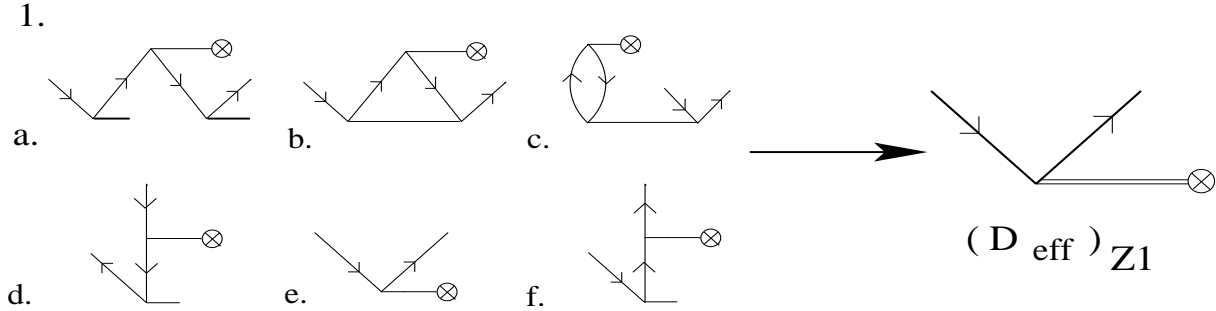


Figure 3.11: Diagrams contributing to $(De^{T^{(0)}})_1$. The diagram named $(D_{\text{eff}})_{Z1}$ is the effective operator obtained by summing the diagrams (a,b,c,d,e,f). All diagrams are *connected*.

In Fig. 3.12, among the $(De^{T^{(0)}})_2$ diagrams, (a), (c), (g) and (j) are *connected* and the remaining are *disconnected*,

$$(De^{T^{(0)}})_2 = \left(De^{T^{(0)}}\right)_2^{\text{conn}} + \left(De^{T^{(0)}}\right)_2^{\text{discon}}, \quad (3.64)$$

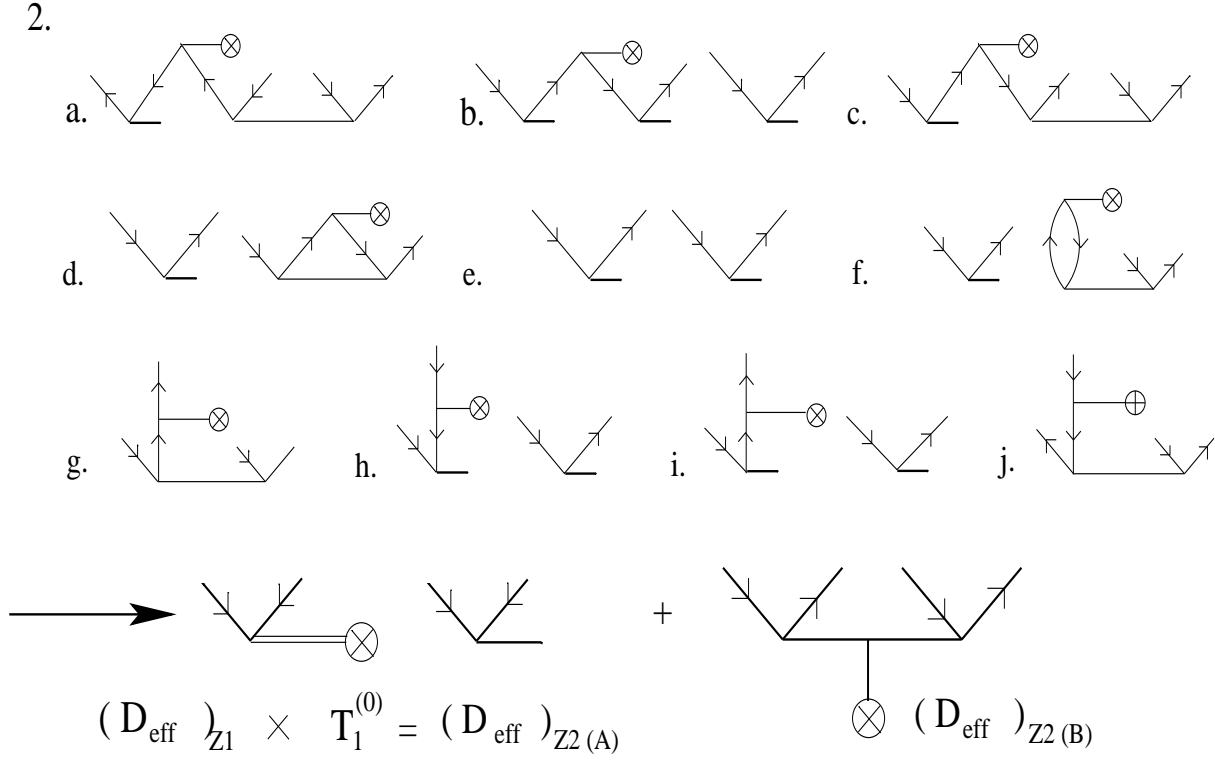


Figure 3.12: Diagrams contributing to $(De^{T(0)})_2$.

where the first and second terms represent the *connected* and *disconnected* terms. The *connected* terms resemble the diagrams contributing to the doubles on the right hand side of the CCEDM equation, again with the H_{EDM} operator replaced by D (see Fig. 3.8). The topology of the diagrams shows that diagrams of $(De^{T(0)})_2$ arise from $(De^{T(0)})_1 \times T_1^{(0)}$ and $(De^{T(0)})_2^{\text{conn}}$ diagrams. That is

$$(De^{T(0)})_2^{\text{discon}} = (De^{T(0)})_1 \times T_1^{(0)} \quad (3.65)$$

All the diagrams having same number of free lines and components are grouped together to obtain effective diagrams shown in Fig. 3.13(II). The diagrams contributing to the zeroth order EDM in Eq. (3.60) are shown in Fig. 3.14 and are obtained from the *contraction* of the effective dressed electric dipole operator with the perturbed cluster operator.

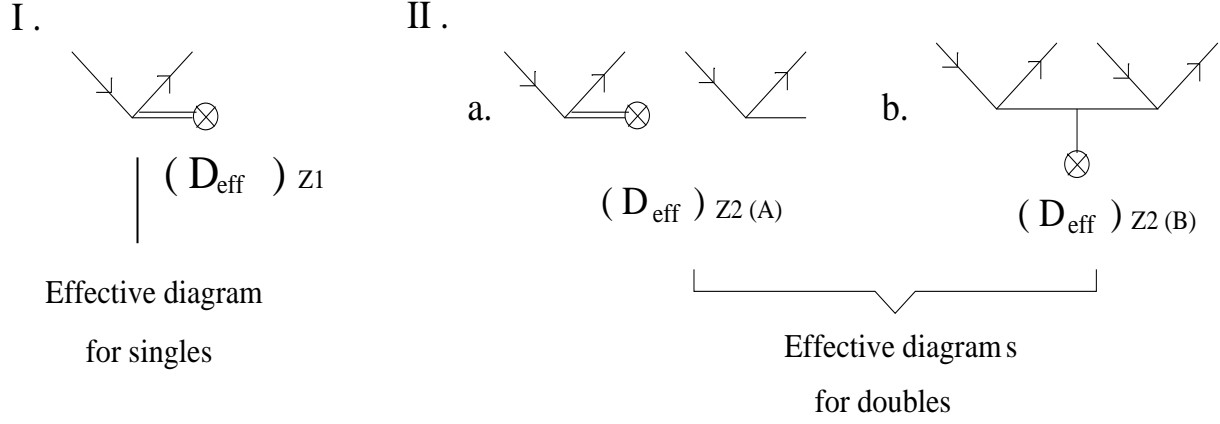


Figure 3.13: Effective diagrams for singles and doubles for zeroth order

3.2.2 First Order EDM

Next, consider the $n = 1$ term in Eq. (3.60), it is the first order in $T^{(0)\dagger}$

$$\begin{aligned} \left\langle \Phi_1 \left| T^{(0)\dagger} De^{T^{(0)}} \right| \Phi_0 \right\rangle &= \left\langle \Phi_0 \left| \left[T_1^{(1)\dagger} + T_2^{(1)\dagger} \right] T^{(0)\dagger} De^{T^{(0)}} \right| \Phi_0 \right\rangle \\ &= \left\langle \Phi_0 \left| \underbrace{T_1^{(1)\dagger} T^{(0)\dagger} De^{T^{(0)}}}_{F1} \right| \Phi_0 \right\rangle + \left\langle \Phi_0 \left| \underbrace{T_2^{(1)\dagger} T^{(0)\dagger} De^{T^{(0)}}}_{F2} \right| \Phi_0 \right\rangle \end{aligned}$$

We now determine the terms contributing to F1 and F2, expanding $T^{(0)\dagger}$ in F1

$$\left\langle \Phi_0 \left| T_1^{(1)\dagger} T^{(0)\dagger} De^{T^{(0)}} \right| \Phi_0 \right\rangle = \underbrace{\left\langle \Phi_0 \left| T_1^{(1)\dagger} \left(T_1^{(0)\dagger} De^{T^{(0)}} \right)_1 \right| \Phi_0 \right\rangle}_{F1(A)} + \underbrace{\left\langle \Phi_0 \left| T_1^{(1)\dagger} \left(T_2^{(0)\dagger} De^{T^{(0)}} \right)_1 \right| \Phi_0 \right\rangle}_{F1(B)}$$

Further, expanding $De^{T^{(0)}}$ in F1(A),

$$\begin{aligned} \left(T_1^{(0)\dagger} De^{T^{(0)}} \right)_1 &= T_1^{(0)\dagger} \left(De^{T^{(0)}} \right)_2 \\ &= T_1^{(0)\dagger} \left[\frac{1}{3!} DT_1^{(0)3} + DT_1^{(0)} T_2^{(0)} + \frac{1}{2!} DT_1^{(0)2} + DT_2^{(0)} + DT_1^{(0)} \right]_2 \\ &= T_1^{(0)\dagger} \left[\left(De^{T^{(0)}} \right)_2^{\text{conn}} + \left(De^{T^{(0)}} \right)_1 \times T_1^{(0)} \right] \end{aligned} \quad (3.66)$$

As discussed in the zeroth order case, the $(De^{T^{(0)}})_2$ diagrams arise from $(De^{T^{(0)}})_1 \times T_1^{(0)}$ and the actual $(De^{T^{(0)}})_2^{\text{conn}}$ diagrams. We saw that the effective diagrams listed in Fig. 3.13 are sum of all the diagrams arising from $(De^{T^{(0)}})_1 \times T_1^{(0)}$ and $(De^{T^{(0)}})_2$. Hence,

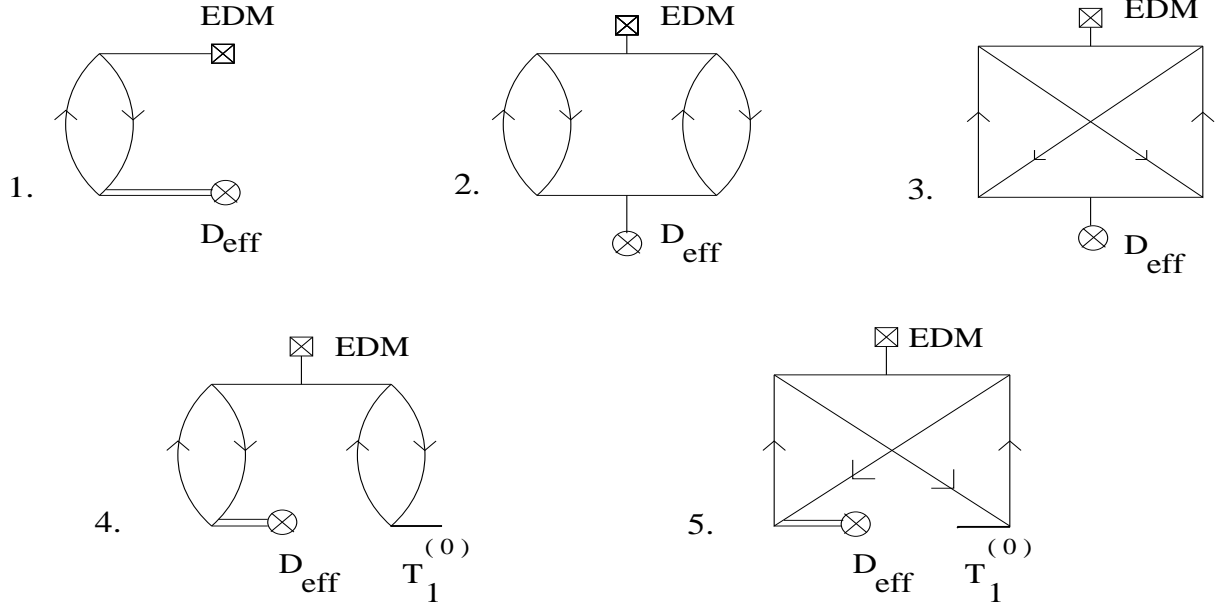


Figure 3.14: Diagrams contributing to EDM from the effective diagrams at zeroth order

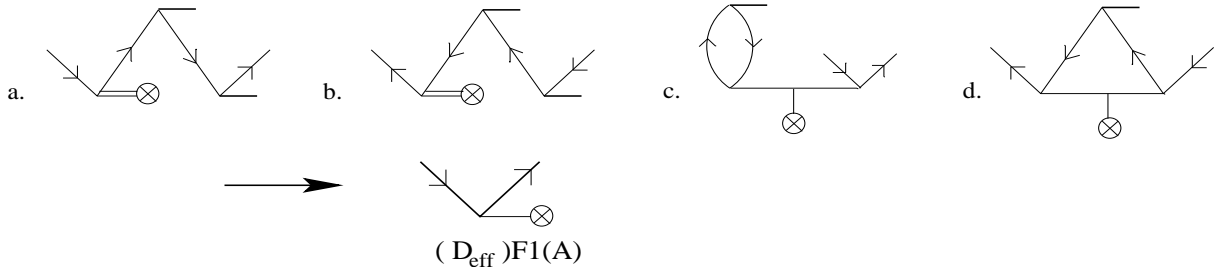


Figure 3.15: Effective diagrams at first order contributing to F1(A)

the effective diagrams of $(T_1^{(0)\dagger} De^{T^{(0)}})_1$ are *contraction* of the effective diagrams in Fig. 3.13 and $T_1^{(0)\dagger}$, these are shown in Fig. 3.15. To calculate the contribution from F1(B), consider

$$\begin{aligned}
 (De^{T^{(0)}})_3 &= \left[\frac{1}{4!} DT_1^{(0)4} + \frac{1}{2!} DT_2^{(0)2} + \frac{1}{2!} DT_1^{(0)2} T_2^{(0)} + \frac{1}{3!} DT_1^{(0)3} + \right. \\
 &\quad \left. DT_1^{(0)} T_2^{(0)} + \frac{1}{2!} DT_1^{(0)2} + DT_2^{(0)} \right]_3 \\
 &= (De^{T^{(0)}})_3^{\text{conn}} + (De^{T^{(0)}})_2^{\text{conn}} \times T_1^{(0)} + (De^{T^{(0)}})_1 \left[\frac{1}{2!} T_1^{(0)2} + T_2^{(0)} \right] \quad (3.67)
 \end{aligned}$$

Similar to the previous cases, $(De^{T^{(0)}})_3$ is the sum of $(De^{T^{(0)}})_1 \times T_1^{(0)2}$, $(De^{T^{(0)}})_1 \times T_2^{(0)}$ and $(De^{T^{(0)}})_2^{\text{conn}} \times T_1^{(0)}$. In the present calculation, we do not include the $(De^{T^{(0)}})_3^{\text{conn}}$,

which are true three body diagrams. That is, we define

$$\left(De^{T^{(0)}}\right)_3 = \left(De^{T^{(0)}}\right)_2^{\text{conn}} \times T_1^{(0)} + \left(De^{T^{(0)}}\right)_1 \left[\frac{1}{2!} T_1^{(0)2} + T_2^{(0)} \right]. \quad (3.68)$$

The diagrams in Fig. 3.16 represent the sum of all the diagrams arising from these terms. The effective diagrams at first order can be obtained by the action of $T_2^{(0)\dagger}$ on

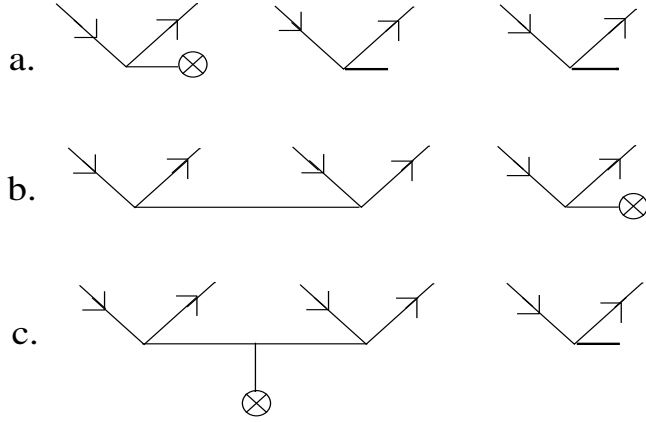


Figure 3.16: Open diagrams at first order for the term $(De^{T^{(0)}})_3$. Multiplication of $T_2^{(0)\dagger}$ with these diagrams gives the effective diagrams contributing to F1(B)

the diagrams listed in Fig. 3.16, then

$$\left(T_2^{(0)\dagger} De^{T^{(0)}}\right)_1 = T_2^{(0)\dagger} \left[\left(De^{T^{(0)}}\right)_2^{\text{conn}} \times T_1^{(0)} + \left(De^{T^{(0)}}\right)_1 \left(\frac{1}{2!} T_1^{(0)2} + T_2^{(0)} \right) \right]. \quad (3.69)$$

The contribution to EDM are then obtained by the *contraction* of these terms with $T_1^{(1)\dagger}$.

Adding Eq. (3.66) and Eq. (3.69), define an effective operator of \bar{D} as

$$\bar{D}_1^1 = \left(T_1^{(0)\dagger} De^{T^{(0)}}\right)_1 + \left(T_2^{(0)\dagger} De^{T^{(0)}}\right)_1, \quad (3.70)$$

where the subscript represents the one-body character of the operator and superscript indicates the order of $T^{(0)\dagger}$.

Similar to F1, expanding F2

$$\left\langle \Phi_0 \left| T_2^{(1)\dagger} T^{(0)\dagger} De^{T^{(0)}} \right| \Phi_0 \right\rangle = \underbrace{\left\langle \Phi_0 \left| T_2^{(1)\dagger} \left(T_1^{(0)\dagger} De^{T^{(0)}} \right)_2 \right| \Phi_0 \right\rangle}_{\text{F2(A)}} + \underbrace{\left\langle \Phi_0 \left| T_2^{(1)\dagger} \left(T_2^{(0)\dagger} De^{T^{(0)}} \right)_2 \right| \Phi_0 \right\rangle}_{\text{F2(B)}} \quad (3.71)$$

Consider F2(A), expanding the term within the parenthesis

$$\left\langle \Phi_0 \left| T_2^{(1)\dagger} \left(T_1^{(0)\dagger} D e^{T^{(0)}} \right)_2 \right| \Phi_0 \right\rangle = \left\langle \Phi_0 \left| T_2^{(1)\dagger} T_1^{(0)\dagger} \left(D e^{T^{(0)}} \right)_3 \right| \Phi_0 \right\rangle. \quad (3.72)$$

From the definition of $(D e^{T^{(0)}})_3$ in Eq. (3.68)

$$= \left\langle \Phi_0 \left| T_2^{(1)\dagger} T_1^{(0)\dagger} \left[\left(D e^{T^{(0)}} \right)_2^{\text{conn}} \times T_1^{(0)} + \left(D e^{T^{(0)}} \right)_1 \left(\frac{1}{2!} T_1^{(0)2} + T_2^{(0)} \right) \right] \right| \Phi_0 \right\rangle. \quad (3.73)$$

As mentioned earlier, the open diagrams contributing to $(D e^{T^{(0)}})_3$ are listed in Fig. 3.16.

The \bar{D} diagrams are then the *contraction* of $T_1^{(0)\dagger}$ with $(D e^{T^{(0)}})_3$, these are shown in Fig.

3.17. Fig. 3.18 shows the effective diagrams arising from summing the diagrams listed

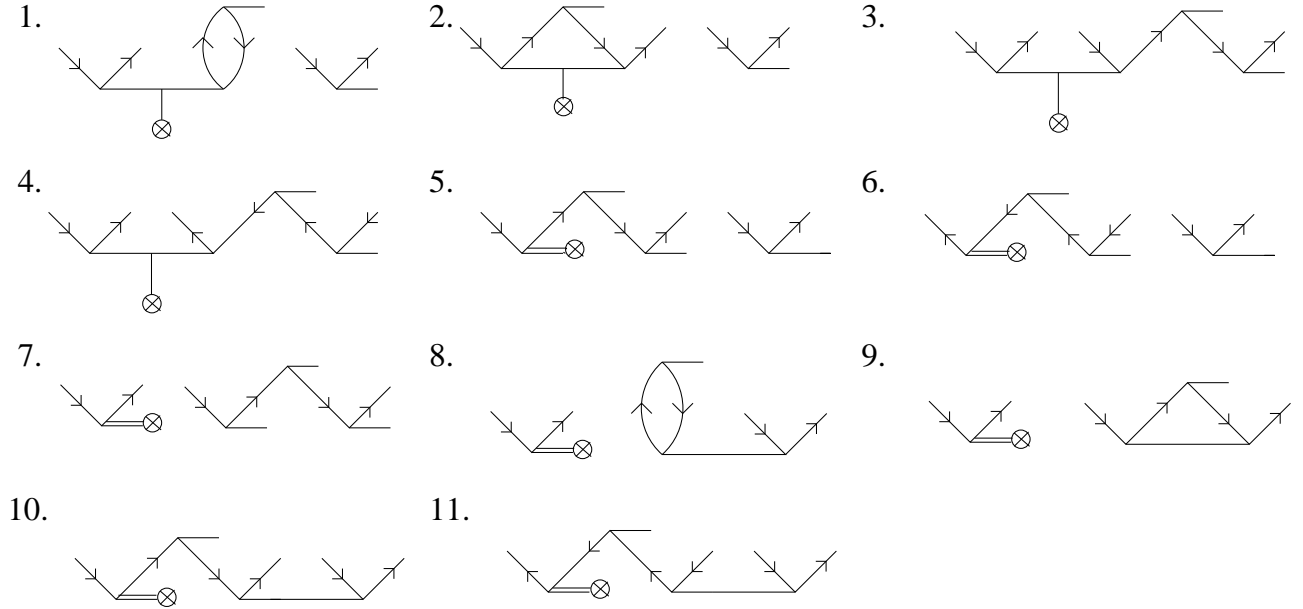


Figure 3.17: Effective diagrams at first order for F2(A) - $T_1^{(0)\dagger} (D e^{T^{(0)}})_3$

in Fig. 3.17.

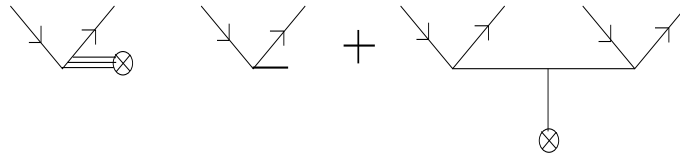


Figure 3.18: Effective diagrams at first order for F2(A) - $T_1^{(0)\dagger} (D e^{T^{(0)}})_3$

Now, consider the F2(B),

$$\left\langle \Phi_0 \left| T_2^{(1)\dagger} \left(T_2^{(0)\dagger} D e^{T^{(0)}} \right)_2 \right| \Phi_0 \right\rangle = \left\langle \Phi_0 \left| T_2^{(1)\dagger} T_2^{(0)\dagger} \left(D e^{T^{(0)}} \right)_4 \right| \Phi_0 \right\rangle. \quad (3.74)$$

Similar to $(De^{t^{(0)}})_3$, we can define

$$\left(De^{T^{(0)}}\right)_4 = \left(De^{T^{(0)}}\right)_2^{\text{conn}} \left[\frac{1}{2!}T_1^{(0)2} + T_2^{(0)} \right] + \left(De^{T^{(0)}}\right)_1 \left[\frac{1}{3!}T_1^{(0)3} + T_2^{(0)}T_1^{(0)} \right]. \quad (3.75)$$

We can define effective \overline{D} diagrams of $(T_1^{(0)\dagger}De^{T^{(0)}})_2$ and $(T_2^{(0)\dagger}De^{T^{(0)}})_2$. However, unlike \overline{D}_1^1 these terms have *connected* as well as *disconnected* diagrams

$$\overline{D}_2^1 = \overline{D}_2^{1\text{conn}} + \overline{D}_2^{1\text{discon}} = \left(T_1^{(0)\dagger}De^{T^{(0)}}\right)_2 + \left(T_2^{(0)\dagger}De^{T^{(0)}}\right)_2, \quad (3.76)$$

where $\overline{D}_2^{1\text{conn}}$ and $\overline{D}_2^{1\text{discon}}$ are the *connected* and *disconnected* contributions respectively.

The EDM contribution from second order $T^{(0)\dagger}$ can be calculated from \overline{D}_1^2 and \overline{D}_2^2 . Substituting $n = 2$ in Eq. (3.58), we get the second order contribution to EDM from the terms,

$$\begin{aligned} \overline{D}^2 &= \frac{T^{(0)\dagger 2}}{2!}De^{T^{(0)}} \\ &= \left(\frac{T_1^{(0)\dagger 2}}{2!} + \frac{T_2^{(0)\dagger 2}}{2!} + \frac{2}{2!}T_1^{(0)\dagger}T_2^{(0)\dagger} \right) De^{T^{(0)}} \end{aligned}$$

where $T^{(0)} = T_1^{(0)} + T_2^{(0)}$. Diagrammatically, the effective diagrams of F2(B) are obtained by the multiplication of $T_2^{(0)}$ by diagrams of $(De^{T^{(0)}})_4$ as shown in Fig. 3.19.

Action of $T_2^{(0)\dagger}$ on

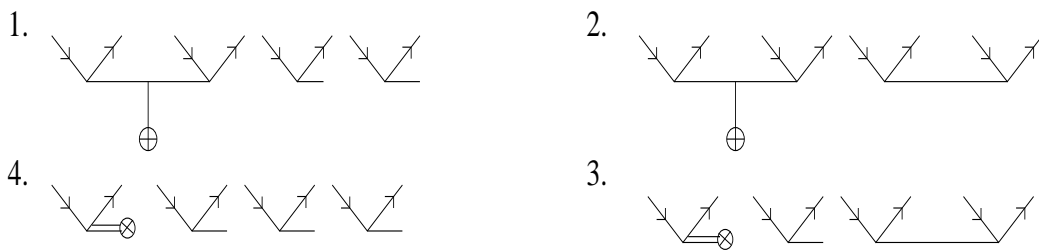


Figure 3.19: Effective diagrams at first order for F2(B) - $T_2^{(0)\dagger}(De^{T^{(0)}})_4$. As shown, the action of $T_2^{(0)\dagger}$ on the diagrams labelled 1 to 4, give rise to the effective diagrams of F2(B).

The results presented in the thesis correspond to the contributions of zeroth and the F1 terms. Following are the terms contributing to the EDM expectation value at the

linear level :

$$D_{\text{atom}} = \left\langle \Phi_0 \left| \overline{D}T^{(1)} + T^{(1)\dagger}\overline{D} \right| \Phi_0 \right\rangle$$

where

$$\overline{D} = e^{T^{(0)\dagger}} D e^{T^{(0)}}.$$

At the linear level,

$$\begin{aligned} &= \left(1 + T^{(0)}\right)^\dagger D \left(1 + T^{(0)}\right) \\ &= D + DT^{(0)} + T^{(0)\dagger}D = D + DT_1^{(0)} + D + DT_2^{(0)} + T_1^{(0)\dagger}D + T_2^{(0)\dagger}D \end{aligned}$$

Now the EDM expectation value becomes,

$$D_{\text{atom}} = 2 \left\langle \Phi_0 \left| \left[T_1^{(1)\dagger}D + T_1^{(1)\dagger}DT_1^{(0)} + T_1^{(1)\dagger}DT_2^{(0)} + T_2^{(1)\dagger}DT_2^{(0)} + T_2^{(1)\dagger}DT_1^{(0)} \right] \right| \Phi_0 \right\rangle \quad (3.77)$$

3.3 Comparison of Coupled-Perturbed Hartree-Fock and Coupled-Cluster Theories

3.3.0.1 The Coupled-Perturbed Hartree-Fock Equations

In this section, we give an outline of the coupled-perturbed Hartree-Fock (CPHF) equations and explain how the diagrams arising from the CPHF theory can be related to the diagrams present in coupled-cluster theory. The results of the numerical comparison are presented in Chapter.5. Consider the Hartree-Fock equation Eq. (3.6),

$$\left(h^0 + g^0 - \epsilon_a^0 \right) \left| \psi_a^0 \right\rangle = 0 \quad (3.78)$$

The introduction of P and T violating interaction, h_{EDM} , as a perturbation, modifies the Hamiltonian and the single particle wavefunctions

$$\left| \psi_a^0 \right\rangle \rightarrow \left| \psi_a^0 \right\rangle + \lambda \left| \psi_a^1 \right\rangle, \quad \text{and} \quad h^0 \rightarrow h^0 + \lambda h_{\text{EDM}}$$

where λ is the perturbation parameter and $|\psi_a^1\rangle$ is the first order correction to wavefunction. The operator h_{EDM} is used to distinguish from H_{EDM} operator at the single

and many-particle levels respectively. There is no first order energy correction as the perturbing Hamiltonian h_{EDM} is an odd parity operator. We then get the perturbed Hartree-Fock equation

$$\begin{aligned} & \left(h^0 + \lambda h_{\text{EDM}} \right) \left(\left| \psi_a^0 \right\rangle + \lambda \left| \psi_a^1 \right\rangle \right) + \sum_{b=1}^{N_{\text{occ}}} \left[\left\langle \psi_b^0 + \lambda \psi_b^1 \left| v \left| \psi_b^0 + \lambda \psi_b^1 \right\rangle \right| \psi_a^0 + \lambda \psi_a^1 \right\rangle \right] \\ & - \sum_{b=1}^{N_{\text{occ}}} \left[\left\langle \psi_b^0 + \lambda \psi_b^1 \left| v \left| \psi_a^0 + \lambda \psi_a^1 \right\rangle \right| \psi_b^0 + \lambda \psi_b^1 \right\rangle \right] - \epsilon_a^0 \left| \psi_a^0 + \lambda \psi_a^1 \right\rangle = 0 \end{aligned} \quad (3.79)$$

Keeping only the terms linear in λ ,

$$\begin{aligned} & \left(h^0 \left| \psi_a^1 \right\rangle + h_{\text{EDM}} \left| \psi_a^0 \right\rangle \right) + \sum_{b=1}^{N_{\text{occ}}} \left(\left\langle \psi_b^0 \left| v \left| \psi_b^1 \right\rangle \right| \psi_a^0 \right\rangle + \left\langle \psi_b^1 \left| v \left| \psi_b^0 \right\rangle \right| \psi_a^0 \right\rangle + \left\langle \psi_b^0 \left| v \left| \psi_b^0 \right\rangle \right| \psi_a^1 \right\rangle \right) \\ & - \left(\left\langle \psi_b^0 \left| v \left| \psi_a^1 \right\rangle \right| \psi_b^0 \right\rangle + \left\langle \psi_b^1 \left| v \left| \psi_a^0 \right\rangle \right| \psi_b^0 \right\rangle + \left\langle \psi_b^0 \left| v \left| \psi_a^0 \right\rangle \right| \psi_b^1 \right\rangle \right) - \epsilon_a^0 \left| \psi_a^1 \right\rangle = 0 \end{aligned} \quad (3.80)$$

Rearranging

$$\left(h^0 + g^0 - \epsilon_a^0 \right) \left| \psi_a^1 \right\rangle = \left(-h_{\text{EDM}} - g^1 \right) \left| \psi_a^0 \right\rangle \quad (3.81)$$

where the perturbed Hartree-Fock potential is given by

$$g^1 \left| \psi_a^0 \right\rangle = \sum_{b=1}^{N_{\text{occ}}} \left[\left\langle \psi_b^0 \left| v \left| \psi_b^1 \right\rangle \right| \psi_a^0 \right\rangle - \left\langle \psi_b^0 \left| v \left| \psi_a^0 \right\rangle \right| \psi_b^1 \right\rangle + \left\langle \psi_b^1 \left| v \left| \psi_b^0 \right\rangle \right| \psi_a^0 \right\rangle - \left\langle \psi_b^1 \left| v \left| \psi_a^0 \right\rangle \right| \psi_b^0 \right\rangle \right] \quad (3.82)$$

The Eq. (3.81) is the CPHF equation. Expanding the perturbed orbitals as a linear combination of the opposite parity unperturbed orbitals

$$\left| \psi_a^1 \right\rangle = \sum_p C_{pa} \left| \psi_p^0 \right\rangle$$

where C_{pa} are the mixing coefficients, then

$$\sum_p \left(h^0 + g^0 - \epsilon_a^0 \right) C_{pa} \left| \psi_p^0 \right\rangle = \left(-h_{\text{EDM}} - g^1 \right) \left| \psi_a^0 \right\rangle$$

Projecting the above equation by $\langle \psi_m^0 |$,

$$\left(\epsilon_p^0 - \epsilon_a^0 \right) C_{pa} = \left\langle \psi_p^0 \left| \left(-h_{\text{EDM}} - g^1 \right) \right| \psi_a^0 \right\rangle$$

Similarly, expanding $|\psi_b^1\rangle = \sum_q C_{qb}|\psi_q^0\rangle$ in g^1 (Eq. (3.82)), the mixing coefficients are the solutions of the linear algebraic equations

$$C_{pa} \left(\epsilon_p^0 - \epsilon_a^0 \right) + \sum_{bq} \left[\tilde{V}_{pqab} C_{qb}^* + \tilde{V}_{pbaq} C_{qb} \right] + \left\langle p \left| h_{\text{EDM}} \right| a \right\rangle = 0 \quad (3.83)$$

where $\tilde{V}_{pqab} = \left(\langle pq|v|ab\rangle - \langle pq|v|ba\rangle \right)$ and $\tilde{V}_{pbaq} = \left(\langle pb|v|aq\rangle - \langle pb|v|qa\rangle \right)$.

The wavefunctions $|\psi_p^0\rangle$, $|\psi_a^0\rangle$, $|\psi_b^0\rangle$ and $|\psi_q^0\rangle$ are represented by the orbital indices (p, a, b, q) respectively and hereafter we follow this notation for the single particle orbitals.

The zeroth order contribution to the coefficients is

$$C_{pa}^{(0,1)} = - \frac{\left\langle p \left| h_{\text{EDM}} \right| a \right\rangle}{\left(\epsilon_p^0 - \epsilon_a^0 \right)} \quad (3.84)$$

The superscripts on the coefficient denotes the order of the residual Coulomb interaction and that of the h_{EDM} perturbation respectively. The diagrammatic representation of this term is given in Fig. 3.20(a).

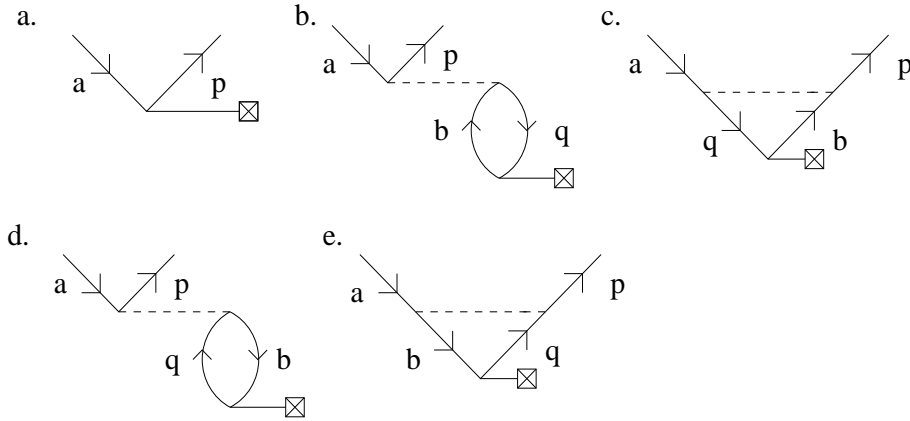


Figure 3.20: CPHF diagrams at zero and one order residual Coulomb interaction. The diagrams (d,e) are called *normal* CPHF diagrams and (b,c) are the *pseudo* CPHF diagrams. The dotted line is the residual Coulomb interaction and the line attached with \boxtimes is the EDM interaction.

The Eq. (3.83) is expressed in the form of a linear matrix equation,

$$\sum_{qb} A_{pa \quad qb} C_{qb} = -B_{pa} \quad (3.85)$$

where $A_{pa\ qb} = \tilde{V}_{pqab} + \tilde{V}_{pbaq} + (\epsilon_p^0 - \epsilon_a^0) \delta_{pq} \delta_{ab}$ and $B_{pa} = \langle p|h_{\text{EDM}}|a\rangle$. This equation is solved iteratively starting with the initial guess for the mixing coefficients given by Eq. (3.84). The coefficients of the k th iteration are obtained from,

$$C_{pa}^{(k,1)} = -\frac{B_{pa}}{\epsilon_p^0 - \epsilon_a^0} - \sum_{bq} \left[\left(\tilde{V}_{pqab} \right) \frac{C_{qb}^{(k-1,1)*}}{\epsilon_p^0 - \epsilon_a^0} + \left(\tilde{V}_{pbaq} \right) \frac{C_{qb}^{(k-1,1)}}{\epsilon_p^0 - \epsilon_a^0} \right] \quad (3.86)$$

With one order in residual Coulomb interaction, we get,

$$C_{pa}^{(1,1)} = -\frac{B_{pa}}{\epsilon_p^0 - \epsilon_a^0} - \sum_{bq} \left[\left(\tilde{V}_{pqab} \right) \frac{C_{qb}^{(0,1)*}}{\epsilon_p^0 - \epsilon_a^0} + \left(\tilde{V}_{pbaq} \right) \frac{C_{qb}^{(0,1)}}{\epsilon_p^0 - \epsilon_a^0} \right] \quad (3.87)$$

The diagrams arising from the above equation are shown in Fig. 3.20.

Substituting the expression of $C_{qb}^{(0,1)}$

$$C_{pa}^{(1,1)} = -\frac{B_{pa}}{\epsilon_p^0 - \epsilon_a^0} - \sum_{bq} \left[\left(\tilde{V}_{pqab} \right) \frac{(B_{qb})^\dagger}{(\epsilon_b^0 - \epsilon_q^0)(\epsilon_p^0 - \epsilon_a^0)} + \left(\tilde{V}_{pbaq} \right) \frac{B_{qb}}{(\epsilon_b^0 - \epsilon_q^0)(\epsilon_p^0 - \epsilon_a^0)} \right] \quad (3.88)$$

The contribution of the *normal* CPHF diagrams for one order in residual Coulomb interaction is,

$$(C_{pa}^{(1,1)})_{\text{normal}} = -\sum_{bq} \left[\left(\tilde{V}_{pbaq} \right) \frac{B_{qb}}{(\epsilon_b^0 - \epsilon_q^0)(\epsilon_p^0 - \epsilon_a^0)} \right] \quad (3.89)$$

This expression is used later to compare with similar expression arising in CCEDM. Consider the two pseudo diagrams of CPHF. Writing only the pseudo diagrams,

$$(C_{pa}^{(1,1)})_{\text{pseudo}} = -\sum_{bq} \left[\left(\tilde{V}_{pqab} \right) \frac{(B_{qb})^\dagger}{(\epsilon_b^0 - \epsilon_q^0)(\epsilon_p^0 - \epsilon_a^0)} + \right] \quad (3.90)$$

These terms are diagrammatically represented by Fig. 3.20(b,c).

3.3.0.2 CCEDM Equations

Consider the CCEDM equations,

$$\left\langle \Phi_a^{p'} \left| \left[\overline{H_N T}^{(1)} \right] \right| \Phi_0 \right\rangle = - \left\langle \Phi_a^{p'} \left| \overline{H_{\text{EDM}}} \right| \Phi_0 \right\rangle \quad (3.91)$$

$$\left\langle \Phi_{ab}^{pq'} \left| \left[\overline{H_N T}^{(1)} \right] \right| \Phi_0 \right\rangle = - \left\langle \Phi_{ab}^{pq'} \left| \overline{H_{\text{EDM}}} \right| \Phi_0 \right\rangle \quad (3.92)$$

In the CCEDM equation for singles, set $\overline{H_N} = H_N$ and $\overline{H_{\text{EDM}}} = H_{\text{EDM}}$ and ignore the doubles for the present.

$$\left\langle \Phi_a^{p'} \left| \overline{H_N T}_1^{(1)} \right| \Phi_0 \right\rangle = - \left\langle \Phi_a^{p'} \left| H_{\text{EDM}} \right| \Phi_0 \right\rangle \quad (3.93)$$

using $\overline{H_N T}^{(1)} = \left\{ \overline{H_N T}^{(1)} \right\}$. Introducing a complete set of singly excited states,

$$\sum_{bq} \left\langle \Phi_a^{p'} \left| H_N \right| \Phi_b^{q'} \right\rangle \left\langle \Phi_b^{q'} \left| T_1^{(1)} \right| \Phi_0 \right\rangle = - \left\langle \Phi_a^{p'} \left| H_{\text{EDM}} \right| \Phi_0 \right\rangle \quad (3.94)$$

we get

$$\sum_{bq} (H_N)_{ap,bq} \left(T_1^{(1)} \right)_{bq} = - (H_{\text{EDM}})_{ap} \quad (3.95)$$

where $(H_N)_{ap,bq} = V_{pb,aq} - V_{pb,qa} + f_{pq} - f_{ba}$ considering only the terms of H_N which have a CPHF counterpart. The operator, $H_N = f_N + V_N$, where f_N and V_N are the normal ordered one- and two-body operators respectively. The one-body terms contribute to the single particle orbital energies. In terms of single-particle wavefunctions, the CCEDM equation becomes

$$\begin{aligned} \sum_{bq} \left[\left\langle pb \left| V \right| aq \right\rangle - \left\langle pb \left| V \right| qa \right\rangle - \left\langle a \left| f \right| b \right\rangle + \left\langle p \left| f \right| q \right\rangle \right] \times \left\langle q \left| t^{(1)} \right| b \right\rangle &= \left\langle p \left| -h_{\text{EDM}} \right| a \right\rangle \\ \Rightarrow \sum_{bq} \left[\tilde{V}_{pb,aq} t_b^{q(1)} \right] + \left(\epsilon_p^0 - \epsilon_a^0 \right) t_a^{p(1)} &= \left\langle p \left| -h_{\text{EDM}} \right| a \right\rangle \end{aligned}$$

The perturbed cluster amplitudes are hence given by,

$$t_a^{p(1)} = \left(-B_{ap} - \sum_{bq} \tilde{V}_{pb,aq} t_b^{q(1)} \right) / \left(\epsilon_p^0 - \epsilon_a^0 \right) \quad (3.96)$$

Where the matrix B_{ap} is given by,

$$B_{ap} = \left\langle p \left| h_{\text{EDM}} \right| a \right\rangle$$

Expressing the above equation in an iterative form,

$$t_a^{p(k,1)} = \left(-B_{ap} - \sum_{bq} \tilde{V}_{pb,aq} t_b^{q(k-1,1)} \right) / \left(\epsilon_p^0 - \epsilon_a^0 \right) \quad (3.97)$$

The perturbed cluster amplitudes are solutions of the Eq. (3.97), where the initial guess is given by,

$$t_a^{p(0,1)} = \frac{-\left\langle p \left| h_{\text{EDM}} \right| a \right\rangle}{\left(\epsilon_p^0 - \epsilon_a^0 \right)}$$

For one order in residual Coulomb interaction, $k = 1$ and get,

$$t_a^{p(1,1)} = \left(-B_{ap} - \sum_{bq} \tilde{V}_{pb,aq} t_b^{q(0,1)} \right) / \left(\epsilon_p^0 - \epsilon_a^0 \right) \quad (3.98)$$

Substituting for $t_b^{q(0,1)}$, we get,

$$t_a^{p(1,1)} = \frac{\left\langle p \left| -h_{\text{EDM}} \right| a \right\rangle}{\left(\epsilon_p - \epsilon_a \right)} - \sum_{bq} \left(\left\langle pb \left| V \right| aq \right\rangle - \left\langle pb \left| V \right| qa \right\rangle \right) \frac{\left\langle q \left| -h_{\text{EDM}} \right| b \right\rangle}{\left(\epsilon_q^0 - \epsilon_b^0 \right) \left(\epsilon_p^0 - \epsilon_a^0 \right)} \quad (3.99)$$

The second term of the above equation is exactly equivalent to the equation for the CPHF mixing coefficient, Eq. (3.89). The diagrammatic representation of the terms in Eq. (3.89) and the second term of Eq. (3.99) are shown in Fig. 3.20 (d-e). This establishes the equivalence of *normal* CPHF diagrams and the corresponding diagrams arising in the coupled-cluster theory. A detailed comparison of the mixing coefficients of CPHF and the cluster amplitudes from coupled-cluster theory is performed and is demonstrated numerically for atomic mercury. The results of the comparison are summarized in Chapter.5. Now consider the contribution of the atomic EDM in terms of the CPHF mixing coefficients,

$$\text{EDM} = \sum_{ap} \left\langle \psi_a^0 \left| D \right| \psi_p^0 \right\rangle C_{pa}^{(\infty,1)} + C_{pa}^{*(\infty,1)} \left\langle \psi_p^0 \left| D \right| \psi_a^0 \right\rangle$$

The zeroth order contribution to EDM is,

$$EDM = 2 \sum_{ap} \frac{\langle \psi_a^0 | D | \psi_p^0 \rangle \langle \psi_p^0 | h_{EDM} | \psi_a^0 \rangle}{(\epsilon_a^0 - \epsilon_p^0)}$$

since $C_{pa}^* = C_{pa}$. The diagrams contributing to atomic EDM in CPHF theory are shown in Fig. 3.21. The atomic EDM in terms of the cluster operators is

$$EDM = \left\langle \Phi_0 \left| T^{(1)\dagger} \bar{D} + \bar{D} T^{(1)} \right| \Phi_0 \right\rangle \quad (3.100)$$

where $\bar{D} = e^{T^{(0)\dagger}} D e^{T^{(0)}}$. The same diagrams in coupled-cluster theory (Fig. 3.22(III)) arise from the term $D (T_1^{(1)})_{\text{eff}}$ at the level of the final EDM matrix element. The effective operator $(T_1^{(1)})_{\text{eff}}$ results from the *contraction* of singles cluster amplitude operator $(T_1^{(1)\dagger})$ and the residual Coulomb interaction.

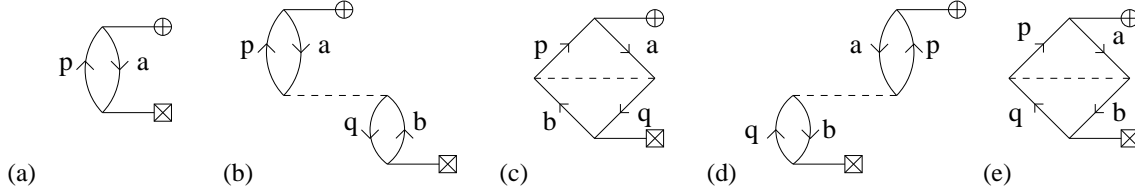


Figure 3.21: CPHF diagrams contributing to EDM

As shown in Fig. 3.22, the CPHF diagrams of the kind shown in Fig. 3.21 (b,c) are obtained by summing the two MBPT diagrams Fig. 3.22(I(a,b) & II(a,b)). These diagrams seem to be arising from the terms $(D(T_1^{(1)})_{\text{eff}} + T_1^{(1)\dagger} D T_2^{(0)})$ where $(T_1^{(1)})_{\text{eff}}$ is the effective diagram arising from the *contraction* of the cluster amplitude $T_1^{(1)\dagger}$ and the residual Coulomb interaction. The diagrams listed under (III) are directly present in the coupled-cluster theory, but (I) and (II) can be shown to be present only indirectly. The CPHF coefficients computed during the first iteration of the CPHF equation contain one order residual Coulomb interaction. The EDM computed using these coefficients can be compared with the coupled-cluster terms as indicated above.

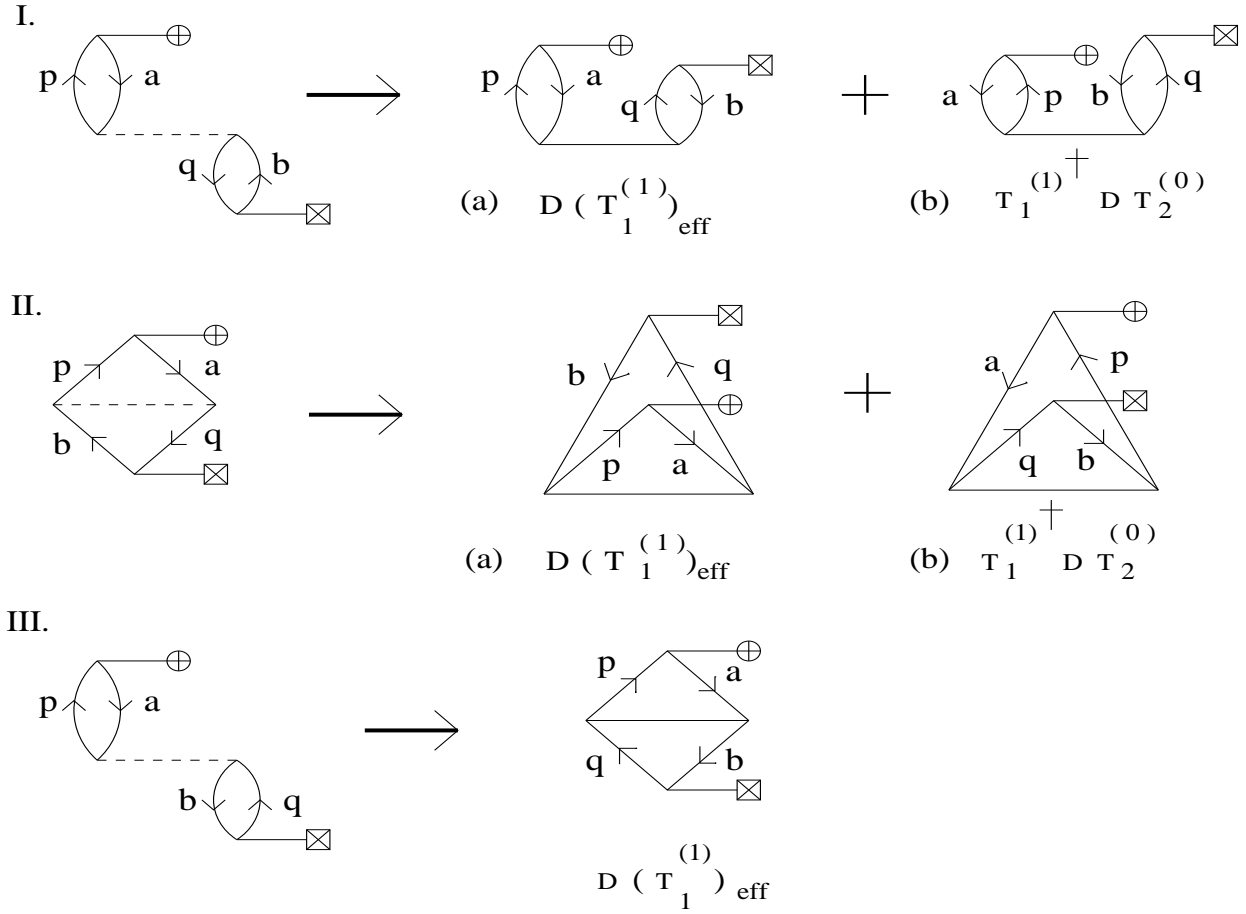


Figure 3.22: Diagrams contributing to EDM - Solid interaction lines in I(a)&(b), II(a)&(b) and III(a)&(b) represent the Coulomb interaction treated to all orders. The operator $(T_1^{(1)})_{\text{eff}}$ is a result of the contraction $T_2^{(0)}T_1^{(1)\dagger}$, which, when contracted with the electric dipole operator (D), gives the diagram contributing to D_a . Here, the diagrams (I) and (II) are the pseudo diagrams of CPHF. We extract the corresponding terms in coupled- cluster theory.

3.4 Comparison of Coupled-Cluster Theory with Configuration Interaction

Before we move on to the calculation of atomic EDMs using CC theory, we make a comparison between the coupled-cluster, the Configuration Interaction (CI) and the many-body perturbation methods. The exact atomic wavefunction in coupled-cluster theory is expressed as

$$|\Psi_{\text{CC}}\rangle = e^T |\Phi_0\rangle$$

where $|\Phi_0\rangle$ is the reference state and T is the hole-particle excitation operator and $|\Psi_{\text{CC}}\rangle$ is the exact atomic state. In the present discussion let $T = T_1 = \sum_{a,p} a_p^\dagger a_a t_a^p$. This gives

$$|\Psi_{\text{CC}}\rangle = \left[1 + T_1 + \frac{T_1^2}{2!} + \dots \right] |\Phi_0\rangle \quad (3.101)$$

and

$$T_1 |\Phi_0\rangle = \sum_{a,p} a_p^\dagger a_a |\Phi_0\rangle t_a^p = \sum_{a,p} |\Phi_a^p\rangle t_a^p$$

t_a^p is the amplitude for the excitation from a to p . Consider the CI wavefunction,

$$|\Psi_{\text{CI}}\rangle = C_0 |\Phi_0\rangle + \sum_s C_s |\Phi_s\rangle + C_d \sum_d |\Phi_d\rangle + \dots \quad (3.102)$$

where $|\Phi_0\rangle$, $|\Phi_s\rangle$ (set of all single excitations), $|\Phi_d\rangle$ (set of all double excitations) and so on form a complete set of basis vectors in Hilbert space. Comparing Eq. (3.101) and Eq. (3.102),

$$T_1 |\Phi_0\rangle = \sum_{a,p} |\Phi_a^p\rangle t_a^p = \sum_s C_s |\Phi_s\rangle$$

Hence, T_1 is equivalent to the set of all the single excitations as given by the CI wavefunction. From Eq. (3.101) and Eq. (3.102) it can also be noted that for double excitations, it is necessary to include them explicitly in the CI wavefunction, but the CC wavefunction can give the same through T_1^2 term at a lower level of truncation of the exponential. The $|\Phi_s\rangle$ of the CI is identical to $|\Phi_a^p\rangle$ of CC theory. Now consider the exact wavefunction as described in the many-body perturbation theory,

$$|\Psi\rangle = |\Phi_0\rangle + |\Phi_0^1\rangle + |\Phi_0^2\rangle + \dots \quad (3.103)$$

where $|\Phi_0\rangle$ is the unperturbed wavefunction and others are the higher order corrections to $|\Phi_0\rangle$. We have,

$$|\Phi_0^1\rangle = \sum_{I \neq 0} |\Phi_I\rangle \frac{\langle \Phi_I | H' | \Phi_0 \rangle}{E_0 - E_I}$$

where for $|\Phi_0^1\rangle$, 'I' stands for all the single excited intermediate states and H' is the perturbation. $|\Phi_0^1\rangle$ can be expanded in terms of the complete set,

$$|\Phi_0^1\rangle = \sum_s C_s^1 |\Phi_s\rangle + \sum_d C_d^1 |\Phi_d\rangle + \dots$$

Similarly,

$$|\Phi_0^2\rangle = \sum_s C_s^2 |\Phi_s\rangle + \sum_d C_d^2 |\Phi_d\rangle + \dots$$

The exact wavefunction $|\Psi\rangle$ can now be written as

$$|\Psi\rangle = |\Phi_0\rangle + \sum_s [C_s^1 + C_s^2 + \dots] |\Phi_s\rangle + \sum_d [C_d^1 + C_d^2 + \dots] |\Phi_d\rangle + \dots \quad (3.104)$$

$|\Phi_0^1\rangle$ has one order of the residual Coulomb interaction(perturbation), $|\Phi_0^2\rangle$ has two orders, and so on. This implies that there are infinite number of residual Coulomb interactions giving rise to a single excitation, infinite Coulomb interactions giving rise to double excitations and so on, where C_s^1, C_s^2 etc. represent one order in the residual Coulomb interaction with one intermediate state(I), two orders in residual Coulomb interaction with two intermediate states (I,J) respectively. Comparing Eq. (3.101) and Eq. (3.104), we get

$$T_1 |\Phi_0\rangle = \sum_s [C_s^1 + C_s^2 + \dots] |\Phi_s\rangle \quad (3.105)$$

which indicates that T_1 contains infinite orders of Coulomb interaction corresponding to all possible single excitations. The above T_1 refers to the unperturbed cluster operator $T_1^{(0)}$. The H_{EDM} perturbed operator $T_1^{(1)}$ contains, in addition to infinite orders in Coulomb perturbation, one order in H_{EDM} . The above equations also demonstrate that under a given approximation of singles and doubles, the summation over the corresponding mixing coefficients is equivalent to treating the perturbation to all orders. Hence, the calculations of the coupled-cluster amplitudes t_a^p and t_{ab}^{pq} is equivalent to the calculation of the mixing coefficients to all orders using the many-body perturbation theory.

3.5 Size Consistency and Size Extensivity

Size consistency : A method is ‘size consistent’ if the corresponding energy of two well-separated (in the limit of infinite separation) subsystems A and B is equal to $(E_A + E_B)$, the sum of the energies of the two systems computed independently.

Consider a CI wavefunction $|\Psi_{\text{CI}}\rangle$, which is expanded in terms of a linear excitation operator, unlike the CC wavefunction,

$$|\Psi_{\text{CI}}\rangle = (1 + C) |\Phi_0\rangle$$

where C is a linear combination of various excitation operators,

$$C = C_s + C_d + C_t + \dots$$

which can be represented in a second quantized form as,

$$C = \sum_{i,a} c_i^a a_a^\dagger a_i + \frac{1}{4} \sum_{ij,ab} c_{ij}^{ab} a_a^\dagger a_b^\dagger a_i a_j + \dots \quad (3.106)$$

Truncation of the operator C to singles and double excitations (CISD) leads to a wavefunction with exactly same number of amplitudes c_i^a and c_{ij}^{ab} , as that needed for the CC singles and doubles (CCSD) approximation, t_i^a and t_{ij}^{ab} . However, the CCSD theory implicitly includes the higher excitations like triples, quadruples, through the inclusion of higher powers of T which arise inherently due to the CC exponential ansatz. Both the full CI and full CC produce exact wavefunctions. Consider the structure of the CC and CI wavefunctions for a system involving two non-interacting and infinitely separated components, A and B. It is possible to dissociate the cluster operators for the two components, assuming that the orbitals used to define T and C are localized on each of the two components,

$$T = T_A + T_B \text{ and } C = C_A + C_B$$

Hence,

$$|\Psi_{\text{CC}}\rangle = e^T |\Phi_0\rangle = e^{T_A} e^{T_B} |\Phi_0\rangle$$

Under the localized orbital description, the reference determinant $|\Phi_0\rangle$ is factorizable into independent determinants of each fragment, the total CC wavefunction can be written as a product of CC wavefunctions of each fragment. The resulting energies would then be a sum of energies of each of the fragments and would be the same as that computed for the system as a whole. In other words,

$$E_{CC} = E_{CC}^A + E_{CC}^B$$

This property is known as size consistency. Since for CI, multiplicative separability is not possible,

$$|\Psi_{CI}\rangle = (1 + C) |\Phi_0\rangle = (1 + C_A + C_B) |\Phi_0\rangle$$

the sum of the energies of the separate fragments is not equal to the energy of the system computed as a whole,

$$E_{CI} \neq E_{CI}^A + E_{CI}^B$$

If CI is nontruncated, then it is possible to write the full CI wavefunction as a product of wavefunctions for separate fragments by transforming the linear operator into an exponential. For a Hydrogen molecule, there are only two electrons to be correlated and hence CCSD and CISD are exact for this system. But the CCSD gives correct total energy and CISD doesn't due to the inseparability of the CI wavefunction.

Size extensivity : A method is said to be 'size extensive', if the energy calculated thereby scales linearly with the number of particles. The SCF and the CC methods are both 'size extensive'. Size consistency applies only to non-interacting molecular fragments, but size extensivity is a more general mathematical concept that applies to any point on the potential energy surface.

Consider the structure of the CI Shroedinger equation,

$$H_N \left(1 + C_1 + C_2 + \dots \right) \left| \Phi_0 \right\rangle = \left(E_{CI} - E_0 \right) \left(1 + C_1 + C_2 + \dots \right) \left| \Phi_0 \right\rangle$$

where H_N is the normal ordered Hamiltonian and intermediate normalization⁵ is as-

⁵ $\langle \Phi_0 | \Psi \rangle = 1$, where $|\Psi\rangle$ is the exact state.

sumed. Projecting the reference state from the left,

$$(E_{\text{CI}} - E_0) = \langle \Phi_0 | H_N (C_1 + C_2) | \Phi_0 \rangle$$

where CI expansion is truncated using Slater rules. By the application of the Wick theorem, this equation can be written in algebraic form as,

$$(E_{\text{CI}} - E_0) = \sum_{i,a} f_{ia} c_i^a + \frac{1}{4} \sum_{ij,ab} \langle ij | v | ab \rangle c_{ij}^{ab}$$

For the HF choice of the single particle orbitals, the first term is zero due to the Brillouin theorem. Assuming a localized orbital basis, for a given orbital $|\phi_i\rangle$, the two-electron integral will be zero, unless the orbitals $|\phi_j\rangle$, $|\phi_a\rangle$ and $|\phi_b\rangle$ are reasonably close to $|\phi_i\rangle$ due to the relatively short range nature of the inter-electronic potential.

Full CI is a size extensive and size consistent theory, but most truncated CI methods are neither size extensive nor size consistent.

Chapter 4

Computational Aspects of CC Theory of Closed-shell Atomic EDMs

In this chapter some important steps in the implementation of the coupled-cluster program to compute closed-shell atomic EDMs are discussed. The program is written in FORTRAN-77. The basic skeleton of the program is presented in Appendix C. The number of diagrams contributing to the EDM perturbed CC amplitudes in Eq. (3.27) are $n_{\text{total}} = 154$ with $n_{\text{sing}} = 42$ and $n_{\text{dbl}} = 102$ where n_{sing} and n_{dbl} are the number of diagrams representing the single and the double excitations respectively. The additional 10 diagrams arise from the right hand side of Eq. (3.27) from singles and doubles. The program is composed of 54 subroutines. Details of the diagrams, the angular factors, description of the program etc. can be obtained from the documentation [33].

4.1 Conventions and Symbols

The coupled-cluster equations consist of the matrix elements of the dressed residual Coulomb operator, the cluster amplitudes and the EDM operators (Eq. (3.27)). Each of these operators are expressed in terms of the creation and annihilation operators, which are represented diagrammatically as explained in Chapter 3. The matrix elements present in the coupled-cluster equations are computed by separating them into the radial and the angular parts. The angular part is manually calculated by representing each

cluster amplitude diagram by its corresponding angular momentum diagram. The closed part of an angular momentum diagram is evaluated using the JLV theorems [24]. The conventions used for the evaluation of the angular factors are shown in Fig. 4.1. In addition to the rules shown in Fig. 4.1, the arrow on the incoming free hole line is removed and the sign at the vertex formed by the three multipoles of the $T_2^{(1)}$ operator ($\lambda_1, \lambda_2, K_2$) (see Fig. 3.9) is given a ‘+’ sign by our convention. For the complete details of the angular factor evaluation, see the documentation [33].

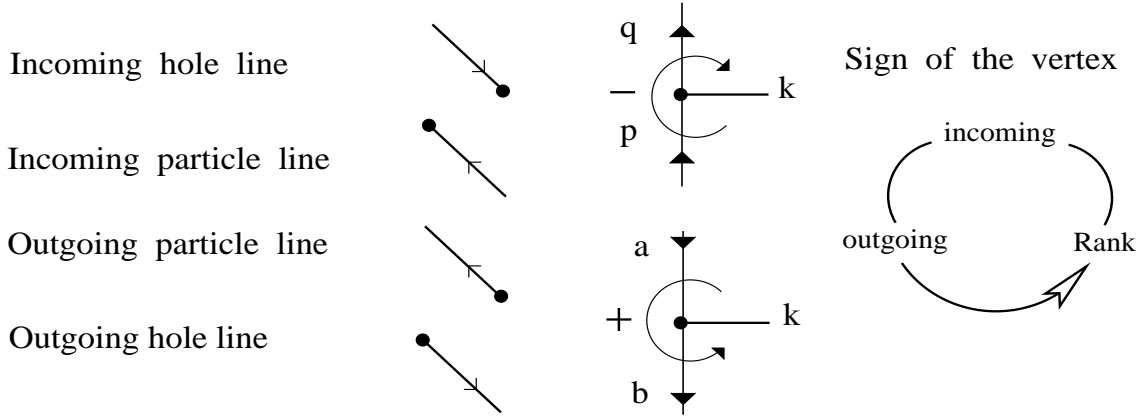


Figure 4.1: Notation for orbital lines

4.2 Implementation of the Iterative Scheme

The EDM perturbed CC equations given by Eq. (3.27) are,

$$\begin{aligned} \left\langle \Phi_a^r \left| \left\{ \overline{H}_N T^{(1)} \right\} \right| \Phi_0 \right\rangle &= - \left\langle \Phi_a^r \left| \overline{H}_{\text{EDM}} \right| \Phi_0 \right\rangle \\ \left\langle \Phi_{ab}^{rs} \left| \left\{ \overline{H}_N T^{(1)} \right\} \right| \Phi_0 \right\rangle &= - \left\langle \Phi_{ab}^{rs} \left| \overline{H}_{\text{EDM}} \right| \Phi_0 \right\rangle \end{aligned} \quad (4.1)$$

Introducing a complete set of orbitals and expanding $T^{(1)} = T_1^{(1)} + T_2^{(1)}$,

$$\begin{aligned} \sum_I \left\langle \Phi_a^r \left| \overline{H}_N \right| \Phi_I \right\rangle \left\langle \Phi_I \left| T_1^{(1)} \right| \Phi_0 \right\rangle + \sum_J \left\langle \Phi_a^r \left| \overline{H}_N \right| \Phi_J \right\rangle \left\langle \Phi_J \left| T_2^{(1)} \right| \Phi_0 \right\rangle &= - \left\langle \Phi_a^r \left| \overline{H}_{\text{EDM}} \right| \Phi_0 \right\rangle \\ \sum_I \left\langle \Phi_{ab}^{rs} \left| \overline{H}_N \right| \Phi_I \right\rangle \left\langle \Phi_I \left| T_1^{(1)} \right| \Phi_0 \right\rangle + \sum_J \left\langle \Phi_{ab}^{rs} \left| \overline{H}_N \right| \Phi_J \right\rangle \left\langle \Phi_J \left| T_2^{(1)} \right| \Phi_0 \right\rangle &= - \left\langle \Phi_{ab}^{rs} \left| \overline{H}_{\text{EDM}} \right| \Phi_0 \right\rangle \end{aligned}$$

which can be written in the form of a set of matrix equations,

$$A_1 T_1^{(1)} + A_2 T_2^{(1)} = B_1 \quad (4.2)$$

$$A_3 T_1^{(1)} + A_4 T_2^{(1)} = B_2 \quad (4.3)$$

which can be compactified as

$$A T^{(1)} = B \quad (4.4)$$

In terms of the elements of the matrices, Eq. (4.4) can be written as,

$$\begin{pmatrix} A_{11} & A_{12} \\ A_{21} & A_{22} \end{pmatrix} \begin{pmatrix} T_1^{(1)} \\ T_2^{(1)} \end{pmatrix} = \begin{pmatrix} B_{10} \\ B_{20} \end{pmatrix} \quad (4.5)$$

where A_i are identified as the dressed Coulomb Hamiltonian matrix elements which form a square matrix and B_{i0} , the matrix of the dressed EDM Hamiltonian operator, and the cluster amplitude matrix $T^{(1)}$ is a column vector. The Eq. (4.2) is first solved for $T_1^{(1)}$, with an initial guess for $T_2^{(1)}$, and is used in Eq. (4.3) to obtain a new set of $T_2^{(1)}$'s. The $T_2^{(1)}$ amplitudes are then used in Eq. (4.2) to obtain a new set of $T_1^{(1)}$ amplitudes. This procedure is repeated until convergence is achieved for both $T_1^{(1)}$ and $T_2^{(1)}$ amplitudes. In other words, we have,

$$T_{1i}^{(1,k)} = \frac{\left(B_{10,i} - \sum_j A_{ij} T_{2j}^{(1,k-1)} \right)}{A_{ii}}$$

$$T_{2j}^{(1,k)} = \frac{\left(B_{20,j} - \sum_j A_{ij} T_{2j}^{(1,k)} \right)}{A_{jj}}$$

where $k = 1, 2, 3, \dots$ is the iteration count.

Usage of the latest determined amplitudes in each iteration helps speed up the convergence of the EDM perturbed CC equations.

4.3 Complementary and Equivalent Diagrams

Complementary diagrams arise due to the contraction of an asymmetric operator ($T_2^{(1)}$) with a symmetric operator such as V_N or $T_2^{(0)}$. The asymmetric character of $T_2^{(1)}$ arises

due to the product of the parities of the two orbitals at the two vertices being opposite in sign, which gives rise to two distinct diagrams from a single contraction with any symmetric operator. While it is necessary to calculate the contributions from *complementary* diagrams, it is important to avoid repetition of the diagrams that are generated whenever the *complementary* diagrams turn out to be topologically equivalent to *normal* diagrams. One example of the diagram for which the actual and its *complementary* are distinct is shown in Fig. B.2 (CD4). The cluster amplitude diagrams are calculated in the subroutines, named after the form of the two-body Coulomb operator they arise from and are ‘called’ in the *driver* routine. The *complementary* diagrams are calculated by calling the routines of the cluster amplitudes twice, where the first and the second call to the routine differs in the arguments of the routine. The arguments corresponding to the open orbital lines of the $T_2^{(1)}$ operator ($ia, ip, ib, iq, l1, l2$) are flipped and those corresponding to the internal lines (ir, ic) are fixed. As an example consider the diagram CD4 of Fig. B.2. The *normal* and the *complementary* calls are :

```
call dpphh(ia, ip, ib, iq, ir, ic, l1, l2, ..... ) (Normal)
call dpphh(ib, iq, ia, ip, ir, ic, l2, l1, ..... ) (Complementary)
```

where the routine is named `dpphh()`, to mean that it calculates the cluster amplitude diagrams arising from the PP-HH form of the Coulomb operator ($\langle PP|V_N|HH \rangle$). It is important to note that the parity of the vertices ($ia, ip, l1$) is fixed to be odd and that of ($ib, iq, l2$), fixed to be even. The evaluation of the *complementary* diagrams this way gives rise to equivalent diagrams when the *normal* and the *complementary* diagrams are symmetric with respect to the interchange of the open orbital lines and hence are not distinct. Equivalent diagrams for the unperturbed and perturbed coupled-cluster amplitudes originate due to the presence of diagrams of symmetric topology, which results in the repeated evaluation of the cluster diagrams that are not distinct. In this thesis, we discuss only the equivalent diagrams arising from the implementation of the linear EDM perturbed CC amplitudes. These diagrams in particular arise from the contraction of the diagrams of the kind where the Coulomb operator and a cluster amplitude operator are involved ($V_N T_2^{(1)}$). The cluster diagrams arising from the contraction of the four-

particle, (two-particle, two-hole) and four-hole forms of the Coulomb operator and the cluster amplitude $T_2^{(1)}$, generate equivalent diagrams. In the next few sections, we explain in detail, the diagrams that contribute to the double counting of cluster amplitude diagrams in linear CCEDM and the numerical factors associated with them to account for it. For the $T_2^{(1)}$ diagrams, the outermost loops correspond to the orbital indices $(ia, ip, ib, iq, l1, l2)$. Due to the parity condition at the two vertices of the $T_2^{(1)}$ diagram, the simultaneous flip of (ia, ib) and (ip, iq) is not allowed during the loop execution. But, the flip of either (ia, ib) or (ip, iq) is possible. In the following sections, we consider these issues separately for the cluster diagrams arising from the (four-particle), (four-hole), (two-particle — two-hole), (three-particle (three-hole) — one-hole (one-particle)) form of the Coulomb operator and deduce the factors associated with them. For the cluster diagrams arising from the (four-particle) and (four-hole) form of the Coulomb operator, evaluation of the equivalent diagrams amounts to evaluating the diagrams identical to the mirror reflection of the original diagrams.

4.3.1 Four Particle Form of the Coulomb Operator

Consider the diagram shown in Fig. 4.2. The *normal* and the *complementary* diagrams are equivalent for the cluster diagram with the bare Coulomb operator, but not for the diagram with the dressed Coulomb operator, which contributes through linear CCEDM. Therefore, the *complementary* diagrams need to be calculated with a factor (1/2) for the diagram Fig. 4.2 (I).

Exactly the same arguments given above are valid for the cluster amplitude diagrams arising from the (four-hole) form of the Coulomb operator. Hence, these diagrams are calculated along with the *complementary* diagrams, including a numerical factor (1/2) for the cluster diagram arising from the bare Coulomb operator and no factor is associated with the cluster diagrams arising from the dressed Coulomb operator.

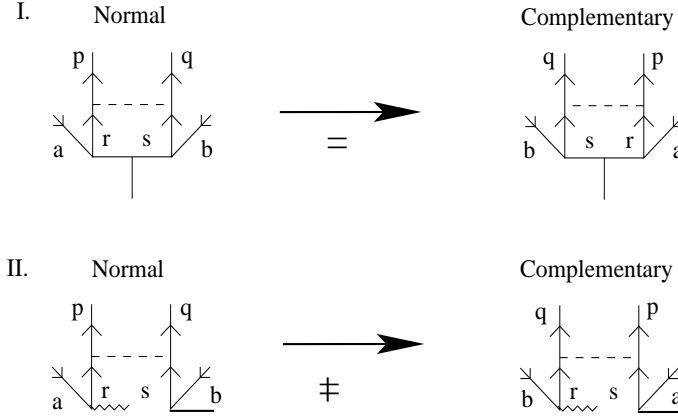


Figure 4.2: Equivalent diagrams - Diagram (I) shows the contraction between the bare-Coulomb and $T_2^{(1)}$ operators and diagram (II), the dressed Coulomb ($H_N T_1^{(0)}$) and $T_1^{(1)}$ operator.

4.3.2 Two-Particle – Two-Hole Form of the Coulomb Operator

The cluster diagrams arising from the (two-particle — two-hole) form of the Coulomb operator contributing to the linear CCEDM is shown in Fig. 4.3. Note that there are no equivalent diagrams as the *normal* and *complementary* diagrams are distinct.

4.3.3 Three-Particle (Three-Hole) – One-Hole (One-Particle) Form of the Coulomb Operator

The cluster diagrams arising from the (three-particle, one-hole) and (one-particle, three-hole) form of the Coulomb operator are shown in Fig. 4.4. The *complementary* diagrams are distinct from the *normal* diagrams and hence there is no numerical factor associated with the diagrams.

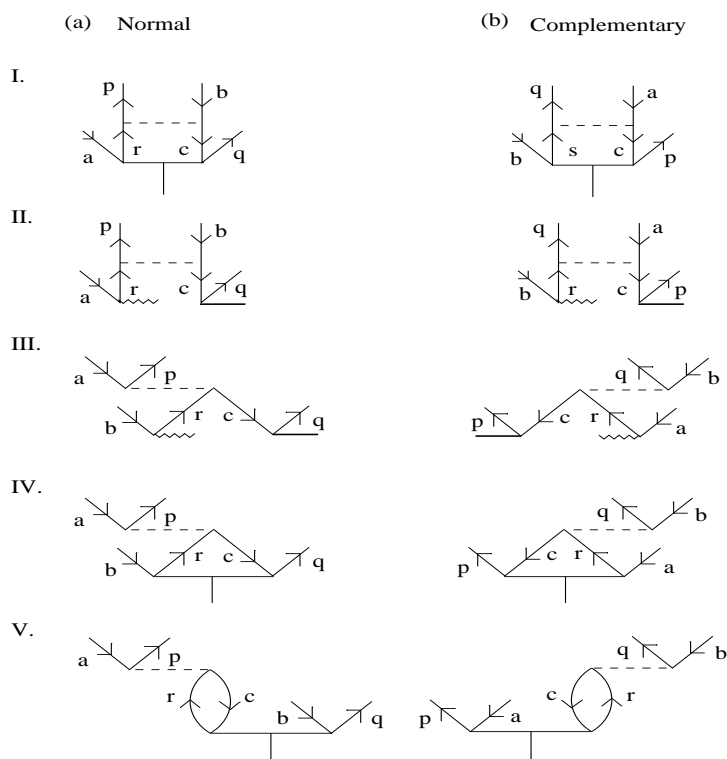


Figure 4.3: The *normal* and *complementary* diagrams are all distinct and hence there is no numerical factor associated with these diagrams.

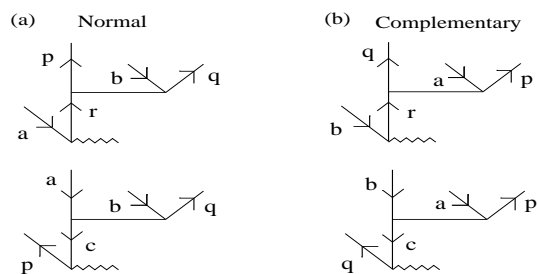


Figure 4.4: The *normal* and *complementary* diagrams are all distinct and hence there are no numerical factors associated with them.

4.4 Intermediate Storage Scheme

Consider a diagram contributing to CCEDM equations shown in Fig. 4.5(a). This diagram contains four particle and four hole lines. To calculate this diagram, the total number of operations required is $= n_h^4 \times n_p^4$. For a reasonable basis, with number of occupied (holes) and unoccupied (particles) orbitals given by $n_h = 22$ and $n_p = 40$, the number of operations would be $\approx 6 \times 10^{11}$. Such diagrams demand a large amount of computational time. Using the Intermediate Storage Scheme (IMS), it is possible to reduce the number of operations by calculating an intermediate diagram, (a portion of the complete diagram) that is commonly present in a set of diagrams, only once and storing it. Such diagrams are termed as effective diagrams and the cluster amplitude diagrams are then calculated in terms of these effective diagrams. The diagram in Fig. 4.5(a) is termed as an EDM-IMS diagram, where the portion of the diagram, $\overline{V_N T_2^{(1)}}$ is calculated and stored in terms of an effective diagram and used later to calculate the actual diagram as shown in Fig. 4.5(b). The number of operations now become $= n_h^2 \times n_p^3 + n_h^3 \times n_p^2 = 2n_h^2 \times n_p^3 = 6 \times 10^7$ which is reduced by a factor $(1/2)n_h^2 n_p = 10^4$. The CCEDM diagrams arising from the (2-particle — 2-hole) form of the Coulomb operator have been classified into EDM-IMS and Coulomb-IMS diagrams based on the topology of the diagram and the number of orbital lines connected to $T_2^{(0)}$ and $T_2^{(1)}$ respectively. The IMS diagrams are calculated only once and are used for further calculation of the complete cluster amplitude diagrams arising from the particular kind of IMS diagrams. At present, this scheme has been implemented only for the (2-particle — 2-hole), but in general can be used for the diagrams involving orbital lines as large as 6 - 8 because such diagrams consume a large amount of CPU time due to the execution of loops corresponding to the orbital lines. The Fig. 4.6 shows the cluster diagrams that require EDM-IMS storage. The diagrams contributing to EDM-IMS diagrams are shown in Fig. 4.7, 4.8 and those contributing to the Coulomb-IMS are shown in Fig. 4.9. These diagrams are of (hole - hole) or (particle - particle) form. The actual cluster amplitudes are then obtained by the contraction of the effective IMS diagrams with the corresponding cluster operator diagrams - the $T_2^{(1)}$ diagram for Coulomb-IMS and $T_2^{(0)}$ for EDM-IMS

diagrams. The possible cluster diagrams in terms of the IMS diagrams are shown in Fig. 4.10. For details on the cluster diagrams calculated using Coulomb-IMS diagrams, refer to the documentation [33]. The pseudo code is presented in Appendix C.

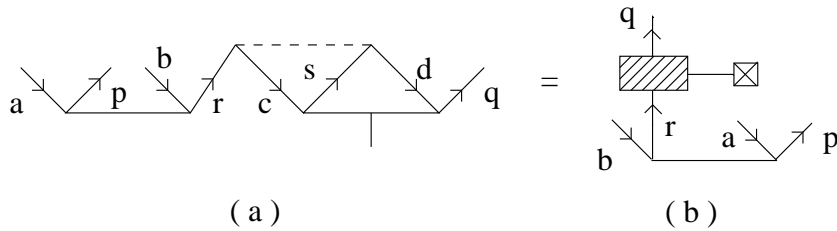


Figure 4.5: EDM-IMS diagram (particle-particle type) contracted with $T_2^{(0)}$.

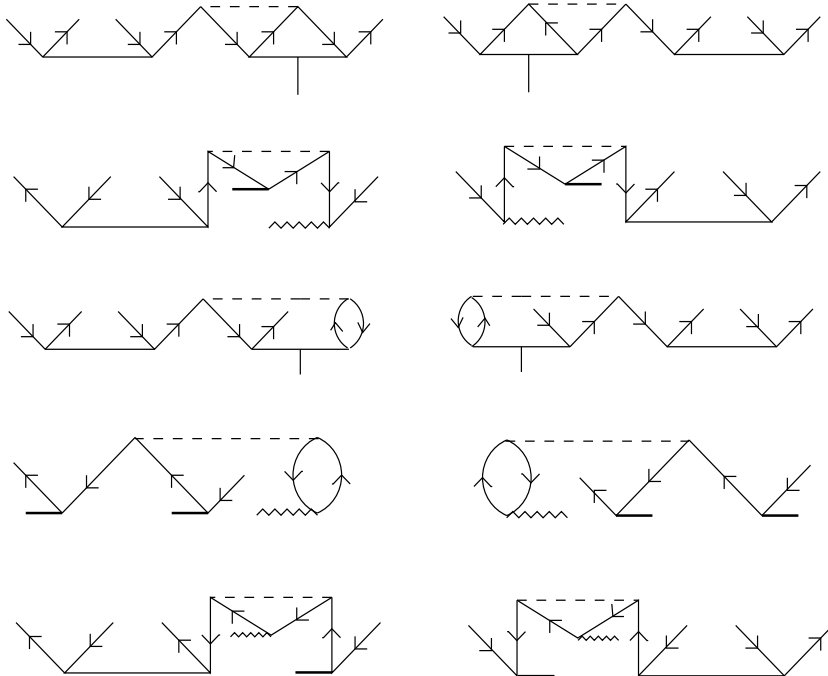


Figure 4.6: Cluster diagrams that are calculated using EDM-IMS diagrams - They arise from the terms $V_N T_2^{(1)}$ and $V_N T_1^{(0)} T_1^{(1)}$.

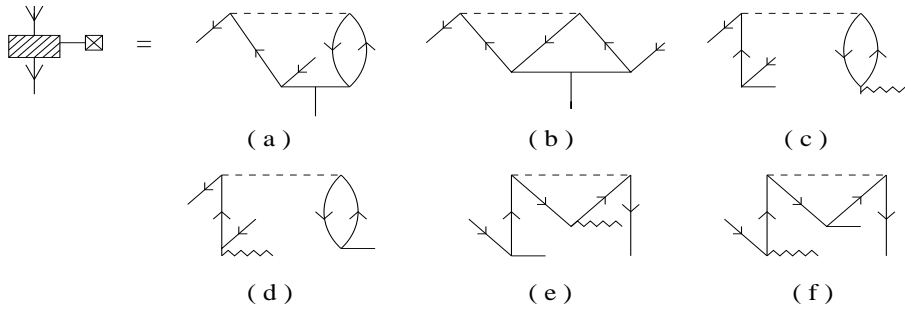


Figure 4.7: H_{EDM} perturbed hole-hole one-body IMS diagrams.

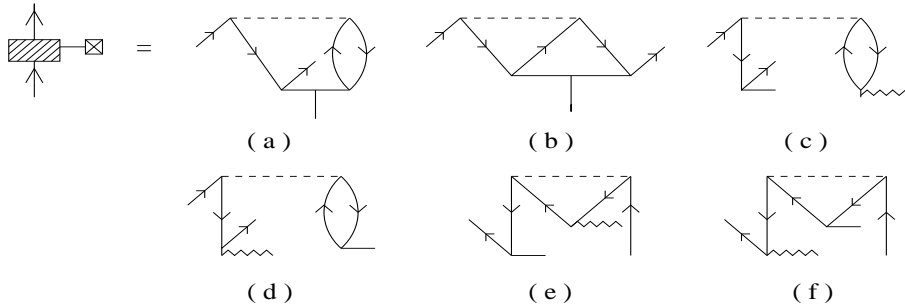


Figure 4.8: H_{EDM} perturbed particle-particle one-body IMS diagrams.

From the topology of the EDM-IMS diagrams it is interesting to note that the rotation of the free lines of the Coulomb vertices generates a diagram which is topologically identical to the cluster diagrams arising from the singles CCEDM equations. This is a very useful observation which enabled us to use our program where the singles cluster amplitude diagrams are calculated (in particular, the cluster diagrams arising from the (3-particle — 1-hole) and (3-hole — 1-particle) form of Coulomb diagrams).

The EDM-IMS diagrams are only a one-body kind, whereas the Coulomb-IMS diagrams are both one- and two - body kind. The two-body Coulomb-IMS diagrams are shown in Fig. 4.11. The angular factors of the IMS diagrams can be obtained from the documentation [33].

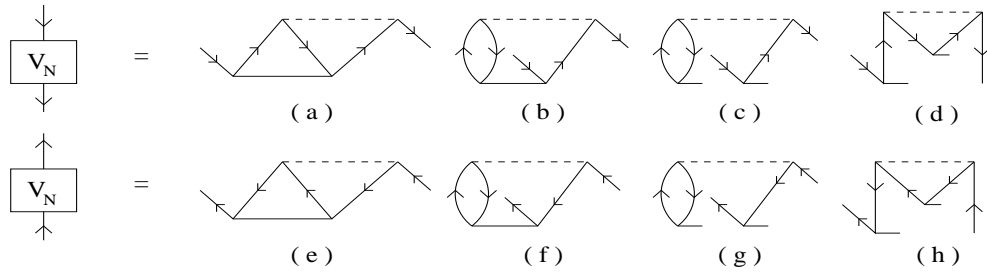


Figure 4.9: One-body V_N effective diagrams

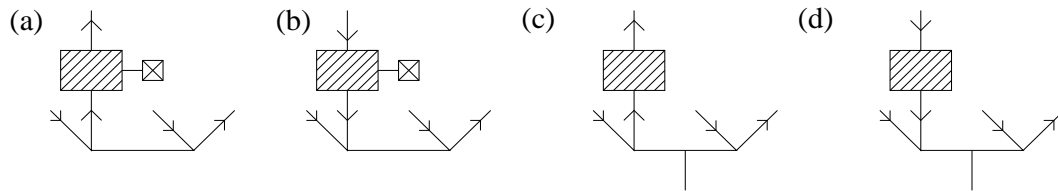


Figure 4.10: (a)& (b) - Cluster diagrams arising from hole-hole and particle-particle H_{EDM} perturbed IMS diagrams, (c)& (d) - cluster diagrams arising from hole-hole and particle-particle Coulomb-IMS diagrams.

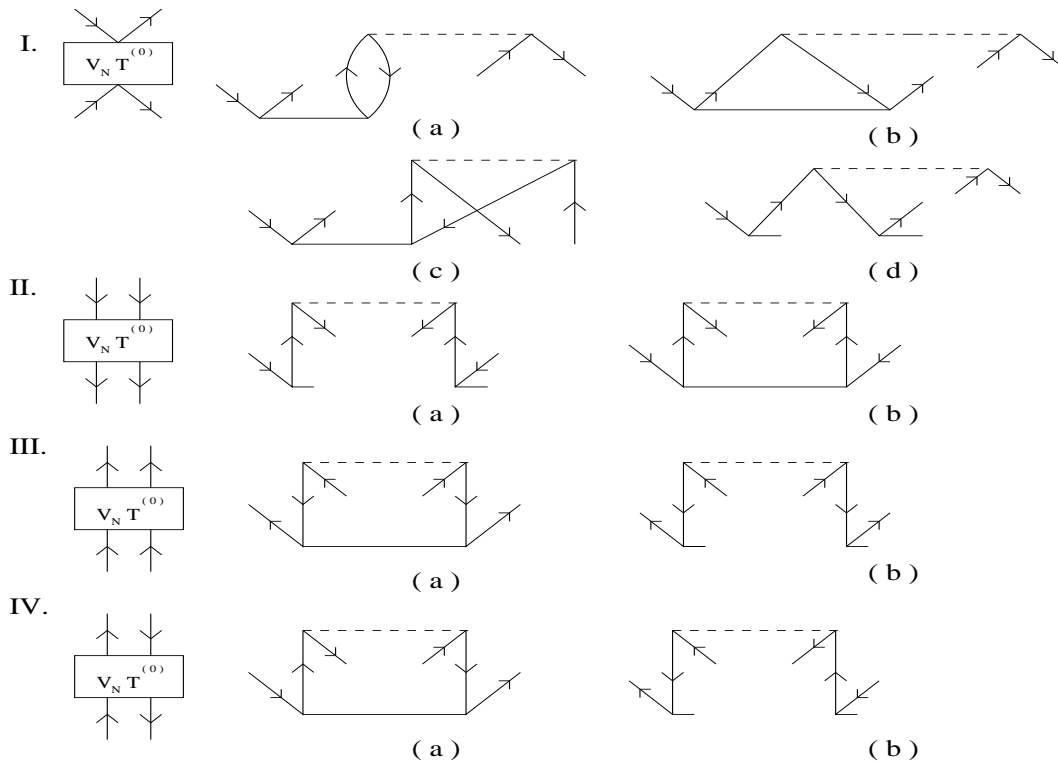


Figure 4.11: Two-body V_N effective diagrams - ph-hp(I), hh-hh(II), pp-pp(III), ph-ph(IV)

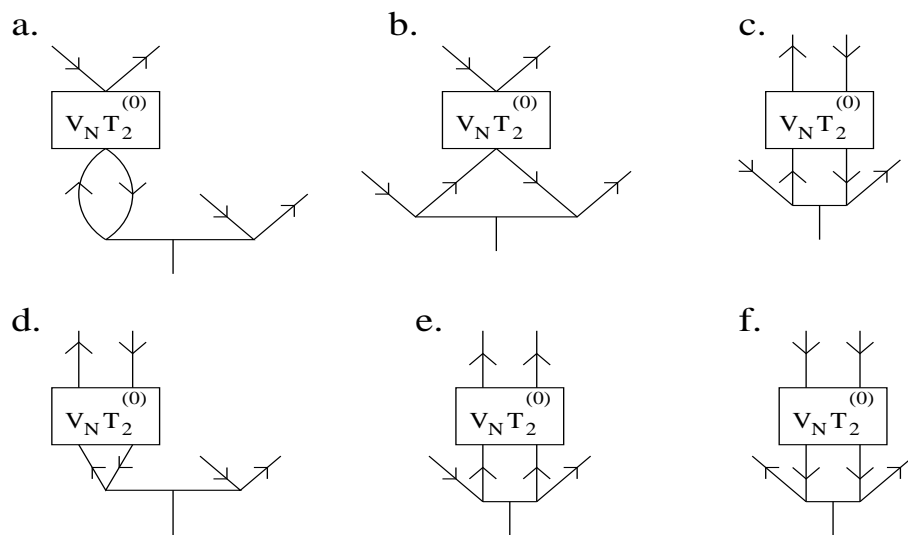


Figure 4.12: Cluster diagrams arising from the two-body Coulomb-IMS diagrams - contraction of IMS diagrams with $T_2^{(1)}$.

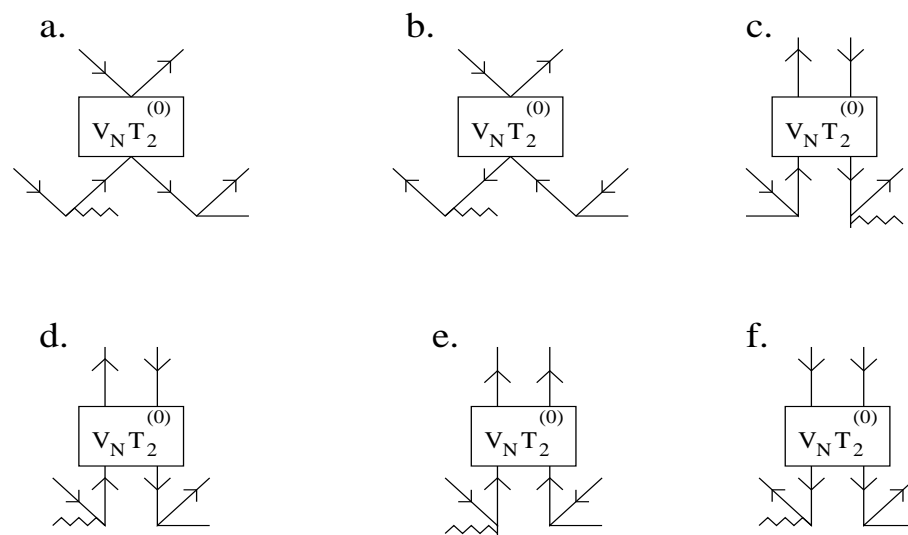


Figure 4.13: Cluster diagrams arising from the two-body Coulomb-IMS diagrams - contraction of IMS diagrams with $T_1^{(0)}T_1^{(1)}$.

4.5 Evaluation of Atomic EDM

The atomic EDM in the coupled-cluster formalism is given by Eq. (3.60),

$$D_a = 2 \left[\left\langle \Phi_1 \left| D e^{T^{(0)}} \right| \Phi_0 \right\rangle + \left\langle \Phi_1 \left| \sum_{n=1}^{\infty} \frac{1}{n!} \left(T^{(0)\dagger} \right)^n D e^{T^{(0)}} \right| \Phi_0 \right\rangle \right] \quad (4.6)$$

The terms contributing to the zeroth and the first order (n=1 in Eq. (4.6)) are

$$D_a^0 = \left\langle \Phi_1 \left| D e^{T^{(0)}} \right| \Phi_0 \right\rangle \quad (4.7)$$

$$= \left\langle \Phi_1 \left| D e^{T^{(0)}} \right| \Phi_0 \right\rangle = \underbrace{\left\langle \Phi_0 \left| T_1^{(1)\dagger} D e^{T^{(0)}} \right| \Phi_0 \right\rangle}_{Z1} + \underbrace{\left\langle \Phi_0 \left| T_2^{(1)\dagger} D e^{T^{(0)}} \right| \Phi_0 \right\rangle}_{Z2} \quad (4.8)$$

and

$$\begin{aligned} \left\langle \Phi_1 \left| T^{(0)\dagger} D e^{T^{(0)}} \right| \Phi_0 \right\rangle &= \left\langle \Phi_0 \left| \left[T_1^{(1)\dagger} + T_2^{(1)\dagger} \right] T^{(0)\dagger} D e^{T^{(0)}} \right| \Phi_0 \right\rangle \\ &= \left\langle \Phi_0 \left| \underbrace{T_1^{(1)\dagger} T^{(0)\dagger} D e^{T^{(0)}}}_{F1} \right| \Phi_0 \right\rangle + \left\langle \Phi_0 \left| \underbrace{T_2^{(1)\dagger} T^{(0)\dagger} D e^{T^{(0)}}}_{F2} \right| \Phi_0 \right\rangle \end{aligned}$$

The terms F1 and F2 are given by,

$$F1 = F1(A) + F1(B); F2 = F2(A) + F2(B)$$

where

$$\begin{aligned} F1(A) &= \left\langle \Phi_0 \left| T_1^{(1)\dagger} \left(T_1^{(0)\dagger} D e^{T^{(0)}} \right)_1 \right| \Phi_0 \right\rangle \\ F1(B) &= \left\langle \Phi_0 \left| T_1^{(1)\dagger} \left(T_2^{(0)\dagger} D e^{T^{(0)}} \right)_1 \right| \Phi_0 \right\rangle \\ &\quad \underbrace{\hspace{10em}}_{F1(B)} \end{aligned}$$

and

$$\begin{aligned} F2(A) &= \left\langle \Phi_0 \left| T_2^{(1)\dagger} \left(T_1^{(0)\dagger} D e^{T^{(0)}} \right)_2 \right| \Phi_0 \right\rangle \\ F2(B) &= \left\langle \Phi_0 \left| T_2^{(1)\dagger} \left(T_2^{(0)\dagger} D e^{T^{(0)}} \right)_2 \right| \Phi_0 \right\rangle \end{aligned}$$

As explained in Chapter.3, the terms contributing through the dressed electric dipole operator in Eq. (4.8) are,

$$\begin{aligned} \left(De^{T^{(0)}}\right)_1 &= \frac{1}{2!}DT_1^{(0)2} + DT_2^{(0)} + DT_1^{(0)} + D \\ \left(De^{T^{(0)}}\right)_2 &= \frac{1}{3!}DT_1^{(0)3} + DT_1^{(0)}T_2^{(0)} + \frac{1}{2!}DT_1^{(0)2} + DT_2^{(0)} + DT_1^{(0)} \end{aligned}$$

The diagrams arising from the term $\left(De^{T^{(0)}}\right)_1$ shown in Fig. 3.11 are topologically identical to the diagrams contributing to the right hand side of the singles CCEDM equations (Eq. (3.7)), with the H_{EDM} operator replaced by the D operator. Similarly, the connected diagrams arising from the term $\left(De^{T^{(0)}}\right)_2$ are topologically identical to the diagrams on the right hand side of the CCEDM equation for the doubles. Hence, the programs developed for the calculation of the B matrix (see Eq. (3.49)) for the singles and the doubles are used to calculate $Z1$, $Z2$ and $F1(A)$, with the replacement of the H_{EDM} operator by the D operator. The term $F1(B)$ involves the calculation of $\left(De^{T^{(0)}}\right)_3$, given by

$$\left(De^{T^{(0)}}\right)_3 = \left(De^{T^{(0)}}\right)_2^{\text{conn}} \times T_1^{(0)} + \left(De^{T^{(0)}}\right)_1 \left[\frac{1}{2!}T_1^{(0)2} + T_2^{(0)} \right].$$

The diagrams representing $F1(B)$ are topologically equivalent to the nonlinear EDM cluster amplitude diagrams for singles arising from the (particle-hole — particle hole) form of the Coulomb operator, where $T_1^{(1)\dagger}$ is replaced by the electric dipole operator, D .

The effective diagrams of $F2(B)$ are obtained by the multiplication of $T_2^{(0)}$ by diagrams of $\left(De^{T^{(0)}}\right)_4$ given by,

$$\left(De^{T^{(0)}}\right)_4 = \left(De^{T^{(0)}}\right)_2^{\text{conn}} \left[\frac{1}{2!}T_1^{(0)2} + T_2^{(0)} \right] + \left(De^{T^{(0)}}\right)_1 \left[\frac{1}{3!}T_1^{(0)3} + T_2^{(0)}T_1^{(0)} \right].$$

The resultant diagrams have the same topology as the diagrams arising from the terms $\left(V_N T_1^{(0)} T_1^{(0)} T_2^{(1)}\right)$, $\left(V_N T_2^{(0)} T_2^{(1)}\right)$, $\left(V_N T_1^{(0)} T_1^{(0)} T_1^{(0)} T_1^{(1)}\right)$, $\left(V_N T_1^{(0)} T_2^{(0)} T_1^{(1)}\right)$, where the residual Coulomb operator has a PH-PH form and is hence replaced by the operator $T_2^{(0)\dagger}$. This enabled us to use the same programs that were written for the calculation of the cluster amplitude diagrams mentioned above, for calculating $F2(A)$.

Chapter 5

Analysis of Hg EDM Results

The single particle orbitals for all calculations in the subsequent sections were generated using the Gaussian basis set expansion whose salient features are presented in this section. In the central field approximation, the solution of the Dirac equation in terms of the four component spinors is given by

$$\Psi_{n\kappa m}(r, \theta, \phi) = r^{-1} \begin{pmatrix} P_{n\kappa}(r) \chi_{\kappa m}(\theta, \phi) \\ iQ_{n\kappa}(r) \chi_{-\kappa m}(\theta, \phi) \end{pmatrix}$$

where $P_{n\kappa}(r)$ and $Q_{n\kappa}(r)$ are the large and the small components of the radial wavefunctions expanded in terms of the basis set[34],

$$\begin{aligned} P_{n\kappa}(r) &= \sum_p C_{\kappa p}^L g_{\kappa p}^L(r) \\ Q_{n\kappa}(r) &= \sum_p C_{\kappa p}^S g_{\kappa p}^S(r) \end{aligned}$$

where the summation over the index p runs over the number of basis functions N , $g_{\kappa p}^L(r)$ and $g_{\kappa p}^S(r)$ correspond to the large and small components and $C_{\kappa p}^L$ and $C_{\kappa p}^S$ are their expansion coefficients for each value of κ . This is known as the method of Finite Basis Set Expansion (FBSE). The functions $g_{\kappa p}^L(r)$ are chosen to be Gaussian Type Orbitals (GTOs) of the form,

$$g_{\kappa p}^L(r) = C_{N_{\kappa p}}^L r^{n_{\kappa}} e^{-\alpha_p r^2}$$

where $\alpha_p = \alpha_0 \beta^{p-1}$, where α_0 and β are input parameters and $n_{\kappa} = 1$ for s , 2 for p and so on and $C_{N_{\kappa p}}^L$ is the normalization factor for the large component. The large and small components are related by [35, 36]

$$g_{\kappa p}^S(r) = C_{N_{\kappa p}}^S \left(\frac{d}{dr} + \frac{\kappa}{r} \right) g_{\kappa p}^L(r)$$

where

$$C_{N\kappa p}^L = \sqrt{\frac{\alpha_p}{2n_\kappa - 1} \left[4(\kappa^2 + \kappa + n_\kappa) - 1 \right]}$$

The coefficients $C_{N\kappa p}^{L,S}$ are obtained by the diagonalization of the Fock matrix [34]. The calculations presented in this thesis correspond to the Even Tempered (ET) basis set, where the parameters α_0 and β are different for different symmetries. Though ET basis leads to a huge number of basis functions, large scale coupled-cluster calculations have been performed with the currently available computational resources. The nuclear density $\rho_N(r)$ for the Fermi type distribution of the nuclear structure is given by,

$$\rho_N(r) = \frac{\rho_0}{1 + e^{(r-c)/a}}$$

where r is the electronic coordinate. The nuclear radius is taken as the root mean square radius of the nucleus [37]. It is approximately related to the isotope number via the formula,

$$\sqrt{\langle r_{\text{rms}}^2 \rangle} = 0.836A^{1/3} + 0.570 \text{ fm}$$

where A is the mass number of the nucleus. a and c are the nuclear parameters, where a is the skin thickness parameter, $a = 2.3/4\ln 3$ and c is the half-charge radius given by, $\sqrt{(5r_{\text{rms}}^2/3 - 7a^2\pi^2/3)}$ [38]. The quantity ρ_0 is determined by normalising the nuclear density over a spherical volume. The radial grid has the form, $r_k = r_0 (e^{(k-1)h} - 1)$, $k = 1, 2, 3, \dots, n_p$, n_p is the total number of grid points.

5.1 Accuracy of the Single Particle Wavefunctions

The comparison of the single particle basis sets used in all the subsequent calculations, with the orbitals generated using the numerical approach with the GRASP2 DF code [39] is presented in this section. In this approach, the Dirac-Fock equation is solved numerically. The single particle wavefunctions and the energies of the core and the virtual orbitals are calculated step by step. This approach generates only the bound orbitals, but the analytical approach explained in the previous section using the FBSE method, produces both the bound and the continuum orbitals in one stroke. The accuracy of the

orbitals generated using the FBSE approach depends on the choice of the parameters α_0 and β . The large and the small components of the relativistic wavefunction generated using the analytical approach for a particular choice of these parameters can be compared with those generated using the numerical approach. The most important criterion which determines the accuracy of the properties is the convergence of the basis set. The convergence of the properties with the size of the basis and the choice of the α_0 and β parameters is related to the completeness of the basis considered. The results of this comparison are shown for the large component in Fig. 5.1, 5.2, 5.3, 5.4, 5.5 for selected orbitals in each symmetry. The horizontal axis corresponds to the radial grid in atomic units whose form is given in the previous section and the vertical axis is the relative percentage error given by $\left| \left| P_{\text{Grasp}}(r) \right| - \left| P_{\text{Gauss}}(r) \right| \right| / \left| P_{\text{Grasp}}(r) \right|$.

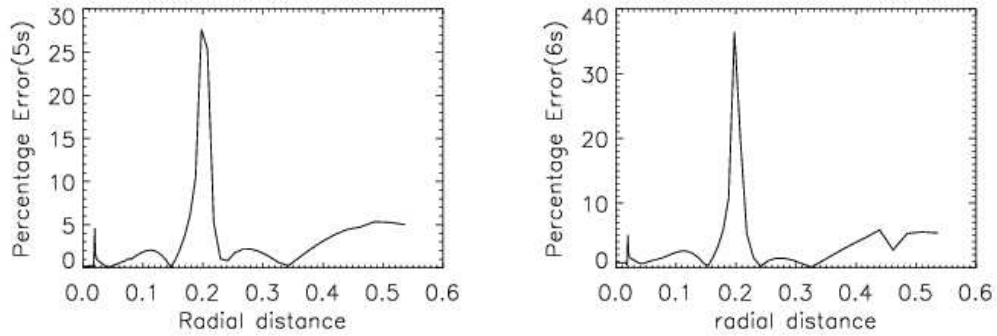


Figure 5.1: Relative percentage error for $5s_{1/2}$ and $6s_{1/2}$. The distance is presented in atomic units.

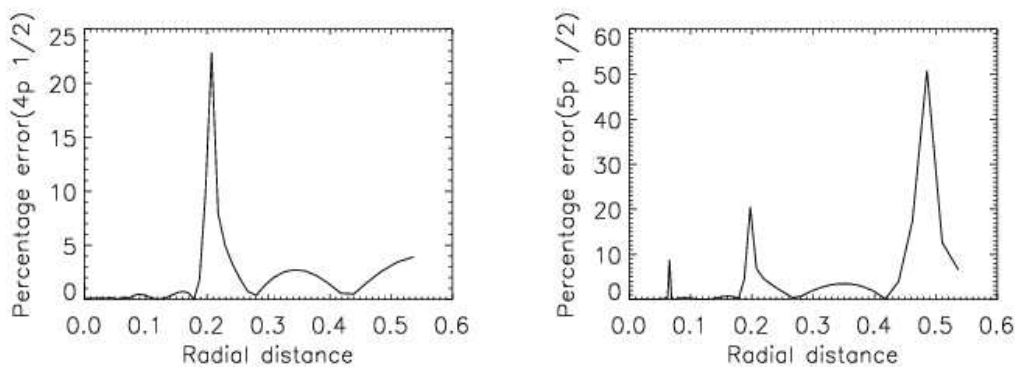


Figure 5.2: Relative percentage error for $4p_{1/2}$ and $5p_{1/2}$. The distance is presented in atomic units.

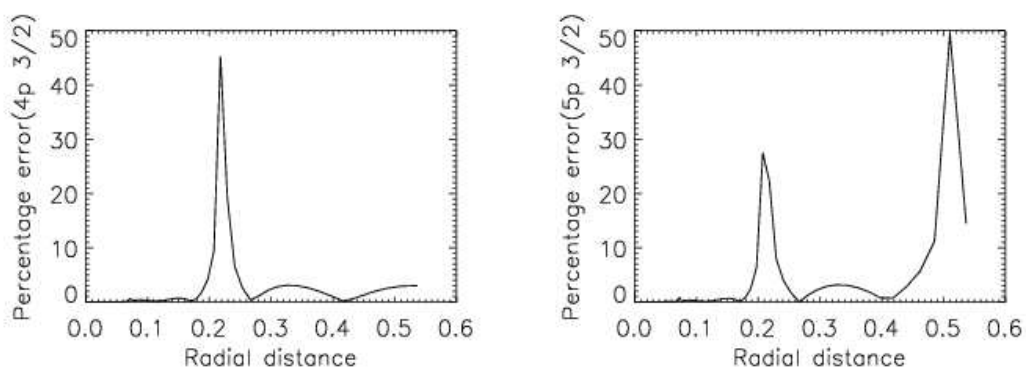


Figure 5.3: Relative percentage error for $4p_{3/2}$ and $5p_{3/2}$. The distance is presented in atomic units.

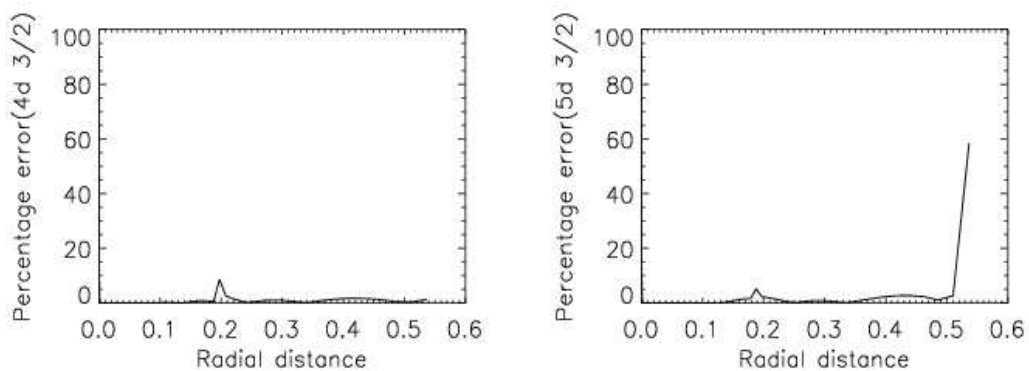


Figure 5.4: Relative percentage error for $4d_{3/2}$ and $5d_{3/2}$. The distance is presented in atomic units.

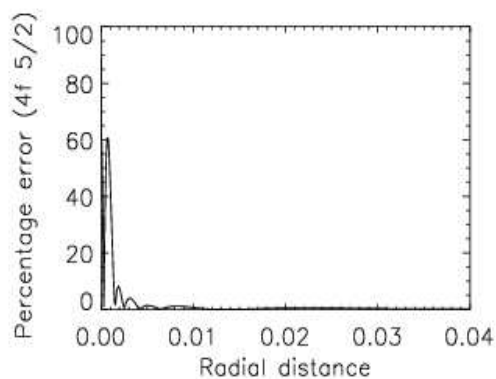


Figure 5.5: Relative percentage error for $4f_{5/2}$. The distance is presented in atomic units.

Table 5.1: Number of basis functions used to generate the even tempered Dirac-Fock orbitals and the corresponding value of α_0 and β used. The total number of active orbitals are shown in the brackets for ‘Active holes’.

	$s_{1/2}$	$p_{1/2}$	$p_{3/2}$	$d_{3/2}$	$d_{5/2}$	$f_{5/2}$	$f_{7/2}$	$g_{7/2}$	$g_{9/2}$
Number of basis	31	32	32	20	20	20	20	10	10
$\alpha_0(\times 10^{-5})$	725	715	715	700	700	695	695	655	655
β	2.725	2.715	2.715	2.700	2.700	2.695	2.695	2.655	2.655
Active holes (36)	2	2	2	2	2	1	1	1	1
Active holes (39)	3	3	3	2	2	1	1	1	1
Active holes (43)	3	3	3	3	3	2	2	1	1
Active holes (45)	3	3	3	3	3	3	3	1	1
Active holes (51)	5	5	5	3	3	3	3	1	1
Active holes (57)	7	7	7	3	3	3	3	1	1
Active particles	6	4	4	3	3	1	1	0	0

For all the subsequent calculations in this thesis, the details of the basis used is shown in Table 5.1.

5.2 Calculation of Correlation Energy

The reduction of the perturbed CC equations to the unperturbed CC equations as shown in Section 3.1.3 can serve as a good check for the CCEDM code. After a suitable reduction, the perturbed CC equations acquire the same mathematical structure as the unperturbed CC equations. The calculation of the unperturbed amplitudes from CCEDM equations in the limit $H_{\text{EDM}} \rightarrow 0$ at the linear level has been performed and compared with a completely independent program, known as the CC with Singles and the Doubles (CCSD)[40] under the linear approximation. The $T^{(0)}$ amplitudes obtained from the two methods are in good agreement.

The correlation energy is calculated starting from the Eq. (3.8),

$$e^{-T} \left(H_N + E_{\text{HF}} \right) e^T \left| \Phi_0 \right\rangle = E \left| \Phi_0 \right\rangle$$

Projecting by the reference state on both sides of the above equation,

$$\left\langle \Phi_0 \left| e^{-T} \left(H_N + E_{\text{HF}} \right) e^T \right| \Phi_0 \right\rangle = E \left\langle \Phi_0 \left| \Phi_0 \right\rangle \right. \quad (5.1)$$

Hence,

$$E_{\text{corr}} = \left\langle \Phi_0 \left| \overline{H}_N \right| \Phi_0 \right\rangle$$

where $E_{\text{corr}} = E - E_{\text{HF}}$. In linear CC theory, the diagrams contributing to the correlation energy are shown in Fig. 5.6.

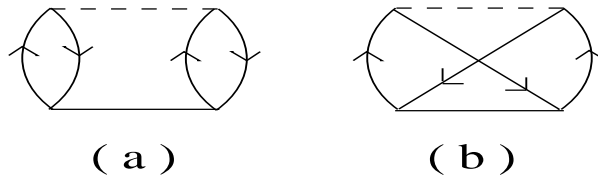


Figure 5.6: Correlation energy diagrams in linear coupled-cluster theory.

Table 5.1 shows the details of the number of basis functions used to generate the Gaussian basis set and the active orbitals used in the present calculation. The comparison of the correlation energy calculated using the cluster amplitudes generated by two

independent codes has been done for a variety of basis sets. The results obtained in the two cases are in good agreement with each other. This constitutes a very good check for the validity of the linear CCEDM code used in the atomic EDM calculations. The results of the correlation energy using the CCEDM code after appropriate changes are shown in Table 5.2.

Table 5.2: Correlation energies calculated with converged unperturbed cluster amplitudes in atomic units

Basis	E_{corr} (linear CCEDM reduced to CCSD)
36	-2.33×10^{-3}
39	-1.64×10^{-2}
43	-1.86×10^{-2}
45	-1.91×10^{-2}
51	-0.78×10^{-1}
57	-1.79×10^{-1}

5.2.1 Application of CC Theory to Polarizability

5.2.1.1 Static Polarizability

The concept of polarizability arises from the interaction of electric field with matter. In the presence of an external electric field, a neutral atom gets polarized, where the positive and negative charge distributions shift from their original positions and reach an equilibrium. This gives rise to an induced electric dipole moment on the atom \mathbf{D}_{ind} which points in the same direction as the external electric field \mathcal{E} and is proportional to it : $\mathbf{D}_{\text{ind}} = \alpha \mathcal{E}$. The constant of proportionality α is called the atomic polarizability. An external time dependent electric field gives rise to dynamic polarizability. We now derive the expression for static polarizability from first principles using quantum mechanics. The polarizability is identified by considering the interaction of an atom with an uniform external electric field.

The induced electric dipole moment is the expectation value of the electric dipole operator in the states perturbed by the interaction $H' = -\vec{D} \cdot \vec{\mathcal{E}}$. It is given by,

$$D_{\text{ind}} = \left\langle \Psi_a \left| D \right| \Psi_a \right\rangle$$

where $|\Psi_a\rangle = |\Psi_a^{(0)}\rangle + |\Psi_a^{(1)}\rangle$ and

$$|\Psi_a^{(1)}\rangle = \sum_I |\Psi_I^{(0)}\rangle \frac{\langle \Psi_I^{(0)} | H' | \Psi_a^{(0)} \rangle}{E_a^{(0)} - E_I^{(0)}}$$

Hence,

$$D_{\text{ind}} = 2 \times \left\langle \Psi_a^{(0)} \left| D \right| \Psi_a^{(1)} \right\rangle \quad (5.2)$$

$$= -2 \sum_I \frac{\langle \Psi_a^{(0)} | D | \Psi_I^{(0)} \rangle \langle \Psi_I^{(0)} | D | \Psi_a^{(0)} \rangle}{E_a^{(0)} - E_I^{(0)}} \mathcal{E} \quad (5.3)$$

Hence, the polarizability can be identified as,

$$\alpha = -2 \sum_I \frac{\langle \Psi_a^{(0)} | D | \Psi_I^{(0)} \rangle \langle \Psi_I^{(0)} | D | \Psi_a^{(0)} \rangle}{(E_a^{(0)} - E_I^{(0)})} \quad (5.4)$$

The above expression suggests that the polarizability of a system in a given state can be determined by taking the expectation value of the electric dipole operator D in that state when it is perturbed by D itself. Let

$$|\Psi_a^{(D)}\rangle = \sum_I |\Psi_I^{(0)}\rangle \frac{\langle \Psi_I^{(0)} | D | \Psi_a^{(0)} \rangle}{(E_a^{(0)} - E_I^{(0)})} \quad (5.5)$$

where $|\Psi^{(0)}\rangle$ and $|\Psi^{(D)}\rangle$ are the unperturbed and the first order electric dipole perturbed wavefunctions respectively and $E^{(0)}$ are the unperturbed energy eigenvalues. The unperturbed atomic Hamiltonian H_0 satisfies the Schrödinger equation,

$$\left(H_0 - E_a^{(0)} \right) |\Psi_a^{(0)}\rangle = 0$$

Operate $(H_0 - E_a^{(0)})$ on both sides of Eq. (5.5),

$$\begin{aligned} (H_0 - E_a^{(0)}) \left| \Psi_a^{(D)} \right\rangle &= \sum_I (H_0 - E_a^{(0)}) \left| \Psi_I^{(0)} \right\rangle \frac{\langle \Psi_I^{(0)} | D | \Psi_a^{(0)} \rangle}{(E_a^{(0)} - E_I^{(0)})} \\ &= - \sum_I \left| \Psi_I^{(0)} \right\rangle \langle \Psi_I^{(0)} | D | \Psi_a^{(0)} \rangle \end{aligned}$$

since $|\Psi_I^{(0)}\rangle$ is an eigen function of H_0 . Since D is an odd parity operator, $|\Psi_I^{(0)}\rangle$ must be opposite in parity to $|\Psi_a^{(0)}\rangle$. Using this fact and the completeness condition, we get

$$(H_0 - E_a^{(0)}) \left| \Psi_a^{(D)} \right\rangle = -D \left| \Psi_a^{(0)} \right\rangle \quad (5.6)$$

The polarizability can therefore be determined as $\alpha = -2 \langle \Psi_a^{(0)} | D | \Psi_a^{(D)} \rangle$ (see Eq. (5.4)). The CC equations for polarizability are similar to the CCEDM equations (Eq. (3.27)) with the H_{EDM} operator being replaced by the electric dipole operator. (Eq. (3.27)) The polarizability calculations are necessary in principle to get an idea about the accuracy of our perturbed CC approach and our code based on it to calculate the EDM of closed-shell atoms. The sample calculation of polarizability for atomic ^{199}Hg is shown in Section 5.2.2. This could have served as a very good check on the CCEDM program, if the polarizability of Hg had been known to high accuracy. However, the uncertainty in the measurement of this quantity is about 50 % [41]. Nevertheless, we have calculated the polarizability of Hg in its ground state, as no other experimental data is available to test our EDM calculation.

5.2.2 Sample Calculation of Polarizability of ^{199}Hg

The polarizability of a closed-shell atomic system is calculated by replacing the H_{EDM} operator by the induced dipole operator (see Section 5.2.1.1). With the same input given in Table 5.1 for 57 active orbitals, the individual contributions of terms in Eq. (3.77) are presented in Table 5.3

Table 5.3: Individual contributions

Contributions in units of ea_0^3	
$T_1^{(1)\dagger}D$	25.40
$T_1^{(1)\dagger}DT_1^{(0)}$	-0.16
$T_1^{(1)\dagger}DT_2^{(0)}$	-2.21
$T_2^{(1)\dagger}DT_2^{(0)}$	0.298
$T_2^{(1)\dagger}DT_1^{(0)}$	-0.01
Total	23.32

The Dirac-Fock contribution is = 34.66 a.u. The leading contribution arises from the term $T_1^{(1)\dagger}D$ and the next dominant is the term $T_1^{(1)\dagger}DT_2^{(0)}$. The experimental value of the polarizability in atomic units [41] is $34.45ea_0^3$, the uncertainty in the measurement being 50 %. The earlier calculation [13] with V^N form of orbitals gave a value 40.91 a.u for the Dirac-Fock and 44.92 a.u with the CPHF. The difference is due to the nature of the orbitals and the basis used. Though the results for the polarizability of ^{199}Hg might not reflect the validity of the linear CCEDM program due to the large error bars in its measured value, our result nevertheless is within the error bars of the measurement.

5.3 Linear CCEDM for Atomic Hg

The calculation presented in this chapter is for a test basis of 57 active orbitals. A summary of the results obtained by gradually increasing the size of the basis set is presented towards the end of this chapter. The single particle wavefunctions are calculated using GTOs which are generated with the input for 57 active orbitals are shown in Table 5.1. The individual contributions presented further in this chapter correspond to this basis. This is followed by the generation of the unperturbed cluster amplitudes using an independent coupled-cluster program. The perturbed cluster amplitudes are then calculated using the CCEDM program. The program converged in 8 iterations for a tolerance of 10^{-7} . The terms contributing to the atomic EDM at the level of the linearised CCEDM

are,

$$D_{\text{atom}} = 2 \left\langle \Phi_0 \left| \left[T_1^{(1)\dagger} D + T_1^{(1)\dagger} D T_1^{(0)} + T_1^{(1)\dagger} D T_2^{(0)} + T_2^{(1)\dagger} D T_2^{(0)} + T_2^{(1)\dagger} D T_1^{(0)} \right] \right| \Phi_0 \right\rangle \quad (5.7)$$

It must be noted that the operators D and H_{EDM} are both single particle operators and have the same rank ($K_2 = 1$). Also, diagrammatically both the operators have same representations. Hence the atomic EDM calculated by considering H_{EDM} as the perturbation and subsequently calculating the expectation value of the induced dipole operator between the perturbed states or treating the induced dipole operator as the perturbation and taking the expectation value of the H_{EDM} operator, are identical. Computationally, it is much more efficient to calculate the EDMs induced by the T-PT, NSM interactions and also properties like the polarizability, by using the cluster amplitudes perturbed by the induced dipole operator so that the calculation of the perturbed amplitudes is performed only once.

5.3.1 Results for Hg EDM Induced by the P and T Violating T-PT Interaction

Contributions from each of the terms in Eq. (5.7) are shown in Table 5.4 for the basis with the number of active orbitals = 57. The final result can be expressed in units of e-m,

Table 5.4: Individual contributions

Contributions in units of $e a_0 G_F C_T \sigma_N$	
$T_1^{(1)\dagger} D$	-47.830
$T_1^{(1)\dagger} D T_1^{(0)}$	0.0815
$T_1^{(1)\dagger} D T_2^{(0)}$	14.320
$T_2^{(1)\dagger} D T_2^{(0)}$	-0.386
$T_2^{(1)\dagger} D T_1^{(0)}$	-0.059
Total	-33.874

$D_{\text{Hg}} = -1.125 \times 10^{-22} C_T \sigma_N \text{ e m}$ The Dirac-Fock contribution is $-73.89 C_T G_F \sigma_N e a_0 =$

$-2.45 \times 10^{-22} C_T \sigma_{Ne}$ m. It can be noticed from the above table that the largest contribution comes from the term $T_1^{(1)\dagger} D$. This can be inferred from the fact that the Dirac-Fock effect, which is the dominant, is contained in it. In addition, certain types of pair correlation effects are also present, some of which are given in Fig. 5.7. The trend shown by the individual contributions in Table 5.4 is related to the fact that the $T_1^{(0)}$ cluster amplitudes are smaller in magnitude compared to the $T_2^{(0)}$ cluster amplitudes. Also, the $T_1^{(1)}$ amplitudes are larger in magnitude compared to the $T_2^{(1)}$ amplitudes again due to the presence of the Dirac-Fock contribution in $T_1^{(1)}$. For example, from the above table, we see that the contribution of $T_1^{(1)\dagger} DT_2^{(0)}$ is greater than that of $T_1^{(1)\dagger} DT_1^{(0)}$. Similarly, the contribution of $T_2^{(1)\dagger} DT_2^{(0)}$ is greater than that of $T_2^{(1)\dagger} DT_1^{(0)}$. These arguments are equally valid for the atomic EDM induced by the nuclear Schiff moment shown in the next section, which follows the same trend as above. It is also interesting to note that in both cases contribution of the term $T_1^{(1)\dagger} D$ is ≈ 3 times larger than that of the term $T_1^{(1)\dagger} DT_2^{(0)}$, which is the second largest contribution.

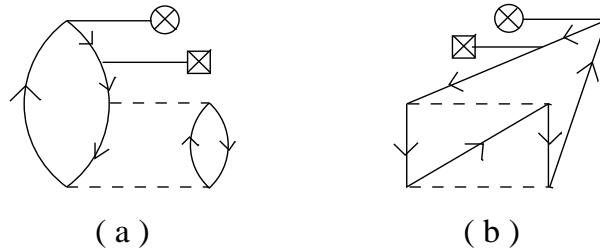


Figure 5.7: Leading diagrams contributing to pair correlation

5.3.2 Results for Hg EDM Induced by the \hat{P} and \hat{T} Violating Nuclear Schiff Moment

The ^{199}Hg atomic EDM induced by the nuclear Schiff moment is calculated for the same input given in the previous Section 5.3.1. The method of generation of the perturbed and the unperturbed cluster amplitudes is the same as described earlier. The Dirac-Fock contribution is $D_{\text{Hg}} = -0.546 \times 10^5 e a_0 S = -0.390 \times 10^{-17} e \text{ cm } \frac{S}{\text{efm}^3}$. Contributions

from each of the above terms is shown in Table 5.5. Again, the leading contribution is that of the term $T_1^{(1)\dagger} D$ and it can also be seen that the contribution of the term $T_1^{(1)\dagger} D$ is ≈ 3 times of that of the term $T_1^{(1)\dagger} DT_2^{(0)}$, which was also true for the results of the T-PT induced EDM. Our result is not in agreement with Dzuba *et al.* [13]. They have used CI + MBPT method for the generation of the orbitals. We have compared the Schiff moment interaction and the electric dipole matrix elements of the $6s_{1/2}$ and the core $p_{1/2}$ orbitals for ^{199}Hg with the results obtained by the authors of Dzuba *et al.* at the Dirac-Fock level and found that the agreement was very good. This suggests that the discrepancy in our results could be majorly due to the different choices of the virtual orbitals in the two calculations. We have used Dirac-Fock orbitals in our calculation but the details of the orbitals used in the calculation of Dzuba *et al.* [13] is not clear.

Table 5.5: Individual contributions

Contributions in atomic units of $S e \times a_0$	
$T_1^{(1)\dagger} D$	-0.177×10^5
$T_1^{(1)\dagger} DT_1^{(0)}$	0.030×10^3
$T_1^{(1)\dagger} DT_2^{(0)}$	0.525×10^4
$T_2^{(1)\dagger} DT_2^{(0)}$	-14.258×10^1
$T_2^{(1)\dagger} DT_1^{(0)}$	0.252×10^{-4}
Total	-0.126×10^5

The final result is in the units where S is expressed in $e \text{ fm}^3$,

$$D_{\text{Hg}} = -0.126 \times 10^5 \times \frac{2 \times 10^{-23}}{0.529^2} \times \frac{S}{e \text{ fm}^3} e \text{ cm}$$

$$D_{\text{Hg}} = -0.0901 \times 10^{-17} e \text{ cm} \frac{S}{e \text{ fm}^3}$$

5.3.3 Summary of the EDM Results for ^{199}Hg

In this section, a summary of all the results obtained for the atomic EDM induced by the T-PT, NSM and also the polarizability, with basis sets of different sizes is presented.

The interaction Hamiltonian for the T-PT and the NSM are both dependent on the nuclear density $\rho_N(r)$ and hence their matrix elements are sensitive to the $s_{1/2}$ and the $p_{1/2}$ orbitals, which have a nonzero probability density inside the nuclear radius. In addition, the NSM interaction Hamiltonian is proportional to the electron coordinate \vec{R} . Also, the matrix elements of the atomic EDM contain the electric dipole operator \vec{D} . Hence the atomic EDMs arising from these interactions require the single particle orbitals to be very accurate all through the radial coordinate. The trend followed by the T-PT and NSM induced EDM is shows that the atomic EDM is very sensitive to the inclusion of $s_{1/2}$ and the $p_{1/2}$ virtuals. On the otherhand, there is not much variation in the polarizability as it is more sensitive to the orbitals having higher orbital angular momenta. We have also performed linear CCEDM calculations, without including any $T^{(0)}$ cluster amplitudes. This in other words, amounts to the linear CCEDM calculation with the cluster amplitudes generated under the approximations $\overline{H}_N \approx H_N$ and $\overline{H}_{\text{EDM}} \approx H_{\text{EDM}}$ in Eq. (3.27). Hence all the correlation effects that are present through the $T^{(0)}$ amplitudes have been omitted. The results of this calculation for a basis of 39 active orbitals are presented here. The Dirac-Fock contribution for this basis is $D_{\text{Hg}} = -3.17 \times 10^{-22} C_T \sigma_{Ne}$ m. The total contribution is $D_{\text{Hg}} = -5.77 \times 10^{-22} C_T \sigma_{Ne}$ m. For this basis, the CPHF calculation gives $D_{\text{Hg}} = -4.64 \times 10^{-22} C_T \sigma_{Ne}$ m. Similar comparison can be made for a basis of 57 active orbitals, for which the Dirac-Fock contribution is $D_{\text{Hg}} = -2.45 \times 10^{-22} C_T \sigma_{Ne}$ m, the bare-Coulomb calculation without $T^{(0)}$ amplitudes gives $D_{\text{Hg}} = -6.60 \times 10^{-22} C_T \sigma_{Ne}$ m, CPHF calculation gives $D_{\text{Hg}} = -5.61 \times 10^{-22} C_T \sigma_{Ne}$ m. This comparison helps in understanding the interplay between the various many-body effects at the CPHF level, which contains the Coulomb effects only of the two particle-two hole kind, the bare-Coulomb, which contains all the effects of the Coulomb interaction and the linear CCEDM, which collectively contains the effects of the CPHF, the bare Coulomb and more.

5.4 Results for the CCEDM-CPHF Comparison

The details of the basis used are shown in Table 5.7.

Table 5.6: Summary of all the results.

Basis size	In units of $10^{-22}C_T\sigma_N$ e m	In units of 10^{-17} e cm $\frac{S}{e\text{fm}^3}$	Polarizability in e a_0^3
36	-2.703	1.830	28.89
39	-2.968	-0.228	30.83
42	-2.205	-0.146	23.59
45	-1.414	-0.112	22.60
51	-1.404	-0.112	23.22
57	-1.125	-0.090	23.31

Table 5.7: Number of basis functions used to generate the even tempered Dirac-Fock orbitals and the corresponding value of α_0 and β used.

	$s_{1/2}$	$p_{1/2}$	$p_{3/2}$	$d_{3/2}$	$d_{5/2}$	$f_{5/2}$	$f_{7/2}$	$g_{7/2}$	$g_{9/2}$
Number of basis	31	32	32	20	20	20	20	10	10
$\alpha_0(\times 10^{-5})$	725	715	715	700	700	695	695	655	655
β	2.725	2.715	2.715	2.700	2.700	2.695	2.695	2.655	2.655
Active holes	6	6	6	4	4	4	4	3	3
Active particles	6	4	4	3	3	1	1	0	0

The calculated $T_1^{(1)}$ amplitudes are in excellent agreement with the CPHF mixing coefficients to an accuracy of 99% (Table 5.10). We attribute this difference to the type of orbitals used. The variation of D_a with *normal* diagrams for the chosen basis, with the inclusion of higher angular momentum virtual states shows the following trend with the inclusion of *normal* diagrams : The Table 5.8 indicates that the higher angular momentum states give a positive contribution. The dominant contribution arises from the $6s_{1/2}$ - $p_{1/2}$ and $6s_{1/2}$ - $p_{3/2}$ intermediate states, whose matrix elements are tabulated in Table 5.9. Total contribution (*normal* + *pseudo*) from $6s_{1/2}$ - $np_{1/2}$ is $D_a = -1.78 \times 10^{-11}C_T e a_0 \sigma_N$. The contribution of all the core is $D_a = -5.81 \times 10^{-22}C_T e m \sigma_N$. We attribute the slight discrepancy between this and the result of an earlier calculation [10] to the numerical differences arising primarily from the generation of the single particle orbitals used and the size of the basis in our calculation and the coefficients calculated by

Table 5.8: Variation of D_a with the inclusion of higher angular momentum virtual states. Here *nsym* refers to the symmetry of the orbital.

S.No.	nsym	EDM ($\times 10^{-22} C_T \sigma_N$ e m)	
		Normal	(Normal+Pseudo)
1	3	-6.30	-5.48
2	5	-6.31	-5.53
3	7	-6.16	-5.81
4	9	-6.16	-5.81

solution of differential equation approach in [10]. From the present study, it is evident that the contribution from *pseudo* diagrams though important is 6 % of the *normal* diagram contribution and opposite in sign. An increase in the number of virtual orbitals, results in deviation from the values listed in Table 5.9. For example, with the basis (1-14) $s_{1/2}$, (2-14) $p_{1/2,3/2}$, (3-12) $d_{3/2,5/2}$, (4-8) $f_{5/2,7/2}$ and (5-9) $g_{7/2,9/2}$, the total contribution and the contribution from the *normal* is $-6.54 \times 10^{-22} C_T \sigma_N$ e m and $-6.31 \times 10^{-22} C_T \sigma_N$ e m respectively. Hence, there are certain terms in the coupled-cluster theory for EDMs that are exactly equivalent to the terms known as the *normal* diagrams in the CPHF theory. This is demonstrated numerically in the context of electric dipole moments, a property which is sensitive to the accuracy of the wavefunctions in the near-nuclear regions. Such equivalence for *pseudo* diagrams, Fig. 3.20(ii,iii) is not evident. Pseudo diagrams can be realized as the sum of two MBPT diagrams [42]. Hence, in the coupled-cluster expression of D_a Eq. (3.57), the direct and the conjugate terms, which when added give exactly the *pseudo* diagrams of CPHF. This shows that the coupled-cluster theory clearly contains all the CPHF effects and many more. With the increasing number of virtual orbitals in each symmetry, the difference between the Dirac-Fock contributions in the CPHF and the CCEDM-CPHF framework is $\sim 10^{-11} C_T$ e m.

Table 5.9: Dominant contributions to D_a (in units of C_{Tea_0}) from *normal* and *pseudo* diagrams for np intermediate states calculated using the coupled-cluster theory for EDMs.

Core	np	$T_1^{(1)}$ (atomic units)		D (atomic units)		$D_a = T_1^{(1)} \times D$	
		Normal	Pseudo	Normal	Pseudo	Normal	Pseudo
$6s_{1/2}$	$6p_{1/2}$	111.753	95.739	0.872	0.835	-0.204	0.038
$6s_{1/2}$	$7p_{1/2}$	-269.402	-233.805	-1.821	-1.734	-1.027	0.185
$6s_{1/2}$	$8p_{1/2}$	270.725	242.544	1.388	1.311	-0.787	0.126
$6s_{1/2}$	$9p_{1/2}$	-198.267	-189.975	-0.344	-0.319	-0.143	0.017
$6s_{1/2}$	$10p_{1/2}$	-106.923	-108.978	0.068	0.059	0.015	-0.002
$6s_{1/2}$	$6p_{3/2}$	20.542	15.054	0.995	0.904	0.043	-0.015
$6s_{1/2}$	$7p_{3/2}$	-54.653	-39.743	-2.372	-2.109	0.271	-0.104
$6s_{1/2}$	$8p_{3/2}$	-58.035	-41.318	-2.311	-1.876	0.269	-0.118
$6s_{1/2}$	$9p_{3/2}$	30.418	20.049	0.771	0.513	0.049	-0.033
Total						-1.514	0.094

Table 5.10: Comparison of the CPHF mixing coefficients and the CCEDM-CPHF $T^{(1)}$ amplitudes in atomic units.

Index	CCEDM-CPHF	CPHF
1	0.2924205119	0.2924205118
2	-0.7982275466	-0.7982275462
3	-1.1155643358	-1.1155643352
4	1.8377536946	1.8377536937
5	3.7317822454	3.7317822436
6	9.6787847632	9.6787847589
7	-30.008015414	-30.008015412
8	0.0001165862	0.0001165862
9	0.0002421674	0.0002421674
10	-0.6387746775	-0.6387746765
11	1.7436575790	1.7436575763
12	2.4365130942	2.4365130904
13	-4.0126091898	-4.0126091835
14	-8.1347997133	-8.1347997011
15	-20.937517787	-20.937517755
16	60.693370926	60.693370912
17	1.2843746175	1.2843746168
18	-3.5056043989	-3.5056043963
19	-4.8962935559	-4.8962935525
20	8.0527485401	8.0527485326
21	16.227995315	16.227995299
22	40.569138706	40.569138625
23	-95.030635781	-95.030635790
24	0.0006727996	0.0006727997
25	-0.0021685273	-0.0021685274

5.5 Implications of Atomic EDMs for Physics Beyond the Standard Model

The Standard Model of particle physics does not accommodate the tensor-pseudotensor P and T violating electron-nuclear interaction. Any nonzero value of C_T would mean physics beyond the Standard Model. The present limit on $C_T = 0$ is obtained from the comparison of the ratio $R = d_{\text{atom}}/C_T$ using coupled-perturbed Dirac-Fock theory [10] and the latest experimental result [8]. More details of this theory are presented in Section 3.3. The diagrams arising in the CPHF theory Fig. 3.20 form only a subset of the correlation effects shown in Fig. B.2. This comparison gives [8, 9, 10],

$$C_T = \left(1.77 \pm 0.82 \pm 0.67\right) \times 10^{-9} \sigma_N$$

An improved accuracy of the calculation of the quantity R would give an improved estimate of C_T . With our linear CCEDM calculation, we obtain the limit for C_T as

$$C_T = \left(0.94 \pm 0.44 \pm 0.36\right) \times 10^{-8} \sigma_N$$

From the Fig. 1.1, the contribution to the closed-shell atomic EDMs induced by the tensor-pseudotensor electron-nucleus interaction arises from the electron-nucleon interactions which originates from the electron-quark interactions. The interaction involves the nuclear spin σ_N and hence C_T is weighted by the neutron and proton spins :

$$C_T = \left\langle C_{Tp} \sum_p \sigma_p + C_{Tn} \sum_n \sigma_n \right\rangle$$

where σ_p and σ_n are the proton and neutron spins respectively. The nucleus of ^{199}Hg has an unpaired neutron with $I = \frac{1}{2}$. Certain models of CP -violation can in principle predict the coupling constants associated with the T-PT electron-quark interactions. For example, the coupling constant C_T at the quark-electron level can be nonzero in the models that can accommodate the scalar leptoquarks. However, it is difficult to determine C_T at the quark-electron level from a knowledge of the atomic EDMs. This

is associated with the lack of a clear cut approach in finding the contribution that the EDM of a current quark makes to a nucleon EDM [43].

It has already been explained in earlier sections that the EDM of atomic ^{199}Hg could arise from the P and T violating nuclear interactions. These interactions produce the NSM. In this chapter we discuss the connection between the NSM with the P and T violating quark interactions.

The contribution to the nuclear Schiff moment (NSM) can arise from

1. The nucleon EDM : The nuclei which consist of unpaired nucleons can induce an EDM due to the EDMs of the lone nucleons.
2. P and T violating nucleon-nucleon interactions : The presence of CP violation at the quark level can induce nucleon-nucleon interactions which are P and T violating, in addition to the nucleon EDMs of the form

$$H_{\text{PT}} = \frac{G_F}{\sqrt{2}} \eta_{ab} (\bar{N}_a i \gamma_5 N_a) (\bar{N}_b N_b). \quad (5.8)$$

In the nonrelativistic limit, Eq. (5.8), reduces to,

$$H_{\text{PT}} = \frac{G_F}{\sqrt{2}} \frac{\eta_{ab}}{2m_p} \sigma_{\mathbf{a}} \cdot \nabla \rho_b$$

This interaction can be written as an interaction of a single valence nucleon N_a and the nuclear core with the density distribution ρ as,

$$H_{\text{nc}} = \frac{G_F}{\sqrt{2}} \frac{1}{2m_p} \eta_a \sigma_{\mathbf{a}} \cdot \nabla \rho \quad (5.9)$$

where

$$\eta_i = [\eta_{\text{ip}} Z + \eta_{\text{in}} (A - Z)] / A$$

For ^{129}Xe and ^{199}Hg , the unpaired nucleon is a neutron. The NSM caused by the internal proton excitations is parameterized in terms of the constant η_{ip} . It was later shown that the contributions of the internal nucleons to the T-odd nuclear moments is as important as the contribution of external ones [15]. The most accurate measurement of the ^{199}Hg atomic EDM is [8],

$$d_{\text{Hg}} = -(1.06 \pm 0.49 \pm 0.40) \times 10^{-28} \text{ e cm} \quad (5.10)$$

and the numerical calculations of the ^{199}Hg atomic EDM induced by the nuclear Schiff moment with our CCEDM calculations give,

$$d_{\text{Hg}} = -0.090 \times 10^{-17} \left(\frac{S}{\text{e fm}^3} \right) \text{ e cm} \quad (5.11)$$

The NSM, S is related to the parameter η_{np} by [15],

$$\frac{S}{\text{e fm}^3} = -1.4 \times 10^{-8} \eta_{\text{np}} \quad (5.12)$$

From Eq. (5.11) and 5.12, we get,

$$\begin{aligned} d_{\text{Hg}} &= -0.090 \times 10^{-17} \times (-1.4) \times 10^{-8} \eta_{\text{np}} \text{ e cm} \\ &= 0.126 \times 10^{-25} \eta_{\text{np}} \text{ e cm} \end{aligned} \quad (5.13)$$

From Eq. (5.10), we obtain,

$$-(1.06 \pm 0.49 \pm 0.40) \times 10^{-28} = 0.126 \times 10^{-25} \eta_{\text{np}} \quad (5.14)$$

Hence,

$$\begin{aligned} \eta_{\text{np}} &= -\frac{(1.06 \pm 0.49 \pm 0.40) \times 10^{-28}}{0.126 \times 10^{-25}} \\ &= -(8.4 \pm 3.9 \pm 3.2) \times 10^{-3} \end{aligned} \quad (5.15)$$

(see Ref.[13], Table VIII.)

To estimate the η_{np} parameter, it is assumed that the terms $(G_F/\sqrt{2}) \eta_{\text{np}} \bar{N} i \gamma_5 N \bar{N} N$ arise from one pion exchange. The lowest intermediate state contributing to η_{np} is the π^0 meson, which is related to the pion-nucleon coupling constant by,

$$\eta_0 \frac{G_F}{\sqrt{2}} = -\frac{g_{\pi NN} \bar{g}_{\pi NN}}{m_\pi^2} \quad (5.16)$$

where, $G_F = 1.17 \times 10^{-11} (\text{MeV})^{-2}$ is the Fermi's coupling constant, $m_\pi = 140 \text{ MeV}$ is the pion mass, $g_{\pi NN} \approx 13.5$ is the usual pion-nucleon coupling constant, and $\bar{g}_{\pi NN}$ is the P and T violating pion-nucleon coupling constant. For ^{199}Hg , we have,

$$-g_{\pi NN} \bar{g}_{\pi NN} = \eta_{\text{np}} \times \frac{G_F m_\pi^2}{\sqrt{2}} \quad (5.17)$$

where $G_F m_\pi^2 = 2.29 \times 10^{-7}$. Substituting for $G_F m_\pi^2$,

$$\begin{aligned}
 -g_{\pi NN} \bar{g}_{\pi NN} &= -(8.4 \pm 3.9 \pm 3.2) \times 10^{-3} \times \frac{2.29 \times 10^{-7}}{\sqrt{2}} \\
 \bar{g}_{\pi NN} &= (8.4 \pm 3.9 \pm 3.2) \times 10^{-10} \times \frac{2.29}{13.5 \times \sqrt{2}} \\
 &= (8.4 \pm 3.9 \pm 3.2) \times 0.11 \times 10^{-10} \\
 &= (0.92 \pm 0.43 \pm 0.35) \times 10^{-10}
 \end{aligned} \tag{5.18}$$

(see Ref.[13], Table VIII.)

According to [18], the above value of $\bar{g}_{\pi NN}$ for ^{199}Hg can be used to set limit on the QCD vacuum angle θ_{QCD} using,

$$\bar{g}_{\pi NN} \approx -0.027 \theta_{\text{QCD}}$$

which gives,

$$\theta_{\text{QCD}} = (3.4 \pm 1.6 \pm 1.3) \times 10^{-9} \tag{5.19}$$

(See [13] Table VIII).

Apart from the limit on θ_{QCD} , it is also possible to set a limit on the linear combination of quark chromo EDMs using,

$$\eta_{\text{np}} = \frac{1}{4\pi G_F} \frac{3g_{\pi\text{pp}} m_0^2}{f_\pi m_\pi^2} \times (\tilde{d}_d - \tilde{d}_u - 0.012\tilde{d}_s)$$

where f_π is the pion decay constant, $g_{\pi\text{pp}}$ is the CP conserving coupling constant. Also, the $I = 1$ component of $\bar{g}_{\pi NN}$ is related to the chromo electric EDM of the light quarks[17],

$$\bar{g}_{\pi NN}^{I=1} = 2(\tilde{d}_u - \tilde{d}_d) \times 10^{14}$$

where the terms on the right hand side are all expressed in centimeters. From the limit on $\bar{g}_{\pi NN}$, we obtain the limit for the linear combination of the quark chromo EDMs,

$$\begin{aligned}
 e(\tilde{d}_u - \tilde{d}_d) &= \frac{(0.92 \pm 0.43 \pm 0.35) \times 10^{-10}}{2 \times 10^{14}} \\
 &= (0.46 \pm 0.22 \pm 0.18) \times 10^{-24} \text{e cm}
 \end{aligned}$$

(See [13] Table VIII).

It is also possible to obtain a limit on the neutron and proton EDMs from the ^{199}Hg EDM. The neutron EDM d_N is estimated in terms of the the CP -odd θ terms in the QCD Lagrangian [44],

$$d_N \approx (5.2 \times 10^{-16} \text{e cm}) \theta$$

Using Eq. (5.19),

$$d_N = (5.2 \times 10^{-16} \text{e cm}) \times (3.4 \pm 1.6 \pm 1.3) \times 10^{-9} \quad (5.20)$$

we get,

$$d_N = (17.7 \pm 8.3 \pm 6.8) \times 10^{-25} \text{e cm}$$

which can be used to set limit on the proton EDMs [19],

$$Q = s_p d_p + s_n d_n \quad (5.21)$$

where the NSM Q is presented as the sum of proton and neutron EDMs and $s_p = 0.2 \pm 0.02 \text{fm}^2$ and $s_n = 1.895 \pm 0.035 \text{fm}^2$. It is possible from the above relations, to get a limit for the proton EDM from ^{199}Hg EDM.

Chapter 6

Conclusions and Future Directions

The study of atomic electric dipole moments is of fundamental importance involving the fields of atomic, nuclear and particle physics. These can provide an unambiguous test for the Standard Model and some of its extensions. Atoms are rich sources of P and T violating effects and hence can be used to study CP violation in the leptonic, semi-leptonic and hadronic sectors. In particular, the closed-shell atomic EDMs can throw light on the CP violating interactions that originate within the nucleus. The observation of an EDM is a direct evidence of time-reversal violation. Tremendous progress has been made during the past few years in the search for EDMs. Experiments are currently underway on Hg [8], Xe [45] and new experiments are being planned for Ra and Yb. Sophisticated techniques like laser cooling and other state of the art techniques could help in improving the sensitivity of the EDM experiments significantly. Certain molecules and solid state materials also serve as promising candidates to look for EDMs. Molecules can have enhancement factors ≈ 100 -1000 times larger than that for atoms due to their large interaction energy. For example, a limit for the EDM of an electron has been obtained from YbF molecule [46]. Experiments with molecules are more promising compared to atoms because of the elimination of various systematic errors due to the large interaction energy and strong tensor polarizability of the molecules. Solid state materials like gadolinium garnets could also be good candidates for the electron EDM [47].

In this thesis, we have attempted to calculate the EDM of closed-shell atoms using relativistic coupled-cluster theory; an all order relativistic many-body theory. We have obtained new limits for various quantities of fundamental importance — the tensor-

pseudotensor coupling constant (C_T), the nuclear Schiff moment (S), the neutron EDM (d_N), the pion-nucleon coupling constant ($\bar{g}_{\pi NN}$), the QCD vacuum angle (θ_{QCD}) and the EDMs of linear combinations of quarks. This is the most advanced calculation of EDM of closed-shell atoms to date. Inclusion of nonlinear terms in the CCEDM equations would give more accurate limits further and together with the experimental result, would give an improved estimate of the P and T violating coupling constants. The validity of the CCEDM program has been checked at various stages. We have performed the calculations of the unperturbed coupled-cluster amplitudes by appropriate modifications to the CCEDM program. The correlation energy calculated from these amplitudes match fairly well with the results of an independent existing CC program. We have established that the *normal* CPHF diagrams are subsumed in the CCEDM theory and have shown the numerical equivalence of the two theories for *normal* diagrams at all orders of Coulomb perturbation. We found that the pseudo diagrams are present; though not in a transparent way in the CCEDM theory. Our calculation of the T-PT interaction coupling constants and the nuclear Schiff moment includes the correlation effects arising from the four-particle, four-hole, (three-particle — one-hole), (three-hole — one-particle), etc. that are not present in the CPHF theory, which contains only the (two-particle — two-hole) effects. A more detailed study could be performed to understand the importance of each of these effects independently in a heavy atom like Hg. The results of the Dirac-Fock, the CPHF and the CCEDM, reflect the fact that the correlation effects are very important for Hg. One more interesting thing is that the results obey the same trend for the NSM and the T-PT induced atomic EDMs. The CCEDM program can be used to calculate the atomic polarizability by replacing the H_{EDM} operator by the electric dipole operator. This would have been an excellent check for the program if the error bars of the experimental value of atomic Hg were small. Nevertheless, our result of the polarizability of Hg lies within the error bars of its measured value.

An improvement in our CC calculation can be achieved by the inclusion of triple excitations, quadrupole excitations, etc. The demands on the computational resources

become increasingly critical for the inclusion of higher order excitations. As the size of the basis increases, the number of Coulomb integrals proliferate and this consumes an enormous amount of computational time and memory. In addition, the triangular and the parity selection rules satisfied by the EDM operator are also responsible for huge amounts of computational time. An alternative approach to perform these calculations is by [48] which is a string-based algorithm and can handle any level of excitation. In addition, theories like the unitary coupled-cluster (UCC) and the linear response theory (LRT)[42] can be used to perform EDM calculations. The linear CCEDM theory presented in this thesis is applicable to any closed-shell atomic system, but our focus has been on Hg as it is presently the most interesting candidate from an experimental point of view and a new result for this atom is expected soon.

The results shown in Section.5.3 correspond to a linearised coupled-cluster theory applied to the calculations of closed-shell atomic EDMs. The linear CCEDM calculations with accurate and large basis sets are critical for these calculations and are in progress. In particular, there is the challenging task of optimizing the single particle basis. This could be explored to a large extent by using the even-tempered (ET) and the well-tempered (WT) bases. Undoubtedly, the accuracy of the single particle basis is very critical to any many-body calculation. It can be noticed that the basis used in our calculations is quite accurate near the nucleus and also far from the nucleus. Since this is an important requisite for the atomic EDM calculations, particularly the EDMs induced by the T-PT and the NSM, which are sensitive to the $s_{1/2}$ and $p_{1/2}$ wavefunctions near the nucleus, the quality of the basis used in our calculations is indeed very good. The high accuracy calculations of the coupling constants are underway and it should be possible to obtain the results of the nonlinear CCEDM calculation in the near future considering the present status of the CCEDM program, and the accessibility of the techniques of parallelization. The stage is now well set for further research on the EDM of atomic Hg. Given the prospect of an improved measurement of this quantity, there is clearly a necessity for accurate calculations of R ; the ratio of the atomic EDM to the P and T violating coupling constant. The accurate calculations of the coupling constants would help in providing

important insights into many models of particle physics that predict CP violation.

From the nuclear physics point of view, there is a necessity for an improvement in the calculation of the nuclear Schiff moment, which can connect the CP violating coupling constants at the atomic level to those predicted by the models of particle physics. Clearly, atomic physics has the potential to probe new physics beyond the Standard Model.

Appendix A

P and T Violation and Electric Dipole Moments

Implications of P symmetry on intrinsic electric dipole moments

The permanent electric dipole moment(EDM) is defined as the expectation value of the electric dipole operator between non-degenerate atomic states. Let \mathcal{D}_{int} denote the intrinsic or the permanent EDM of a non-degenerate physical system in a state $|\Psi\rangle$. Then, its EDM is given by,

$$\mathcal{D}_{\text{int}} = \langle \Psi | D_{\text{ind}} | \Psi \rangle \quad (\text{A.1})$$

where D_{ind} is the induced dipole operator. Consider the above quantity in a parity transformed coordinate system,

$$\mathcal{D}_{\text{int}} = \langle \Psi' | D_{\text{ind}} | \Psi' \rangle$$

where $|\Psi'\rangle = P|\Psi\rangle$. Since $P = P^\dagger = P^{-1}$, the above can be modified into,

$$\begin{aligned} \mathcal{D}_{\text{int}} &= \langle \Psi' | (P P^\dagger) D_{\text{ind}} (P P^\dagger) | \Psi' \rangle \\ &= \langle \Psi | P^\dagger P (P^\dagger D_{\text{ind}} P) P^\dagger P | \Psi \rangle \end{aligned} \quad (\text{A.2})$$

Since, $(P^\dagger D_{\text{ind}} P) = -D_{\text{ind}}$, we have,

$$\mathcal{D}_{\text{int}} = -\langle \Psi | D_{\text{ind}} | \Psi \rangle \quad (\text{A.3})$$

$$\langle \Psi' | D_{\text{ind}} | \Psi' \rangle = -\langle \Psi | D_{\text{ind}} | \Psi \rangle$$

The state $|\Psi\rangle$ is a stationary state and hence if the Hamiltonian determining the system is \mathcal{H} , then, $\mathcal{H}|\Psi\rangle = \mathcal{E}|\Psi\rangle$. Assuming the Hamiltonian to be invariant under P , we have $P^{-1}\mathcal{H}P = \mathcal{H}$. Hence,

$$\begin{aligned}(P\mathcal{H}P^{-1})P|\Psi\rangle &= \mathcal{E}P|\Psi\rangle \\ \mathcal{H}|\Psi'\rangle &= \mathcal{E}|\Psi'\rangle\end{aligned}$$

This implies, both $|\Psi\rangle$ and $|\Psi'\rangle \equiv P|\Psi\rangle$ describe stationary states with same eigenvalue \mathcal{E} . If this energy level is non-degenerate, then the two states cannot be independent and hence $P|\Psi\rangle = c|\Psi\rangle$, where $c = \pm 1$. From A.1 and A.3,

$$\begin{aligned}\langle\Psi|D_{\text{ind}}|\Psi\rangle &= -\langle\Psi'|D_{\text{ind}}|\Psi'\rangle \\ &= -c^2\langle\Psi|D_{\text{ind}}|\Psi\rangle \\ &= -\langle\Psi|D_{\text{ind}}|\Psi\rangle\end{aligned}$$

In other words,

$$\langle\Psi|D_{\text{ind}}|\Psi\rangle = 0$$

It is hence proved that

If the Hamiltonian is invariant under a P transformation, and if the state is non-degenerate, then there can be no permanent electric dipole moment in that state

Implications of T symmetry on intrinsic electric dipole moments

In the previous section, it was shown that there can be no permanent electric dipole moment in a non-degenerate state if the Hamiltonian is invariant under space inversion. It can be shown that electric dipole moments are excluded by invariance under time reversal too. If the Hamiltonian \mathcal{H} is rotationally invariant, it must commute with the angular momentum operators. This further means that there is a complete set of common eigen vectors of \mathcal{H} , \mathbf{J}^2 and \mathbf{J}_z denoted by the state $|E, j, m\rangle$. It is assumed that the only degeneracy of these energy eigen vectors is that associated with the $(2j+1)$ values of m , where m is the projection of j , the eigenvalue of the total angular momentum operator

J. The electric dipole moment operator \mathbf{d} is an irreducible tensor operator of rank 1. Therefore, the average dipole moment on one of these states is, from projection theorem,

$$\langle E, j, m | \mathbf{d} | E, j, m \rangle = C_{E,j} \langle E, j, m | \mathbf{J} | E, j, m \rangle \quad (\text{A.4})$$

where $C_{E,j}$ is a scalar. We know that if the vectors $|u'\rangle = \theta|u\rangle$ and $|v'\rangle = \theta|v\rangle$, then,

$$\langle u'|v'\rangle = \langle u|v\rangle^* \quad (\text{A.5})$$

where θ is the time-reversal operator and is anti-linear. Let $|u\rangle = |\psi\rangle$ and $|v\rangle = d_\alpha|\psi\rangle$ where d_α is one of the components of electric dipole moment operator. Then, $|u'\rangle = |\psi'\rangle = \theta|\psi\rangle$ and $|v'\rangle = \theta d_\alpha|\psi\rangle = d_\alpha|\psi'\rangle$

$\Rightarrow \langle \psi' | d_\alpha | \psi' \rangle = \langle \psi | d_\alpha | \psi \rangle^*$. But d_α is hermitian $\Rightarrow \langle \psi' | \mathbf{d} | \psi' \rangle = \langle \psi | \mathbf{d} | \psi \rangle$ where $|\psi'\rangle = \theta|\psi\rangle$.

Similarly consider J_α , a component of angular momentum in place of d_α . Therefore, $\theta J_\alpha = -J_\alpha \theta$

$$\Rightarrow \langle \psi' | \mathbf{J} | \psi' \rangle = -\langle \psi | \mathbf{J} | \psi \rangle \quad (\text{A.6})$$

Also,

$$\mathbf{J}_z |E, j, m\rangle = m\hbar |E, j, m\rangle \quad (\text{A.7})$$

$\Rightarrow \theta \mathbf{J}_z \theta^{-1} \theta |E, j, m\rangle = m\hbar \theta |E, j, m\rangle$. Therefore,

$$\mathbf{J}_z [\theta |E, j, m\rangle] = -m\hbar \theta |E, j, m\rangle \quad (\text{A.8})$$

Restricting the degeneracy to m values alone, the vector $\theta |E, j, m\rangle$ can differ from $|E, j, -m\rangle$ by at most a phase factor. Therefore by taking, $|\psi\rangle = |E, j, m\rangle$ we have $\langle E, j, -m | \mathbf{d} | E, j, -m \rangle = \langle E, j, m | \mathbf{d} | E, j, m \rangle$ and

$$\langle E, j, -m | \mathbf{J} | E, j, -m \rangle = -\langle E, j, m | \mathbf{J} | E, j, m \rangle \quad (\text{A.9})$$

From these two results, by substituting m by $-m$, the right hand side of Eq. (A.4) changes sign, while left hand side doesn't. This is possible only if both sides vanish separately. Hence the spontaneous dipole moment of the state must vanish under combined assumptions of rotational invariance and time reversal invariance and the degeneracy of the state being only that due to m .

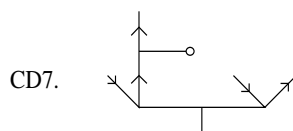
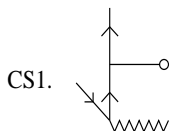
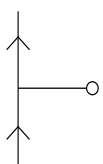
Appendix B

Classification of the CCEDM

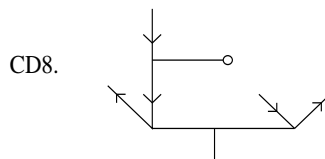
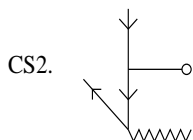
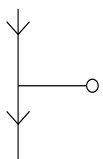
Diagrams

Diagrammatic representation of Coulomb operator and classification of diagrams according to the form of Coulomb operator

F_PP



F_HH



F_PH

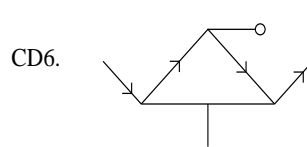
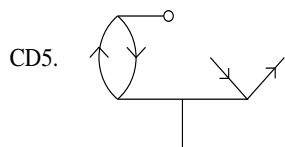
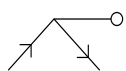


Figure B.1: CCEDM diagrams at the bare Coulomb level listed according to the form of H_N . The operator F denotes the single electron part of H_N . The leftmost side is the list of diagrams of F and on the right side are given the cluster amplitude diagrams arising for each F .

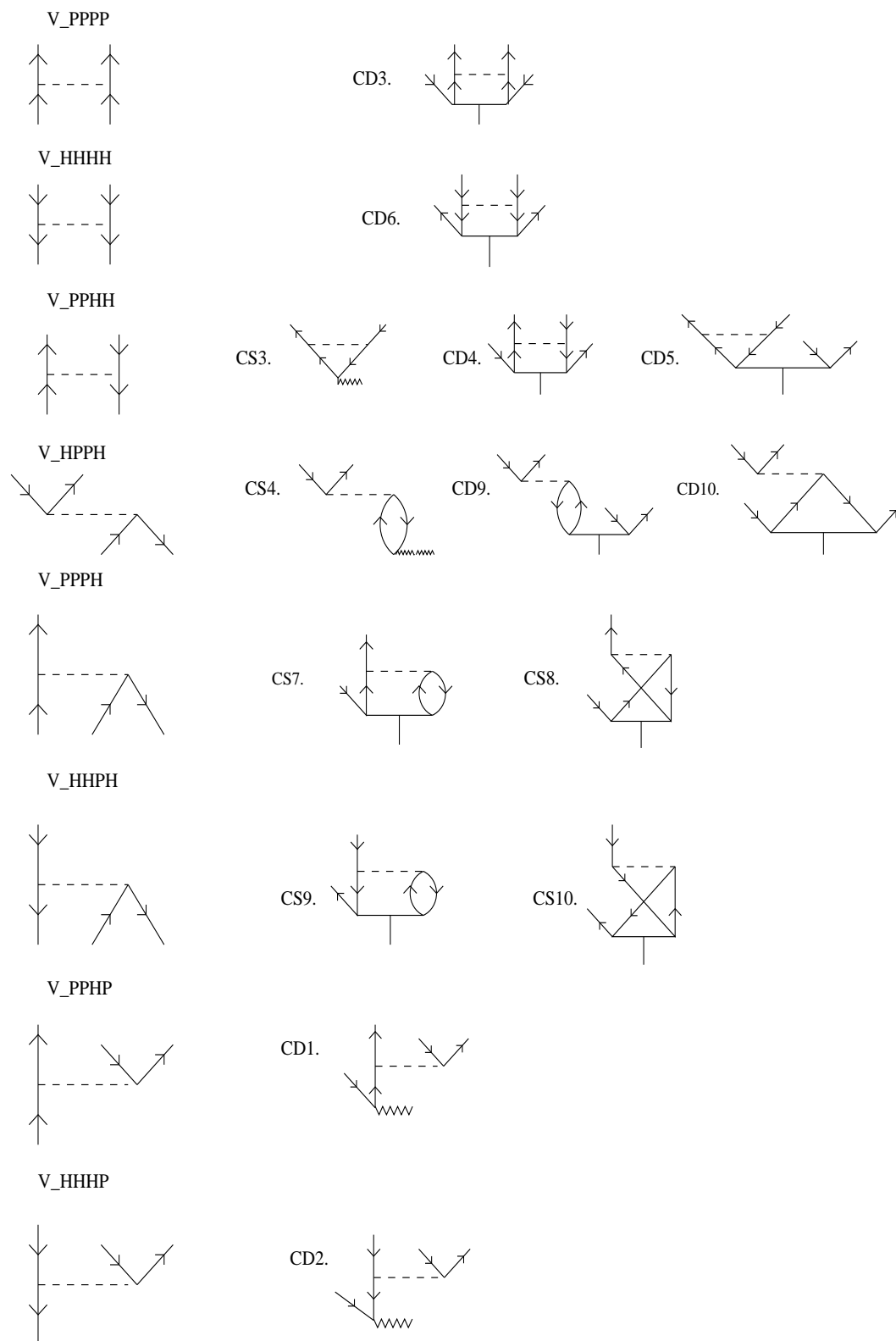


Figure B.2: CCEDM diagrams at the bare Coulomb level listed according to the form of V_N - contd. V_N is the two-electron part. The leftmost side is the list of diagrams of V_N and on the right side are given the cluster amplitude diagrams arising for each V_N .

Appendix C

Technical Details of the CCEDM Program

Flow chart for the CCEDM program is shown in Fig. C.1.

The program consists of routines to calculate various parameters/quantities necessary for setting up the CCEDM equations. The routines important for the actual EDM calculation are described below :¹

- Subroutine `readinp`: Reads the input containing the number of basis, number of occupied orbitals and the rank of the EDM and induced dipole operators.
- Subroutine `symm`: This routine sets up the equation indices for retrieving $T^{(0)}$ amplitudes and also the skip information necessary for defining the locations of the Coulomb integrals.
- Subroutine `symm-edm`: This routine sets up the equation indices for the $T^{(1)}$ amplitudes.
- Subroutine `findlam`: This routine calculates the multipoles (λ_1, λ_2) of the $T_2^{(1)}$ operator, stores them in an array and also defines the locations for storing them.
- Subroutine `coulims`: This routine calculates the bare Coulomb integrals, i.e. (4-particle), (4-hole), (2 particle, 2 hole), (3 particle, 1 hole) diagrams and stores them in memory.

¹For a detailed description of the program refer to the documentation to be put up in our webpage : <http://www.iiap.res.in/research/NAPP/main.html>

- Subroutine `aimshhph`: This routine calculates the (particle - particle) EDM IMS contributions and stores them in memory.
- Subroutine `aimsppph`: This routine calculates the (hole - hole) EDM IMS contributions and stores them in memory.
- Subroutine `edmtp`: This routine calculates the matrix elements of the tensor-pseudotensor EDM operator.
- Subroutine `e1mat`: This routine calculates the matrix elements of the electric dipole matrix element.
- Subroutine `schiff`: This routine calculates the matrix elements of the Schiff moment interaction Hamiltonian.
- Subroutine `vdriver`: This routine solves the CCEDM equations for the unknown $T^{(1)}$ amplitudes. The method employed to solve them is based on the Gauss-Seidel iterative scheme. The amplitudes are then stored in a binary format for property calculations.
- Subroutine `vimsloc`: This routine sets up the equation indices for storing the Coulomb integrals $\langle ij|V|kl\rangle$.
- Subroutine `sppph`: This routine calculates the perturbed cluster amplitude diagrams arising from the (3 particle - 1 hole) form of Coulomb diagrams, contributing to singles CCEDM equations (See Fig. B.2).
- Subroutine `shhph`: This routine calculates the perturbed cluster amplitude diagrams arising from the (3 hole - 1 particle) form of Coulomb diagrams, contributing to singles CCEDM equations (See Fig. B.2).
- Subroutine `sphph`: This routine calculates the perturbed cluster amplitude diagrams arising from the (2 hole - 2 particle) form of Coulomb diagrams, contributing to singles CCEDM equations (See Fig. B.2).

- **Subroutine `dpphp`**: This routine calculates the perturbed cluster amplitude diagrams arising from the (3 particle - 1 hole) form of Coulomb diagrams, contributing to the doubles CCEDM equations (See Fig. B.2).
- **Subroutine `dhhhp`**: This routine calculates the perturbed cluster amplitude diagrams arising from the (1 particle - 3 hole) form of Coulomb diagrams, contributing to the doubles CCEDM equations (See Fig. B.2).
- **Subroutine `dpphh`**: This routine calculates the perturbed cluster amplitude diagrams arising from the (2 hole - 2 particle) form of Coulomb diagrams, contributing to the doubles CCEDM equations (See Fig. B.2).
- **Subroutine `dpppp`**: This routine calculates the perturbed cluster amplitude diagrams arising from the (4 particle) form of Coulomb diagrams, contributing to the doubles CCEDM equations (See Fig. B.2).
- **Subroutine `dhhhh`**: This routine calculates the perturbed cluster amplitude diagrams arising from the (4 hole) form of Coulomb diagrams, contributing to the doubles CCEDM equations (See Fig. B.2).
- **Subroutine `dppph`**: This routine calculates the perturbed cluster amplitude diagrams arising from the (3 particle - 1 hole) form of Coulomb diagrams, contributing to the doubles CCEDM equations (See Fig. B.2).
- **Subroutine `dhhph`**: This routine calculates the perturbed cluster amplitude diagrams arising from the (1 particle - 3 hole) form of Coulomb diagrams, contributing to the doubles CCEDM equations (See Fig. B.2).
- **`compute-edm.f`**: This routine calculates the EDM expectation value for the tensor-pseudotensor, NSM and can also be used for the calculation of atomic polarizabilities.
- **Subroutine `edm-lin`**: This routine is particularly written for calculating the contribution to the EDM expectation value from linear CCEDM calculations. In the

Section 5.3.1, a sample calculation is presented, listing the specific terms contributing to the EDM calculation at the linear CCEDM level.

Further in this chapter, some of the milestones in the project of the implementation of the CCEDM theory program are described.

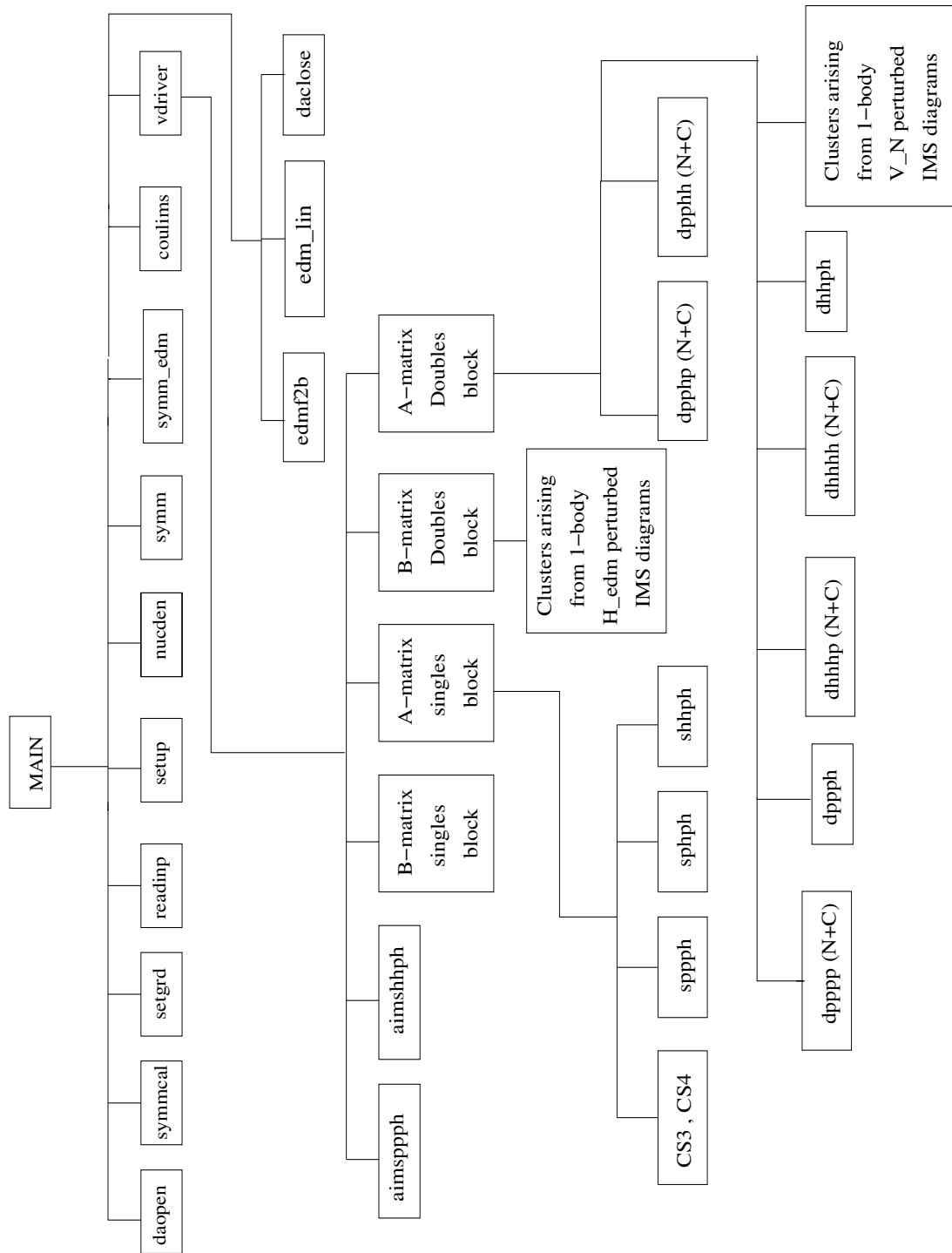


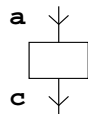
Figure C.1: Flow-chart for the nonlinear CCEDM code - The driver routine calls the routines *sppph*, *sphph*, *shhph*, where the cluster diagrams arising from PPPH, PHPH, HHPH form of the Coulomb operator (V_N) respectively, contributing to singles are calculated. Similarly the routines, *dpphp*, *dppph*, *dpppp*, *dppph*, *dhhhp*, *dhhhh* are called where the diagrams arising from corresponding form of the Coulomb operator contributing to doubles are calculated. The driver routine also calculates the diagrams contributing to the right hand side -(B matrix) of the CCEDM equation.

Loop over two holes & two particles

Loop over 'ic'
 Loop over 'ir'
 Loop over 'id'
 Loop over 'is'

Hole-hole H_{EDM} IMS diagrams

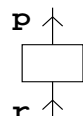
Loop over 'ia'



End 'ia'

Particle-particle H_{EDM} IMS diagrams

Loop over 'ip'



End 'ip'

End 'is'
 End 'id'
 End 'ir'
 End 'ic'

Loop over open lines

Loop over 'ia'
 Loop over 'ip'

Begin singles

Compute B-matrix diagrams
 for singles

Loop over 'ib'
 Loop over 'iq'

Diagrams CS3 & CS4 – T1-T1 block

Loop over 'ir'

Singles clusters arising from
 V_{PPPH}

Loop over 'ic'

Singles clusters arising from
 V_{PHPH}

End 'ic'
 End 'ir'
 Loop over 'ic'

Singles clusters arising from
 V_{HHPH}

End 'ic'
 End 'iq'
 End 'ib'

Compute $T_1^{(1)}$ for iteration

End singles
Begin doubles

Loop over 'ib'
 Loop over 'iq'

Compute B-matrix diagrams
 for doubles

Loop over 'ir'

Doubles clusters arising from
 V_{PPPH}

Figure C.2: Loop structure for the driver routine

Loop over 'ic'

Doubles cluster arising from
V_PPHH

End 'ic'

Loop over 'is'

Doubles cluster arising from
V_PPPP

Loop over 'ic'

Doubles cluster arising from
V_PPPH

End 'ic'

End 'is'

End 'ir'

Loop over 'ic'

Doubles cluster arising from
V_HHHP

Loop over 'id'

Doubles cluster arising from
V_HHHH

Loop over 'ir'

Doubles cluster arising from
V_HHPH

End 'ir'

End 'id'

Hole-Hole V_N IMS diagrams

End 'ic'

Loop over 'ir'

Particle-particle V_N
IMS diagrams

End 'ir'

Compute $T_2^{(1)}$ for
iteration

End doubles

End 'ib'

End 'iq'

End 'ip'

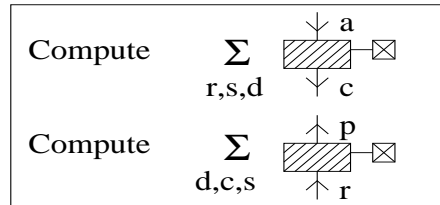
End 'ia'

Figure C.3: Loop structure for the driver routine (contd.)

```

Loop over 'ia'
Loop over 'ip'
  Loop over 'ic'
  Loop over 'ir'
    Loop over 'id'
    Loop over 'is'

```



```

End 'is'
End 'id'
End 'ir'
End 'ic'

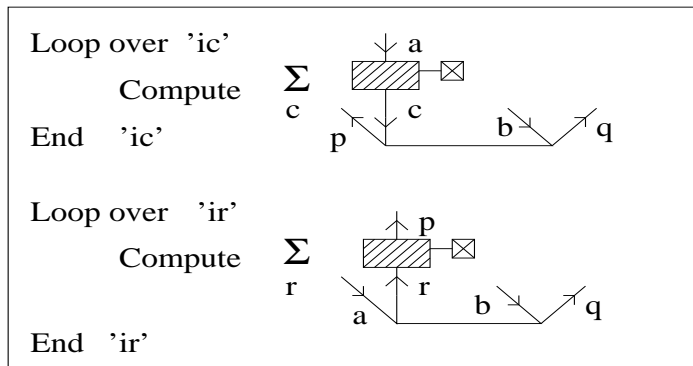
```

End of singles loop

```

Loop over 'ib'
Loop over 'iq'

```



End of doubles loop

```

End 'iq'
End 'ib'
End 'ip'
End 'ia'

```

Figure C.4: Loop structure for inclusion of EDM-IMS diagrams in driver routine and computing the cluster amplitudes using the IMS

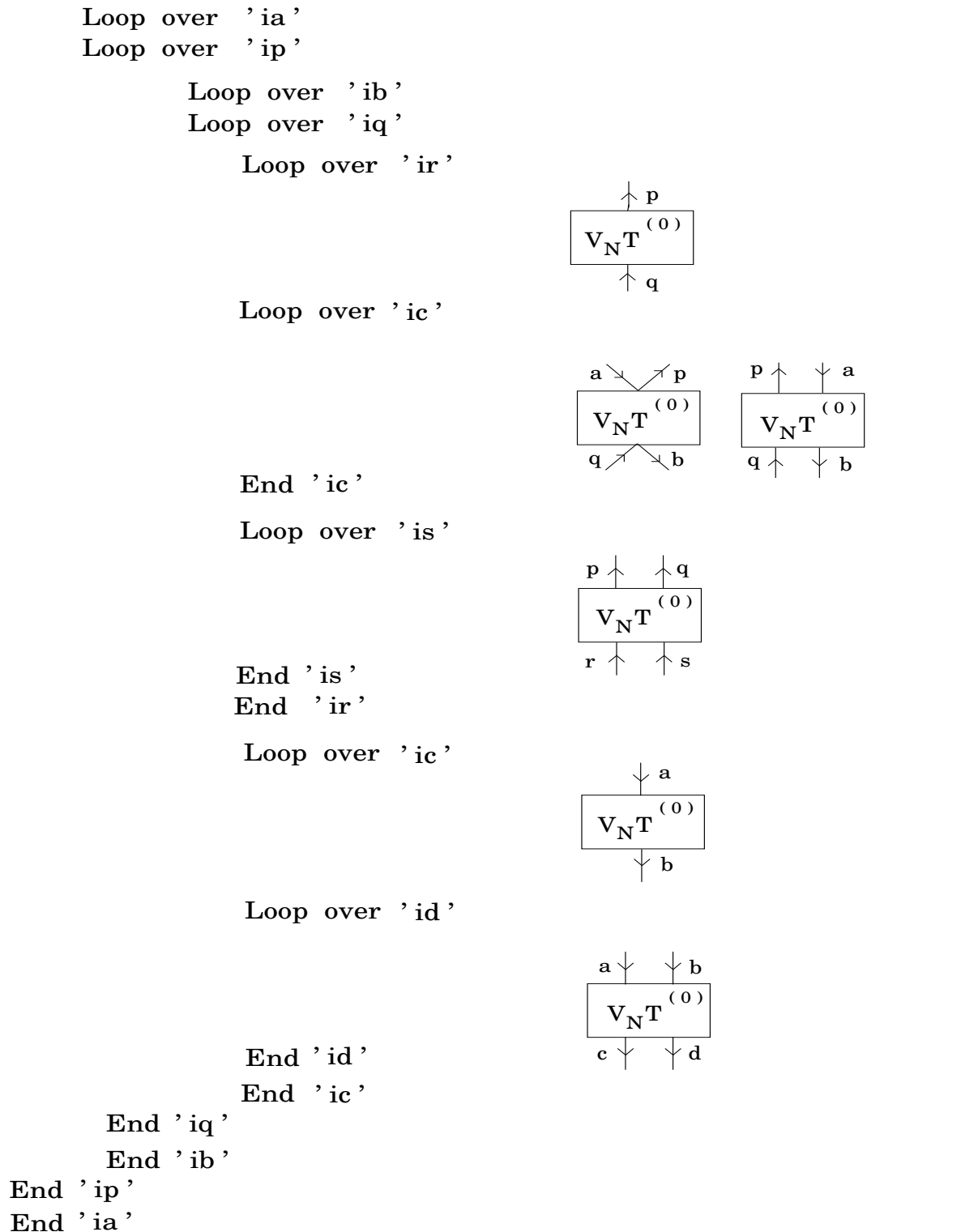


Figure C.5: Loop structure for one-body and two-body Coulomb IMS diagrams in the routine coulims.f.

Appendix D

The Tensor-Pseudotensor H_{EDM} Matrix Element

Consider the general matrix element of H_{EDM} between $|\Phi_a\rangle$ and $|\Phi_b\rangle$, $\langle\Phi_a|H_{\text{EDM}}|\Phi_b\rangle$ where H_{EDM} has the form given in Eq. (2.10). Keeping the numerical constants aside for the moment, consider

$$\langle\Phi_a|H_{\text{EDM}}|\Phi_b\rangle = \langle\Phi_a|i\beta\alpha_z I_z \rho_N(r)|\Phi_b\rangle$$

Consider the Z-axis as the axis of quantization.

$$\langle\Phi_a|H_{\text{EDM}}|\Phi_b\rangle = iI_z \langle\Phi_a|i\beta\alpha_z \rho_N(r)|\Phi_b\rangle \quad (\text{D.1})$$

The wavefunctions $|\Phi_a\rangle$ and $|\Phi_b\rangle$ can be represented in terms of the two-component Dirac wavefunctions given by,

$$\langle\mathbf{r}|\Phi_a\rangle = \frac{1}{r} \begin{pmatrix} P_{n_a \kappa_a}(r) \chi_{\kappa_a m_a}(\theta, \phi) \\ iQ_{n_a \kappa_a}(r) \chi_{-\kappa_a m_a}(\theta, \phi) \end{pmatrix}$$

and

$$\langle\mathbf{r}|\Phi_b\rangle = \frac{1}{r} \begin{pmatrix} P_{n_b \kappa_b}(r) \chi_{\kappa_b m_b}(\theta, \phi) \\ iQ_{n_b \kappa_b}(r) \chi_{-\kappa_b m_b}(\theta, \phi) \end{pmatrix}$$

The Dirac matrices, β and α are given by

$$\beta = \begin{pmatrix} I & 0 \\ 0 & -I \end{pmatrix}; \alpha = \begin{pmatrix} 0 & \sigma \\ \sigma & 0 \end{pmatrix}$$

Substituting for β , α_z in Eq. (D.1), we get

$$\begin{aligned}
 \langle \Phi_a | H_{\text{EDM}} | \Phi_b \rangle &= \\
 \int \frac{1}{r^2} & \left[P_{n_a \kappa_a}(r) \chi_{\kappa_a m_a}^\dagger(\theta, \phi) \quad -i Q_{n_a \kappa_a}(r) \chi_{-\kappa_a m_a}^\dagger(\theta, \phi) \right] \begin{pmatrix} 0 & \sigma_z \\ -\sigma_z & 0 \end{pmatrix} \left[\begin{array}{l} P_{n_b \kappa_b}(r) \chi_{\kappa_b m_b}(\theta, \phi) \\ i Q_{n_b \kappa_b}(r) \chi_{-\kappa_b m_b}(\theta, \phi) \end{array} \right] \\
 & \times \rho_N(r) r^2 dr d\Omega (iI_z) \\
 &= \int \left[P_{n_a \kappa_a}(r) \chi_{\kappa_a m_a}^\dagger(\theta, \phi) \quad -i Q_{n_a \kappa_a}(r) \chi_{-\kappa_a m_a}^\dagger(\theta, \phi) \right] \left[\begin{array}{l} \sigma_z(i) Q_{n_b \kappa_b}(r) \chi_{-\kappa_b m_b}(\theta, \phi) \\ -\sigma_z(i) P_{n_b \kappa_b}(r) \chi_{\kappa_b m_b}(\theta, \phi) \end{array} \right] \\
 & \rho_N(r) dr d\Omega (iI_z)
 \end{aligned}$$

Simplifying further,

$$\begin{aligned}
 \langle \Phi_a | H_{\text{EDM}} | \Phi_b \rangle &= \\
 & \int \left[P_{n_a \kappa_a}(r) \chi_{\kappa_a m_a}^\dagger(\theta, \phi) \sigma_z Q_b(r) \chi_{-\kappa_b m_b}(\theta, \phi)(i) \right] + \\
 & \left[Q_{n_a \kappa_a}(r) \chi_{-\kappa_a m_a}^\dagger(\theta, \phi) \sigma_z P_b(r) \chi_{\kappa_b m_b}(\theta, \phi)(i) \right] \rho_N(r) dr d\Omega (iI_z)
 \end{aligned}$$

Separating the integrals for radial and angular parts,

$$\begin{aligned}
 & \int P_{n_a \kappa_a}(r) Q_{n_b \kappa_b}(r) \rho_N(r) dr \underbrace{\int \chi_{\kappa_a m_a}^\dagger(\theta, \phi) \sigma_z \chi_{-\kappa_b m_b}(\theta, \phi) d\Omega(i)}_{\text{I1}} (iI_z) \quad (\text{D.2}) \\
 & + \int Q_{n_a \kappa_a}(r) P_{n_b \kappa_b}(r) \rho_N(r) dr \underbrace{\int \chi_{-\kappa_a m_a}^\dagger(\theta, \phi) \sigma_z \chi_{\kappa_b m_b}(\theta, \phi) d\Omega(i)}_{\text{I2}} (iI_z)
 \end{aligned}$$

To calculate the specific angular matrix elements corresponding to $\langle \Phi_{K_{S1/2}} | H_{\text{EDM}} | \Phi_{K'_{P1/2}} \rangle$ and $\langle \Phi_{K_{S1/2}} | H_{\text{EDM}} | \Phi_{K'_{P3/2}} \rangle$ we evaluate the respective angular parts, I1 and I2 in Eq. (D.2).

Consider the first integral, I1 for $\langle \Phi_{K_{S1/2}} | H_{\text{EDM}} | \Phi_{K'_{P3/2}} \rangle$:

$$I1 = \int \chi_{\kappa_a m_a}^\dagger(\theta, \phi) \sigma_z \chi_{-\kappa_b m_b}(\theta, \phi) d\Omega$$

$\chi_{\kappa_a m_a}^\dagger(\theta, \phi) : \kappa_a = -1 \ J_a = 1/2$ This angular wavefunction is for the upper component of Φ_a . Hence, $l_a = (J_a + \text{Sign}(\kappa_a) \times 1/2) = 0 \Rightarrow m_a^l = 0$ and $s_a = 1/2$. Choose the projection of the total angular momentum to be the highest value. $M_a = 1/2 = 0 + 1/2$.

The state $|J_a, M_a\rangle = |\frac{1}{2}, \frac{1}{2}\rangle = |0, 0\rangle|\frac{1}{2}, \frac{1}{2}\rangle$ in the L-S basis. Writing $\chi_{\kappa_a m_a}^\dagger(\theta, \phi)$ in the uncoupled basis,

$$\begin{aligned}\chi_{\kappa_a m_a}(\theta, \phi) &= \sum_{m_a^l, m_a^s} |l_a, m_a^l\rangle \times |s_a, m_a^s\rangle \langle l_a, m_a^l, s_a, m_a^s | J_a, M_a\rangle \\ &= |0, 0\rangle |0, 0\rangle = Y_{00} |\alpha\rangle\end{aligned}$$

where $|\alpha\rangle$ represents the wavefunction of a spin-up particle and Y_{00} , the spherical harmonics.

The term $\chi_{-\kappa_b m_b}(\theta, \phi)$ corresponds to the lower component of $|\Phi_b\rangle$. The orbital angular momenta of the upper and lower components l and l' respectively are related as $l' = 2J - l$. We now have, $\kappa_b = -2$ $J_b = 3/2$ The kappa for the lower component, $-\kappa_b = 2$. Therefore, $l'_b = 2J_b - l_b$ and $l_b = 1$. Hence, $l'_b = 2$. From Wigner-Eckart theorem, the multipole moments, M_a , M_b and q satisfy $-M_a + q + M_b = 0$. Hence, $M_a = M_b$. Hence choose $M_b = 1/2$. Therefore,

$$\begin{aligned}\chi_{-\kappa_b m_b}(\theta, \phi) &= |2, 0\rangle |\frac{1}{2}, \frac{1}{2}\rangle \langle 2, 0; \frac{1}{2}, \frac{1}{2} | \frac{3}{2}, \frac{1}{2}\rangle + \\ &\quad |2, 1\rangle |\frac{1}{2}, -\frac{1}{2}\rangle \langle 2, \frac{1}{2}, -\frac{1}{2} | \frac{3}{2}, \frac{1}{2}\rangle \\ &= Y_{20} |\alpha\rangle \langle 2, 0; \frac{1}{2}, \frac{1}{2} | \frac{3}{2}, \frac{1}{2}\rangle + Y_{21} |\beta\rangle \langle 2, 1; \frac{1}{2}, -\frac{1}{2} | \frac{3}{2}, \frac{1}{2}\rangle\end{aligned}$$

Now,

$$\sigma_z \chi_{-\kappa_b m_b}(\theta, \phi) = Y_{20} |\alpha\rangle \langle 2, 0; \frac{1}{2}, \frac{1}{2} | \frac{3}{2}, \frac{1}{2}\rangle - Y_{21} |\beta\rangle \langle 2, 1; \frac{1}{2}, -\frac{1}{2} | \frac{3}{2}, \frac{1}{2}\rangle$$

The integral I1 becomes,

$$I1 = \int \chi_{\kappa_a m_a}^\dagger(\theta, \phi) \sigma_z \chi_{-\kappa_b m_b}(\theta, \phi) d\Omega = 0$$

Consider I2:

$\chi_{\kappa_b m_b}(\theta, \phi)$:

$\kappa_b = -2$, $J_b = \frac{3}{2}$, $l_b = \frac{3}{2} - \frac{1}{2} = 1 \rightarrow m_b^l = -1, 0, 1$. Fix $M_b = \frac{1}{2}$.

$$\chi_{\kappa_b m_b}(\theta, \phi) = Y_{10} |\alpha\rangle \langle 1, 0; \frac{1}{2}, \frac{1}{2} | \frac{3}{2}, \frac{1}{2}\rangle + Y_{11} |\beta\rangle \langle 1, 1; \frac{1}{2}, -\frac{1}{2} | \frac{3}{2}, \frac{1}{2}\rangle$$

$$\sigma_z \chi_{\kappa_b m_b}(\theta, \phi) = Y_{10} |\alpha\rangle \langle 1, 0; \frac{1}{2}, \frac{1}{2} | \frac{3}{2}, \frac{1}{2}\rangle - Y_{11} |\beta\rangle \langle 1, 1; \frac{1}{2}, -\frac{1}{2} | \frac{3}{2}, \frac{1}{2}\rangle$$

$\chi_{-\kappa_a m_a}(\theta, \phi)$:

$\kappa_a = -1, -\kappa_a = 1, J_a = 1/2, l'_a = 2J_a - l_a = 1$. Hence, $m_a^l = -1, 0, 1$. Fix $M_a = \frac{1}{2}$.

$$\chi_{-\kappa_a m_a}(\theta, \phi) = Y_{10} |\alpha\rangle \langle 1, 0; \frac{1}{2}, \frac{1}{2} | \frac{1}{2}, \frac{1}{2}\rangle + Y_{11} |\beta\rangle \langle 1, 1; \frac{1}{2}, -\frac{1}{2} | \frac{1}{2}, \frac{1}{2}\rangle$$

Using the orthogonality property of the Spherical tensors Y_{lm} and Clebsch-Gordan coefficients, we get $I_2 = -\frac{2}{3}\sqrt{2}$. The EDM matrix element,

$$\left\langle \Phi_{K_S 1/2} \left| H_{\text{EDM}} \right| \Phi_{K' P 3/2} \right\rangle = (i^2)(I_z) \left(-\frac{2}{3}\sqrt{2} \right) \int Q_a(r) P_b(r) \rho_N(r) dr \quad (\text{D.3})$$

Appendix E

Radial Matrix Elements of the Nuclear Schiff Moment

Consider the matrix element of the Schiff moment interaction H_{SM} between two states, $\langle \Phi_a | H_{\text{SM}} | \Phi_b \rangle$. The wavefunctions $|\Phi_a\rangle$ and $|\Phi_b\rangle$ can be represented in terms of the two-component Dirac wavefunctions given by,

$$\Phi(\mathbf{r}) = \frac{1}{r} \begin{pmatrix} P_{n_a \kappa_a}(r) \chi_{\kappa_a m_a}(\theta, \phi) \\ i Q_{n_a \kappa_a}(r) \chi_{-\kappa_a m_a}(\theta, \phi) \end{pmatrix} \quad (\text{E.1})$$

Expressing $|\Phi_b\rangle$ in a similar form and setting up of the matrix element of H_{SM} gives,

$$\begin{aligned} \langle \Phi_a | H_{\text{SM}} | \Phi_b \rangle &= \int \left[P_{n_a \kappa_a}(r) \chi_{\kappa_a m_a}^\dagger - i Q_{n_a \kappa_a}(r) \chi_{-\kappa_a m_a}(\theta, \phi)^\dagger \right] (-3 S e) \\ &\quad \left[\begin{matrix} P_{n_b \kappa_b}(r) \chi_{\kappa_b m_b}(\theta, \phi) \\ i Q_{n_b \kappa_b}(r) \chi_{-\kappa_b m_b}(\theta, \phi) \end{matrix} \right] \frac{\rho(r)}{B} dr d\Omega \end{aligned} \quad (\text{E.2})$$

where $d\Omega = \sin\theta d\theta d\phi$ and $B = \int r^4 \rho(r) dr$. Multiplying the matrices,

$$\begin{aligned} &\int_0^\infty \left[\underbrace{P_{n_a \kappa_a}(r) P_{n_b \kappa_b}(r) \chi_{\kappa_a m_a}^\dagger \chi_{\kappa_b m_b}}_{\mathcal{A}} + \underbrace{Q_{n_a \kappa_a}(r) Q_{n_b \kappa_b}(r) \chi_{-\kappa_a m_a}^\dagger \chi_{-\kappa_b m_b}}_{\mathcal{B}} \right] \\ &\quad \left(-3 S e \frac{1}{B} \right) \rho(r) r \cos\theta dr d\Omega \end{aligned} \quad (\text{E.3})$$

Consider,

$$\mathcal{A} = (-3 S e) \int \left[P_{n_a \kappa_a}(r) P_{n_b \kappa_b}(r) \chi_{\kappa_a m_a}^\dagger \chi_{\kappa_b m_b} \right] \frac{\rho(r)}{B} r \cos\theta dr d\Omega$$

and

$$\mathcal{B} = (-3 S e) \int \left[Q_{n_a \kappa_a}(r) Q_{n_b \kappa_b}(r) \chi_{-\kappa_a m_a}^\dagger \chi_{-\kappa_b m_b} \right] \frac{\rho(r)}{B} r \cos\theta dr d\Omega$$

We now evaluate the angular parts of the specific integrals between $s_{1/2}$ and $p_{1/2}$ orbitals. First consider the angular part of,

$$\langle \Phi_{\kappa s_{1/2}} | H_{\text{SM}} | \Phi_{\text{mp}_{1/2}} \rangle$$

given by,

$$\int \chi_{\kappa_a m_a}^\dagger \cos\theta \chi_{\kappa_b m_b} \sin\theta d\theta d\phi$$

$$\kappa_a = -1; J_a = 1/2 \Rightarrow l_a = (J_a + \text{sign}(\kappa_a) \times 1/2) = 0$$

Using the above expression for l_i , the values of κ_i are calculated by fixing the projection of the total angular momentum $J_a = 1/2$ and $J_b = 1/2$ as $M_a = 1/2$ and $M_b = 1/2$ and tabulated in Table E.

κ_a	m_a^l	κ_b	m_b^l
-1	0	1	-1, 0, 1

Table E.1: Possible orbital angular momenta for $\kappa = -1$.

The angular part $\chi_{\kappa_a m_a}$ is expressed in terms of the spherical harmonics and the spin functions α (up-spin) and β (down-spin) as,

$$\begin{aligned} \chi_{\kappa_a m_a} &= \sum_{m_a^l, m_a^s} |l_a m_a^l\rangle \otimes |s_a m_a^s\rangle \times \langle l_a m_a^l s_a m_a^s | J_a M_a \rangle \\ &= \mathcal{Y}_{00} | \alpha \rangle \langle 0 0 \frac{1}{2} \frac{1}{2} | \frac{1}{2} \frac{1}{2} \rangle \\ &= \mathcal{Y}_{00} | \alpha \rangle \langle \frac{1}{2} \frac{1}{2} 0 0 | \frac{1}{2} \frac{1}{2} \rangle \\ &= \mathcal{Y}_{00} | \alpha \rangle \end{aligned} \tag{E.4}$$

Now consider, $\kappa_b = 1$ and $J_b = 1/2$, $\Rightarrow l_b = 1$ and $m_b^l = -1, 0, 1$. Fix $M_b = 1/2$, and using $m_b^s + m_b^l = M_b$, the possible values of $m_b^s = \pm 1/2$. Hence,

$$\begin{aligned} \chi_{\kappa_b m_b} &= \mathcal{Y}_{11} | \beta \rangle \langle 1 1 \frac{1}{2} - \frac{1}{2} | \frac{1}{2} \frac{1}{2} \rangle + \mathcal{Y}_{10} | \alpha \rangle \langle 1 0 \frac{1}{2} \frac{1}{2} | \frac{1}{2} \frac{1}{2} \rangle \\ &= \mathcal{Y}_{11} | \beta \rangle \left(\sqrt{2/3} \right) - \mathcal{Y}_{10} | \alpha \rangle \left(\sqrt{1/3} \right) \end{aligned} \tag{E.5}$$

after substituting for the Clebsch-Gordon coefficients. Combining E.4 and E.5, the angular part of (\mathcal{A}) becomes,

$$\begin{aligned}
 \int \chi_{\kappa_a m_a}^\dagger \cos\theta \chi_{\kappa_b m_b} \sin\theta \, d\theta \, d\phi &= \int [\mathcal{Y}_{00} \langle \alpha |] (\cos\theta) \\
 &\quad \left[\mathcal{Y}_{11} | \beta \rangle \left(\sqrt{2/3} \right) - \mathcal{Y}_{10} | \alpha \rangle \left(\sqrt{1/3} \right) \right] \sin\theta \, d\theta \, d\phi \\
 &= \int -\mathcal{Y}_{00} \mathcal{Y}_{10} \left(\sqrt{1/3} \right) \cos\theta \sin\theta \, d\theta \, d\phi \\
 &= -\left(\frac{1}{3} \right) \tag{E.6}
 \end{aligned}$$

The integral (\mathcal{A}) becomes,

$$\mathcal{A} = (-3 S e) \left(\frac{-1}{3} \right) \int P_{n_a \kappa_a}(r) P_{n_b \kappa_b}(r) \frac{\rho(r)}{B} r \, dr$$

We now evaluate the angular part of (\mathcal{B}) given by,

$$\int \chi_{-\kappa_a m_a}^\dagger \cos\theta \chi_{-\kappa_b m_b} \sin\theta \, d\theta \, d\phi$$

Consider, $\kappa_a = -1 \Rightarrow -\kappa_a = 1$ and $J_a = 1/2$. Hence, $l_a = 1$ and $m_a^l = -1, 0, 1$. Fixing $M - a = 1/2$, $m_a^s = \pm 1/2$. Therefore,

$$\begin{aligned}
 \chi_{-\kappa_a m_a} &= \mathcal{Y}_{10} | \alpha \rangle \langle 1 \, 0 \, \frac{1}{2} \, \frac{1}{2} | \frac{1}{2} \, \frac{1}{2} \rangle + \mathcal{Y}_{11} | \beta \rangle \langle 1 \, 1 \, \frac{1}{2} \, -\frac{1}{2} | \frac{1}{2} \, \frac{1}{2} \rangle \\
 &= \mathcal{Y}_{10} | \alpha \rangle \left(-\sqrt{1/3} \right) + \mathcal{Y}_{11} | \beta \rangle \left(\sqrt{2/3} \right) \tag{E.7}
 \end{aligned}$$

Consider, $-\kappa_b = -1$, $J_b = 1/2 \Rightarrow l_b = 0 \Rightarrow m_b^l = 0$. Fix $M_b = 1/2 \Rightarrow m_b^s = 1/2$. Hence,

$$\chi_{-\kappa_b m_b} = \mathcal{Y}_{00} | \alpha \rangle$$

We now obtain the angular part of (\mathcal{B}) ,

$$\begin{aligned}
 &= \int \left[\mathcal{Y}_{10}^* \langle \alpha | \left(-\sqrt{1/3} \right) + \mathcal{Y}_{11}^* \langle \beta | \left(\sqrt{2/3} \right) \right] \cos\theta [\mathcal{Y}_{00} | \alpha \rangle] \sin\theta \, d\theta \, d\phi \\
 &= \int \mathcal{Y}_{10}^* \mathcal{Y}_{00} \left(-\sqrt{1/3} \right) \cos\theta \sin\theta \, d\theta \, d\phi \\
 &= \left(\frac{-1}{3} \right) \tag{E.8}
 \end{aligned}$$

Substituting in (B),

$$\mathcal{B} = (-3 S e) \left(-\frac{1}{3} \right) \int Q_{n_a \kappa_a}(r) Q_{n_b \kappa_b}(r) \frac{\rho(r)}{B} r dr$$

Combining (A) and (B),

$$\begin{aligned} \langle \Phi_{ks_{1/2}} | H_{SM} | \Phi_{mp_{1/2}} \rangle &= (-3 S e) \left(\frac{-1}{3} \right) \\ &\int_0^\infty [P_{n_a \kappa_a}(r) P_{n_b \kappa_b}(r) + Q_{n_a \kappa_a}(r) Q_{n_b \kappa_b}(r)] \frac{\rho(r)}{B} r dr \end{aligned} \quad (\text{E.9})$$

The matrix element of the Schiff moment operator between the states $|mp_{1/2}\rangle$ and $|ks_{1/2}\rangle$ can be derived similarly and is given by,

$$\begin{aligned} \left\langle \Phi_{mp_{1/2}} \left| H_{SM} \right| \Phi_{ks_{1/2}} \right\rangle &= (-3 S e) \left(\frac{-1}{3} \right) \\ &\int_0^\infty \left[P_{n_a \kappa_a}(r) P_{n_b \kappa_b}(r) + Q_{n_a \kappa_a}(r) Q_{n_b \kappa_b}(r) \right] \frac{\rho(r)}{B} r dr \end{aligned} \quad (\text{E.10})$$

which is exactly same as for $\left\langle \Phi_{ks_{1/2}} \left| H_{SM} \right| \Phi_{mp_{1/2}} \right\rangle$.

Appendix F

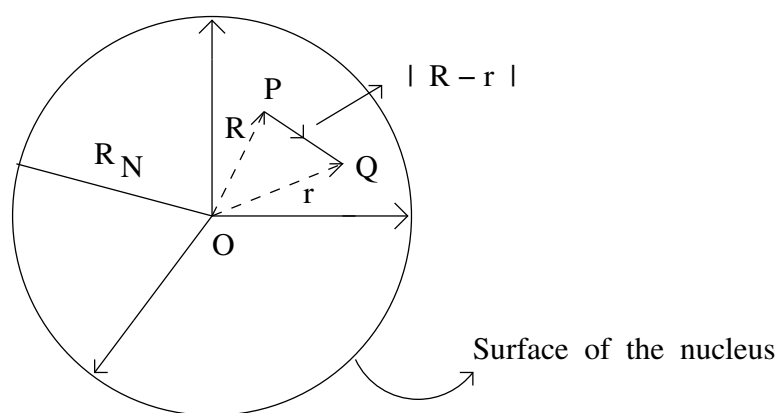
Matrix Elements of the P and T Violating Nuclear Potential

We start with the derivation of a general P , T odd electrostatic potential inside the nucleus, take the electronic matrix element of this potential and show that it is related to the nuclear Schiff moment.

The nuclear electrostatic potential is

$$\Phi(\mathbf{R}) = \int_0^\infty \frac{e\rho(r)}{|\mathbf{R}-\mathbf{r}|} d^3r + \frac{1}{Z}(\mathbf{d}\cdot\nabla) \int_0^\infty \frac{\rho(r)}{|\mathbf{R}-\mathbf{r}|} d^3r \quad (\text{F.1})$$

where $e\rho(r)$ is the nuclear charge density, $\int \rho(r)d^3r = Z$, $\mathbf{d} = e \int \rho(r)d^3r = e\langle\mathbf{r}\rangle$ is the nuclear EDM. The definitions of the vectors \mathbf{R} and \mathbf{r} are given in fig.1.



Note that both \mathbf{R} and \mathbf{r} are lying within the nucleus and R_N is the nuclear radius. The second term cancels the dipole long range electric field in the multipole expansion

of $\Phi(\mathbf{R})$. Consider the multipole expansion of $\Phi(\mathbf{R})$ around $\mathbf{R} = \mathbf{R}_0$

$$\Phi(\mathbf{R}) = \Phi(\mathbf{R}_0) + (\mathbf{R} - \mathbf{R}_0)\Phi'(\mathbf{R}_0) + \frac{(\mathbf{R} - \mathbf{R}_0)^2}{2!}\Phi''(\mathbf{R}_0) + \dots$$

which is equivalent to Eq. (F.1) at $\mathbf{R} = \mathbf{R}_0$ except that the second term in Eq. (F.1) is defined per nucleon. Expanding $\frac{1}{|\mathbf{R}-\mathbf{r}|}$

$$\frac{1}{|\mathbf{R} - \mathbf{r}|} = \sum_l \frac{r_{<}^l}{r_{>}^{l+1}} P_l(\cos\theta)$$

where θ is the angle between \mathbf{R} and \mathbf{r} and $P_l(\cos\theta)$ are the Legendre polynomials. Consider the first term of Eq. (F.1).

$$\int_0^\infty \frac{e\rho(r)}{|\mathbf{R} - \mathbf{r}|} d^3r = \int_0^R \frac{e\rho(r)}{|\mathbf{R} - \mathbf{r}|} d^3r + \int_R^\infty \frac{e\rho(r)}{|\mathbf{R} - \mathbf{r}|} d^3r$$

Only odd multipoles of l give rise to P, T odd potential. All values beyond $l=1$ give negligible contribution. Hence, in the \sum_l only $l=1$ is retained for the first term. Using $P_1(\cos\theta) = \cos\theta$ we get

$$\begin{aligned} &= \frac{1}{R^2} \int_0^R e\mathbf{r}\rho(r) \cos\theta d^3r + R \int_R^\infty \frac{e\rho(r)}{r^2} \cos\theta d^3r \\ &\int_0^\infty \frac{e\rho(r)}{|\mathbf{R} - \mathbf{r}|} d^3r = \frac{\mathbf{R}}{R^3} \cdot \int_0^R e\mathbf{r}\rho(r) d^3r + \mathbf{R} \cdot \int_R^\infty \frac{e\mathbf{r}\rho(r)}{r^3} d^3r. \end{aligned} \quad (\text{F.2})$$

Consider the second term in Eq. (F.1). Retaining only the $l = 0$ term

$$\frac{1}{Z}(\mathbf{d} \cdot \nabla) \int_0^\infty \frac{\rho(r)}{|\mathbf{R} - \mathbf{r}|} d^3r = \frac{1}{Z}\mathbf{d} \cdot \nabla \left(\frac{1}{R} \right) \int_0^R \rho(r) d^3r + \frac{1}{Z}(\mathbf{d} \cdot \nabla) \int_R^\infty \frac{\rho(r)}{\mathbf{r}} d^3r \quad (\text{F.3})$$

Consider the first term in the Eq. (F.2) in the limit $R \rightarrow \text{inf}$

$$e \frac{\mathbf{R}}{R^3} \cdot \int_0^\infty \mathbf{r}\rho(r) d^3r = e \frac{\mathbf{R}}{R^3} \langle \mathbf{r} \rangle.$$

Similarly in the limit $R \rightarrow \text{inf}$ first term in Eq. (F.3) becomes

$$-\frac{\mathbf{R}}{ZR^3}e\langle\mathbf{r}\rangle\int_0^\infty\rho(r)d^3r=-\frac{e\langle\mathbf{r}\rangle}{R^3}\mathbf{R}.$$

These two terms cancel each other. Hence the integral limits in the first terms of Eq. (F.2) and Eq. (F.3) can be changed using

$$\int_0^R=\int_0^\infty-\int_R^\infty=-\int_R^\infty$$

Eq. (F.1) becomes

$$\Phi(\mathbf{R})=\frac{-e\mathbf{R}}{R^3}\int_R^\infty\mathbf{r}\rho(r)d^3r+e\mathbf{R}\int_R^\infty\frac{\rho(r)\mathbf{r}d^3r}{r^3}+\frac{e\langle\mathbf{r}\rangle}{ZR^3}\cdot\mathbf{R}\int_R^\infty\rho(r)d^3r$$

Rewriting the above equation

$$\Phi(\mathbf{R})=e\mathbf{R}\left[\int_R^\infty\left(\frac{\langle\mathbf{r}\rangle}{ZR^3}-\frac{\mathbf{r}}{R^3}+\frac{\mathbf{r}}{r^3}\right)\rho(r)d^3r\right] \quad (\text{F.4})$$

This nuclear potential goes to zero when $\rho(r)$ becomes zero for $\mathbf{R} > \mathbf{R}_N$.

Physical significance of the different terms in Eq. (F.4):

- Consider the first term

$$\int_R^\infty e\mathbf{R}\frac{\langle\mathbf{r}\rangle}{ZR^3}\rho(r)d^3r$$

Rearranging,

$$\int_R^\infty\frac{e\langle\mathbf{r}\rangle}{Z}\frac{\mathbf{R}}{R^3}\rho(r)d^3r$$

This term represents the interaction of the average nuclear electric dipole moment per nucleon due to a charge distribution at a distance of \mathbf{r} between \mathbf{R} and \mathbf{R}_N with the electric field due to a point charge at a distance \mathbf{R} from the centre of the nucleus.

- Consider the second term

$$\int_R^\infty \mathbf{e}\mathbf{r} \cdot \frac{\mathbf{R}}{R^3} \rho(r) d^3r$$

This term is the interaction of the nuclear electric dipole moment produced due to a charge distribution $\rho(r)$ in the region between \mathbf{R} and \mathbf{R}_N with the electric field due to a unit charge at a distance \mathbf{R} from the centre of the nucleus.

- The third term

$$\int_R^\infty \mathbf{R} \frac{e\mathbf{r}}{r^3} \rho(r) d^3r$$

represents an interaction of an electric field produced due to a charge distribution between \mathbf{R} to \mathbf{R}_N with the nuclear dipole moment produced at a distance \mathbf{R} from the centre of the nucleus. The nuclear electrostatic potential, Eq. (F.4) mixes the electron wavefunctions of opposite parity. We consider only the $s_{1/2}$ and $p_{1/2}$ electron wavefunctions as only these have a nonzero probability density inside the nucleus. We are interested in the matrix element

$$\langle \Psi_s | -e\Phi(\mathbf{R}) | \Psi_p \rangle.$$

Using the relativistic form of the electron wavefunctions

$$\Psi(\mathbf{R}) = \begin{pmatrix} f(\mathbf{R})\Omega(jlm) \\ -i(\boldsymbol{\sigma} \cdot \mathbf{n})g(\mathbf{R})\Omega(jlm) \end{pmatrix} \quad (\text{F.5})$$

in the above matrix element and simplifying

$$\int_0^\infty (f_s f_p + g_s g_p) (\Omega_s^\dagger \mathbf{n} \Omega_p) [\Phi(\mathbf{R})] R^2 dR \sin\theta d\theta d\phi$$

Using

$$\int_0^\infty dR \int_R^\infty dr = \int_0^\infty dr \int_0^r dR$$

and $U_{sp} = f_s f_p + g_s g_p$, the above term reduces to

$$= -e^2 \langle s | \mathbf{n} | p \rangle \int_0^\infty \left[\frac{\langle \mathbf{r} \rangle}{ZR^3} - \frac{\mathbf{r}}{R^3} + \frac{\mathbf{r}}{r^3} \right] \rho(r) d^3r \int_0^r R^2 U_{sp} dR$$

$$= -e^2 \langle s | \mathbf{n} | p \rangle \left\{ \int_0^\infty \left[\left(\frac{1}{Z} \langle \mathbf{r} \rangle - \mathbf{r} \right) \int_0^r U_{sp} dR + \frac{\mathbf{r}}{r^3} \int_0^r U_{sp} R^3 dR \right] \rho(r) d^3 r \right\}$$

Now expand $U_{sp} = f_s f_p + g_s g_p = \sum_k b_k R^k$ and substituting in the above equation

$$\begin{aligned} &= -e^2 \langle s | \mathbf{n} | p \rangle \sum_k \left\{ \left[\int_0^\infty \left(\left(\frac{1}{Z} \langle \mathbf{r} \rangle - \mathbf{r} \right) b_k \frac{r^{k+1}}{k+1} + \frac{\mathbf{r}}{r^3} \frac{r^{k+4}}{k+4} b_k \right) \right] \rho(r) d^3 r \right\} \\ &= -e^2 \langle s | \mathbf{n} | p \rangle \sum_k \frac{b_k}{k+1} \left\{ \left[\frac{1}{Z} \langle \mathbf{r} \rangle \langle r^{k+1} \rangle - \frac{3}{k+4} \langle \mathbf{r} r^{k+1} \rangle \right] \right\} \end{aligned}$$

where $\langle s | \mathbf{n} | p \rangle = \int \Omega_s^\dagger \mathbf{n} \Omega_p d\phi \sin \theta d\theta$.

In the nonrelativistic case, ($Z\alpha \rightarrow 0$), only $b_1 \neq 0$. Hence,

$$\begin{aligned} \langle s | -e\Phi^{(1)} | p \rangle &= -\frac{e^2 b_1}{2} \langle s | \vec{n} | p \rangle \cdot \left[\frac{1}{Z} \langle \vec{r} \rangle \langle r^2 \rangle - \frac{3}{5} \langle \vec{r} r^2 \rangle \right] \\ &= 4\pi e \vec{S} \cdot (\nabla \Psi_s^\dagger \Psi_p)_{R \rightarrow 0} \end{aligned}$$

where the Schiff moment \vec{S} is defined as

$$\vec{S} = \frac{e}{10} \left[\langle \vec{r} r^2 \rangle - \frac{5}{3Z} \langle r^2 \rangle \langle \vec{r} \rangle \right] = S\vec{I}/I \quad (\text{F.6})$$

where \vec{I} is the nuclear spin. The above form of the Schiff moment defines the nonrelativistic expression for the P and T violating nuclear potential arising due to the Schiff moment. Note that the quantities defining S refer to the nuclear coordinates.

Appendix G

Additional Notes

G.1 Matrix elements of the Coulomb operator

The term representing the two-body Coulomb interaction can be expanded as [31, 32]

$$\frac{1}{r_{12}} = \sum_k U^k(1, 2) \sum_q (-1)^q C_q^k(1) C_{-q}^k(2) \quad (\text{G.1})$$

where

$$U^k(1, 2) = \frac{r_{<}^k}{r_{>}^{k+1}},$$

$$C_q^k = \sqrt{4\pi/(2k+1)} Y_{kq}(\theta, \phi)$$

The two-electron matrix element is given by,

$$\left\langle ab \left| \frac{1}{r_{12}} \right| cd \right\rangle = \delta(m_a + m_b, m_c + m_d) \sum_k d^k(j_a m_a; j_c m_c) d^k(j_b m_b; j_d m_d) R^k(a, b, c, d, k)$$

The d^k coefficients are the angular factors and $R^k(a, b, c, d, k)$ is a two-electron radial integral dependent on the large and small components of the orbitals a, b, c, d and the multipole k . This can be written as,

$$\left\langle ab \left| \frac{1}{r_{12}} \right| cd \right\rangle = \sum_{\substack{j_a, j_c, j_b, j_d \\ (m_a, m_c, m_b, m_d, k, q)}} X_q^k(j_a, j_b, j_c, j_d) (-1)^{(j_a - m_a + j_d - m_d)} \begin{pmatrix} j_a & k & j_c \\ -m_a & q & m_c \end{pmatrix} \begin{pmatrix} j_d & k & j_b \\ -m_d & q & m_b \end{pmatrix} \quad (\text{G.2})$$

where

$$X_q^k(j_a, j_b, j_c, j_d) = (-1)^{(k-q)} (-1)^{(j_a - \frac{1}{2} + j_b - \frac{1}{2})} \begin{pmatrix} j_a & k & j_c \\ \frac{1}{2} & 0 & -\frac{1}{2} \end{pmatrix} \begin{pmatrix} j_d & k & j_b \\ \frac{1}{2} & 0 & -\frac{1}{2} \end{pmatrix} \\ \left[j_a, j_c, j_b, j_d \right]^{\frac{1}{2}} R^k(a, b, c, d, k)$$

and

$$R^k(a, b, c, d, k) = \int_0^\infty \int_0^\infty \left[P_{n_a \kappa_a}(r_1) P_{n_c \kappa_c}(r_1) + Q_a(r_1) Q_c(r_1) \right] \times \frac{r_1^k}{r_1^{k+1}} \\ \times \left[P_{n_b \kappa_b}(r_2) P_{n_d \kappa_d}(r_2) + Q_b(r_2) Q_d(r_2) \right] dr_1 dr_2$$

With the selection rules,

$$(-1)^{l_a + l_c + k} = (-1)^{l_b + l_d + k} = 1$$

G.2 Matrix elements of the Induced Dipole Operator

Consider the angular matrix element of the induced dipole operator between the states of angular momenta (J_a, M_a) and (J_b, M_b) ,

$$\left\langle \Psi_{J_a, M_a} \left| D_{\text{ind}}^k \right| \Psi_{J_b, M_b} \right\rangle = (-1)^{J_a - M_a} \begin{pmatrix} J_a & k & J_b \\ -M_a & 0 & M_b \end{pmatrix} \times \left\langle J_a \left\| D_{\text{ind}}^k \right\| J_b \right\rangle$$

where the reduced matrix element is

$$\left\langle J_a \left\| D_{\text{ind}}^k \right\| J_b \right\rangle = (-1)^{J_a + \frac{1}{2}} \left[(2J_a + 1)(2J_b + 1) \right] \begin{pmatrix} J_a & 1 & J_b \\ \frac{1}{2} & 0 & -\frac{1}{2} \end{pmatrix} \times \left\langle \Psi_a(r) \left| D_{\text{ind}} \right| \Psi_b(r) \right\rangle$$

and $D_{\text{ind}} = e \mathbf{r}$.

Bibliography

- [1] C. S. Wu, E. Ambler, R. W. Hayward, D. D. Hoppes, and R. P. Hudson. *Phys. Rev.*, 105:1413–1415, 1957.
- [2] J. R. Christensen, J. W. Cronin, V. L. Fitch, and R. Turlay. *Phys. Rev. Lett.*, 138(13), 1964.
- [3] G. Luders. *Annals of Physics*, 2:1, 1957.
- [4] E. D. Commins. *Advances in Atomic, Molecular and Optical Physics*, 40(1), 1999.
- [5] S. M. Barr and W. J. Marciano. Cp violation. World Scientific, Singapore, 1989. edited by C. Jarlkog.
- [6] S. M. Barr. *International Journal of Modern Physics A (IJMPA)*, 8:209–236, 1993.
- [7] J. J. Sakurai. *Modern Quantum Mechanics Revised Edition*. Pearson Education (Singapore), 1994. edited by San Fu Tuan.
- [8] M. V. Romalis, W. C. Griffith, J. P. Jacobs, and E. N. Fortson. *Phys. Rev. Lett.*, 86:2505, 2001.
- [9] J.P. Jacobs, W. M. Klipstein, S. K. Lamoreaux, B. R. Heckel, and E. N. Fortson. *Phys. Rev. Lett.*, 71(23):3782, 1993.
- [10] Ann-Marie Martensson-Pendrill. *Phys. Rev. Lett*, 54(11), 1985.

-
- [11] Toby Falk, Keith A. Olive, Maxim Pospelov, and Radu Roiban. *Nucl. Phys. B*, 560:3–22, 1999.
- [12] A. M. Martensson-Pendrill and E. Lindroth. *Europhys. Lett.*, 15(2):155–160, 1991.
- [13] V. A. Dzuba, V. V. Flambaum, and J. S. M. Ginges. *Phys. Rev. A*, 66:012111, 2002.
- [14] J. S. M. Ginges and V. V. Flambaum. *Physics Reports*, 397:63–154, 2005.
- [15] V. V. Flambaum, I. B. Khriplovich, and O. P. Sushkov. *Nucl. Phys. A*, 449:750, 1986.
- [16] W. C. Haxton. *Chinese Journal of Physics*, 32(S-11), 1994.
- [17] M. Pospelov. *Phys. Lett. B*, 530:123, 2002.
- [18] R. J. Crewther, P. Di Vecchia, G. Veneziano, and E. Witten. *Phys. Lett*, 91B:487(E), 1980.
- [19] V. F. Dmitriev and R. A. Senkov. *Phys. Rev. Lett*, 91:21, 2003.
- [20] Norval Fortson, Patrick Sandars, and Stephen Barr. *Physics Today, June*, page 33, 2003.
- [21] L. I. Schiff. *Phys. Rev.*, 132, 1963.
- [22] P. G. H. Sandars. *Contemporary Physics*, 42:97–111, 2001.
- [23] V. V. Flambaum and J. S. M. Ginges. *Phys. Rev. A*, 65:032113(1)–032113(9), 2002.
- [24] I. Lindgren and J. Morrison. *Atomic Many-Body Theory*. Springer-Verlag, 1982.
- [25] Raymond F. Bishop and Hermann Kummel. *Physics Today, March*, page 52, 1987.

- [26] R. F. Bishop. *Microscopic Quantum Many-Body Theories and their Applications (Lecture notes in Physics)*. Springer-Verlag-Berlin, 1998. J. Navarro and A. Polls.
- [27] R. J. Bartlett. *Modern Electronic Structure Theory*, volume III. World Scientific, Singapore, 1995. edited by D. R. Yarkony.
- [28] Hermann Kummel. Origins of the coupled cluster method. *Theoretica Chimica Acta*, 80:81–89, 1991.
- [29] Geetha K. P. *Relativistic Many-body Studies of Parity Non-Conservation (PNC) in Heavy Atomic Ions*. PhD thesis, Bangalore University, 2001.
- [30] A. Szabo and N. S. Ostlund. *Modern Quantum Chemistry*. Dover Publications, Mineola, New York.
- [31] I. P. Grant. *Adv. Phys.*, 19:747, 1970.
- [32] I. P. Grant. *Proceedings. Royal. Society A*, 262:555, 1961.
- [33] Angom Dilip Kumar Singh and K. V. P. Latha. *Calculation of Atomic Electric Dipole Moment of Closed-shell Atoms using Coupled-cluster Method*. <http://www.iiap.res.in/research/NAPP/main.html>, 2006. unpublished.
- [34] A. K. Mohanty and E. Clementi. *Chemical Physics Letters*, 157:348–352, 1989.
- [35] R. E. Stanton and S. Havriliak. *Journal of Chemical Physics*, 81:1910, 1984.
- [36] I. P. Grant and H. M. Quiney. *Advances in Atomic and Molecular Physics*, 23:37, 1988.
- [37] W. R. Johnson and G. Soff. *At. Data. Nucl. Data Tables*, 33, 1985.
- [38] F. A. Parpia and A. K. Mohanty. *Phys. Rev. A*, 46:3735, 1992.
- [39] F. A. Parpia, C. F. Fischer, and I. P. Grant. *General Relativistic Atomic Structure Program (GRASP2)*. unpublished.

-
- [40] B. P. Das, K. V. P. Latha, B. K. Sahoo, C. Sur, R. K. Chaudhuri, and D. Mukherjee. Relativistic and correlation effects in atoms. *Journal of Theoretical and Computational Chemistry*, 4(1), 2005.
- [41] Thomas M. Miller and Benjamin Bederson. *Advances in Atomic, Molecular Physics*, 13(1), 1977.
- [42] Alok Shukla, B. P. Das, and D. Mukherjee. *Phys. Rev. A*, 50:2096–2107, 1994.
- [43] S. M. Barr. *Phys. Rev. D*, 45:4148–4155, 1992.
- [44] R. J. Crewther, P. Di Vecchia, G. Veneziano, and E. Witten. *Phys. Lett*, 88B:123, 1979.
- [45] M. A. Rosenberry and T. E. Chupp. *Phys. Rev. Lett.*, 86(22), 2001.
- [46] J. J. Hudson, B. E. Sauer, M. R. Tarbutt, and E. A. Hinds. *Phys. Rev. Lett.*, 89:023003, 2002.
- [47] T. N. Mukhamedjanov, V. A. Dzuba, and O. P. Sushkov. *Phys. Rev. A*, 68:012103, 2003.
- [48] Mihalay Kallay and Peter R. Surjan. *Journal of Chemical Physics*, 115(7), 2001.